ULTRAHIGH VACUUM SURFACE ANALYSIS STUDIES OF ELECTROCHEMICAL ATOMIC LAYER DEPOSITION OF METALS AND COMPOUND SEMICONDUCTORS

by

JAY YU KIM

(Under the Direction of John Lewellen Stickney)

ABSTRACT

The main topic of this dissertation is electrochemical atomic layer deposition (ALD) by ultrahigh vacuum (UHV) surface analysis. The purpose of electrochemical ALD is to form smooth thin films at room temperature. The first part of this dissertation will be about platinum (Pt) and copper (Cu) electrochemical ALD on gold (Au) substrate. The surface-limited redox replacements (SLRR) were used in these cases. In case of forming a Pt atomic layer, a Cu atomic layer, as a sacrificial layer, was first formed by underpotential deposition (UPD) on the clean and annealed Au(111) single crystal. Then, it was immersed in the Pt solution at open circuit, and a Cu atomic layer was replaced spontaneously by Pt ions, so a Pt atomic layer was formed on the substrate. To form multiple Pt atomic layers, the subsequent Pt replacements with Cu sacrificial layers were done on the substrate. In order to grow Cu atomic layers on the substrate, lead (Pb) atomic layers were used as the sacrificial layers. I^- and Cl^- anions were used in solutions for electrochemical annealing. Auger electron spectroscopy (AES), low-energy electron diffraction (LEED), and scanning tunneling microscopy (STM) were performed to estimate the quality of the thin films on the substrate.

The second part of this dissertation is about the electrochemical ALD on GaAs(100) substrate. After the substrate was cleaned, an attempt was made to deposit a Te atomic layer on the substrate. A Te atomic layer on the substrate is expected as a precursor to deposit metals, such as cadmium (Cd) or indium (In). From the Auger ratios of In/Te and Te/Ga, the In_2Te_3 atomic layer was attempted to form on the substrate. The deposited In_2Te_3 thin film thickness was calculated from the Auger electron spectra. The future plan with this GaAs(100) substrate is to form atomic layers of InSb, Sb_2Te_3, and $In_2Sb_2Te_3$.

INDEX WORDS: Electrochemical atomic layer deposition, Electrodeposition, Underpotential deposition, Ultrahigh vacuum, Surface-limited redox replacement, Auger electron spectra, Low-energy electron diffraction, Scanning tunneling microscopy, Metal, Compound semiconductor

ULTRAHIGH VACUUM SURFACE ANALYSIS STUDIES OF ELECTROCHEMICAL ATOMIC LAYER DEPOSITION OF METALS AND COMPOUND SEMICONDUCTORS

by

JAY YU KIM

B.S., Korea University, Korea, 2000

M.S., Korea University, Korea, 2002

A Dissertation Submitted to the Graduate Faculty of The University of Georgia in Partial Fulfillment of the Requirements for the Degree

DOCTOR OF PHILOSOPHY

ATHENS, GEORGIA

2008

© 2008

Jay Yu Kim

All Rights Reserved

ULTRAHIGH VACUUM SURFACE ANALYSIS STUDIES OF ELECTROCHEMICAL ATOMIC LAYER DEPOSITION OF METALS AND COMPOUND SEMICONDUCTORS

by

JAY YU KIM

Major Professor: John L. Stickney

Committee: James L. Anderson
I. Jonathan Amster

Electronic Version Approved:

Maureen Grasso
Dean of the Graduate School
The University of Georgia
August 2008

DEDICATION

To My Parents and My Wife

ACKNOWLEDGEMENTS

First of all, I would like to thank my major professor, John L. Stickney. Since I became his student four and a half years ago, he has always been encouraging me to be a scientist, and not just to be a technician. I have been learning not only how to do science, but also how to communicate with people, thanks to him. I would like to acknowledge and thank Professors James Anderson and Jonathan Amster for serving on my committee and for their valuable advice. I would like to thank my former laboratory members: Dr. Mkhulu (Ken) Mathe, Dr. Nattapong (Nat) Srisook, Dr. Madhivanan (Madhi) Muthuvel, and Dr. Venkatram (Ram) Venkatasamy. I would also like to express my gratitude to my present laboratory members: Dr. Youn-Geun Kim, Nagarajan Jayaraju, Dhego Banga, Chandru Thambidurai, Daniel Gebregziabiher, Xuehai Liang, and Leah Sheridan. I would like to thank and give my love to my parents, my parent-in-law, my brother, my sister-in-law, my brother-in-law, and my lovely wife, Mee Kyung, for their supports, advices, and prayers. Finally, I would like to thank and praise God for guiding my life to this point.

"The LORD is my shepherd; I shall not be in want. He makes me lie down in green pastures, he leads me beside quiet waters, and he restores my soul. He guides me in paths of righteousness for his name's sake. Even though I walk through the valley of the shadow of death, I will fear no evil, for you are with me; your rod and your staff, they comfort me. You prepare a table before me in the presence of my enemies. You anoint my head with oil; my cup overflows. Surely goodness and love will follow me all the days of my life, and I will dwell in the house of the LORD forever." (Psalm 23:1~6)

TABLE OF CONTENTS

Page

ACKNOWLEDGEMENTS....................v

CHAPTER

1 INTRODUCTION AND LITERATURE REVIEW....................1

2 STUDIES OF CU ATOMIC LAYER REPLACEMENT, FORMED BY UNDERPOTENTIAL DEPOSITS, TO FORM PT NANOFILMS USING ELECTROCHEMICAL ATMOIC LAYER EPITAXY (EC-ALE)....................25

3 COPPER NANOFILM FORMATION BY ELECTROCHEMICAL ATOMIC LAYER DEPOSITION (ALD) : UHV-EC AND IN-SITU STM STUDIES........40

4 CU NANOFILM FORMATION BY ELECTROCHEMICAL ATOMIC LAYER DEPOSITION (ALD) IN THE PRESENCE OF CHLORIDE IONS....................69

5 SURFACE STRUCTURES OF CLEAN N-GE(111) AND N-GAAS(100) SUBSTRATES : UHV-EC AND IN-SITU EC-STM STUDIES....................97

6 ULTRAHIGH VACUUM SURFACE STUDIES OF THE ELECTROCHEMICAL ATOMIC LAYER DEPOSITION OF INDIUM TELLURIDE ON N-TYPE GAAS(100)....................133

7 ELECTROCHEMICAL ATOMIC LAYER DEPOSITION (ALD) OF INDIUM ANTIMONIDE ON N-TYPE GAAS(100)....................160

8 CONCLUSION AND FUTURE STUDIES....................178

CHAPTER 1

INTRODUCTION AND LITERATURE REVIEW

Introduction

In principle, there are three basic types of thin film growth: island or Volmer-Weber growth, layer or Frank-van der Merwe growth, and island-layer or Stranski-Krastonov growth [1-4]. Island growth occurs when the growth species are more strongly bonded to each other than to the substrate. Many systems of metals on insulator substrates, alkali halides, graphite, and mica substrates display this type of nucleation during the initial film deposition. Subsequent growth results in coalescence of the islands to form a continuous film. The layer growth is the opposite of the island growth, where growth species are equally bound more strongly to the substrate than to each other. A first complete monolayer is formed, before the deposition of a second layer occurs. Providing the decrease in bonding energy is continuous toward the bulk-crystal value, the layer growth mode is sustained. The most important examples of layer growth mode are the epitaxial growth of single crystal films. The island-layer growth is an intermediate combination of layer growth and island growth. In this case, after forming one or more monolayers, subsequent layer growth becomes unfavorable and islands form. Such a growth mode typically involves stress, which is developed during the formation of the nuclei or films. This growth is fairly common and has been observed in metal-metal and metal-semiconductor systems.

Layer-by-layer growth of thin films has been more desirable and applicable in many electronic industries than island growth because of the high crystallinity, low resistance, and continuous characterization of the films [5, 6]. Fundamental to forming high quality structures and devices with thin films of metal and semiconductors is the concept of epitaxy. The epitaxy focuses on the formation of single crystal films on single crystal substrates [7]. Epitaxial deposition with molecular beam epitaxy (MBE) or vapor phase epitaxy (VPE) involves mass transport to and diffusion along the surface. It is generally better to deposit slowly, and to use

higher temperatures, limiting the number of atoms depositing at a given time, and allowing their diffusion to optimal sites, for instance at step edges, to promote epitaxy.

Electrochemical atomic layer epitaxy (ALE) or atomic layer deposition (ALD) has been studied for many years to produce high quality thin films [7]. ALE or ALD is a methodology used initially to improve epitaxy in the growth of thin films by MBE or VPE. The principle of ALE or ALD is to use surface-limited reactions to form each atomic layer of a deposit. If no more than an atomic layer is ever deposited, the growth will be two-dimensional (2-D), layer-by-layer. Surface-limited reactions are developed for the deposition of each component element, and a cycle is formed with them. With each cycle, a compound monolayer is formed, and the deposit thickness is controlled by the number of cycles.

Surface-limited reactions are generally referred to as underpotential deposition (UPD) [7, 8]. UPD is the phenomenon that, in the deposition of one element on a second, frequently the first element will form an atomic layer at a potential prior to, under, that needed to deposit the element on itself. One way of looking at UPD is that a surface compound, or alloy, is formed, and the shift in potential results from the free energy of formation of the surface compound.

Electrochemical ALD is the combination of UPD and ALD. Atomic layers of component elements are deposited at underpotentials in a cycle, to directly form a compound. It is layer-by-layer growth, avoiding three-dimensional (3-D) nucleation, and offering increased degrees of freedom, atomic level control, and promoting of epitaxy. It also offers a way of better understanding compound electrodeposition, a way of breaking it down into its component pieces [7]. It allows compound electrodeposition to be deconvolved into a series of individually controllable steps, resulting in an opportunity to learn more about the mechanisms, and gain a series of new control points for electrodeposition. In this process, each reactant has its own

solution and deposition potential, and there are generally rinse solutions as well. Each solution can be separately optimized, so that the pH, electrolyte, and additives or complexing agents are tailored to fit the precursor. Finally, electrochemical ALD involves growth in a condensed phase with potential control instead of thermal. This increases the variable space for producing materials; the diversity of conditions under which compounds can be formed.

This dissertation mainly focuses on electrochemical ALD of metal and compound semiconductor thin films on Au(111) and n-type GaAs(100) substrates. Chapter 2 first introduces a novel technique to grow smooth Pt thin film in layer-by-layer mode on Au(111) substrate, by surface-limited redox reaction (SLRR). A Cu atomic layer was used as a sacrificial layer in this Chapter. In Chapter 3, the surfaces of the Cu thin film grown on Au(111) substrate, up to 10 replacement cycles, by SLRR with Pb sacrificial layers, are characterized with Auger electron spectra (AES), low-energy electron diffraction (LEED), and in-situ electrochemical scanning tunneling microscopy (EC-STM). In this Chapter, iodine (I) is used for the electrochemical annealing of both substrate and Cu film. In Chapter 4, chlorine (Cl) is used for the electrochemical annealing, and its effects on Cu SLRR are studied. In Chapter 5, semiconductor substrates, n-type Ge(111) and n-type GaAs(100), are cleaned and annealed. Their reconstructed surface structures are studied by LEED and EC-STM. Chapter 6 introduces the first attempt to electrodeposit a Te atomic layer on n-GaAs(100). Electrodeposition of an indium (In) atomic layer on a Te atomic layer on n-GaAs(100) is attempted in this Chapter. An In-Te thin film is then electrodeposited up to thee cycles. In Chapter 7, indium antimonide (InSb) thin film was deposited on n-GaAs(100) by electrochemical ALD. Last but not least, in Chapter 8, the conclusions are drawn and the future studies are presented.

Literature Review

In the Stickney lab, EC-ALE has been intensively studied for 20 years. EC-ALE is an electrochemical analog to ALE [7]. Their early works involved the electrochemical and surface analysis of HCl adsorbed on tri-phase Cu electrodes [9-11]. Compound semiconductors have been formed by EC-ALE on Au substrates; including II-VI compounds such as CdS [12], CdSe [12-14], CdTe [12, 15-21], ZnS [22], ZnSe [22], ZnTe [22], HgSe [23, 24], HgTe [25], and recently MCT ($Hg_xCd_{(1-x)}Te$) [26], IV-VI compounds such as PbSe [27, 28] and PbTe [28], and III-V compounds such as GaAs [29, 30], InAs [31], and InSb [32]. Recently, electrochemical ALD of compound semiconductor thin films of GeTe and GeSb on Au(111) with flow cell system [7, 22] is under study in this laboratory. Several other groups have been using EC-ALE to grow compound semiconductors on various metal substrates, such as CdS on Au(111) [33], Sb_2Te_3 and Bi_2Te_3 on both Au(111) and Pt(111) [34-36], and CdS, ZnS, ZnSe, and InAs on Ag(111) [37-39].

2-D electrochemical epitaxial growth of single-crystal metal thin films has been a difficult task. In general, metals grow as 3-D clusters on the substrate, which can cause difficult analysis of the surface because of their non-uniform coverage of the substrate. It is reported that the 3-D cluster problems can be solved by the replacement of desirable metals by Cu or Pb UPD phenomenon [40-43]. Sieradzki et al. developed an electrochemical technique that serves to significantly enhance ambient-temperature nucleation 2-D islands, called defect-mediated growth (DMG) [41]. The mediator was periodically deposited and stripped from the surface by appropriate cycling of the electrochemical potential. A monolayer (ML) was completed as the growing 2-D clusters eventually merge. Adzic et al. proposed that the UPD adlayer is oxidized by the more noble metal cations, which are simultaneously reduced and deposited on the gold

substrate, and this can be expressed as: $M^0_{UPD} + (m/z)\ P^{z+} \rightarrow M^{m+} + (m/z)\ P^0$, where M^0_{UPD} represents a UPD metal adatom on the electrode surface S and P^{z+} is a noble metal cation with positive charge z+ and valence z [42]. They reported that an interesting novel procedure of near-uniform Pd ML on Au(111) could be formed by the spontaneous redox replacement of a previously prepared Cu UPD layer by Pd (II) solute, confirmed by STM [42]. Figure 1.1 shows the cartoon of Pt surface-limited redox replacement (SLRR) with a Cu sacrificial UPD layer. However, in case of Pt (IV) replacement, a submonolayer of Pt was formed because of the stoichiometry: $2Cu^0_{UPD} + Pt^{4+} \rightarrow 2Cu^{2+} + Pt^0$. Weaver et al. reported the preparation of Pt-group metal films on roughened gold electrodes by utilizing spontaneous redox replacement of a Cu or Pb UPD with a Pt-group metal cation solute, and the resulting films displayed intense surface-enhanced Raman scattering (SERS) for adsorbates bound to the overlayer and free from substrate interferences [43]. Stickney et al. recently have made some progress in the atomic scale studies of Pt [44, 45] and Cu [46-48] thin films, grown a couple of replacement cycles by SLRR on Au(111) single crystal. AES, LEED, and in-situ EC-STM were used to characterize the surfaces of thin films. Iodine and chlorine were used for the electrochemical annealing to modify the surface. Up to date, several attempts have been made in their laboratory to grow smooth and thicker films, 10 ~ 20 nm or thicker, of Pt, Cu, and Ru, by SLRR and flow cell system. The surfaces of these films are characterized by electron probe microanalysis (EPMA) and X-ray diffraction (XRD).

Gallium arsenide (GaAs) is an important III-V compound semiconductor nowadays, and it is substantially replacing the Si substrate in electronic industries because of their higher crystallinity and large mobility [49]. Growing another compound semiconductor on GaAs substrate would be applied to optoelectronic, thermoelectronic, and photovoltaic devices. Several

groups have been attempting to grow chalcogen atomic layers (S, Se and Te) as a passivating layer, by MBE, on GaAs substrates [50-55]. A chalcogen passivating layer on the substrate can also be used as a precursor layer for a metal (such as Cd [56-59], Zn [60, 61], In [62], or Sb [63]) atomic layer, grown by MBE. There have been a number of electrodeposition studies where GaAs was used as a substrate; however, atomic level studies of GaAs surfaces in electrochemical environments have been few. Etcheberry et al. electrodeposited CdSe on InP (100), GaAs(100), and GaAs(111) [64-67]. They co-deposited CdSe from a single solution, at a couple of different potentials on the substrates, and analyzed the surface with XRD, X-ray photoelectron spectroscopy (XPS), LEED, and reflection high-energy electron diffraction (RHEED). Allongue et al. electrodeposited metals such as Pt, Pd, Ni, Co, Cu, and Ag, on n-GaAs(100), from separate solutions, without the use of any passivation layer [68-71]. Recently, Kim and Stickney first attempted to electrodeposit a Te atomic layer on n-type GaAs(100) substrate and to electrodeposit an indium (In) atomic layer on a Te layer to form In_2Te_3 compound, characterized by AES [72]. In addition, we performed three subsequent In-Te ALD cycles on the substrate. The detail of this study is described in Chapter 6.

Experimental Procedure

Cleaning the Substrate

Prior to deposition, the substrates must be clean, which means no oxide or carbon should be formed on the substrates. To clean the gold substrate, it is immersed in hot concentrated nitric acid for about 30 minutes and then annealed in a hydrogen flame for about 10 minutes [73]. Then, the gold substrate can be cleaned by Ar^+ ion bombardment in the ultrahigh vacuum (UHV) chamber [20, 74]. Figures 1.2 and 1.3 show the schematic diagrams of the UHV chamber and

Ar^+ ion bombardment, respectively. The cryopump and ion pump are attached to the main chamber so that the UHV state (~ 10^{-9} Torr) can be reached. The sorption pumps (roughing pumps) are attached to the chamber, which are not shown in Figure 1.2. For the Ar^+ ion bombardment to clean substrates, an Ar gas line is connected to the main chamber. When Ar gas is purged into the chamber and the gas molecules are hit by electrons from the electron gun (~ 1 keV of Ar^+ ions with a current density of ~ 2.5 μA), the gas molecules would be ionized, the Ar^+ ions would sputter the grounded substrate, and the impurities would be removed. However, the surface after the ion bombardment would be rough, and it would be hard to see a LEED pattern; therefore, the substrate needs to be annealed [20, 74]. The annealing can be performed, simply by connecting the substrate with tungsten wire and applying some current to the wire.

Electrochemistry in the ante-chamber

Electrochemistry can be done in the ante-chamber attached to the main chamber (Figure 1.2). The electrochemical cell container is attached to the ante-chamber with a gate valve and each solution is filled in the electrochemical cell and drained to the waste bottle after electrodeposition. All solutions were deaerated with ultrahigh purity (UHP) (99.998 %) Ar gas for at least 30 minutes prior to each experiment. Figure 1.4 shows the substrate holder and the electrochemical cell in the ante-chamber. In the electrochemical cell, there are a working electrode (the substrate), a Ag/AgCl reference electrode (3 M KCl, Bioanalytical System, Inc.), and a gold wire auxiliary electrode, connected to a potentiostat. Before immersing the substrate in a solution, the ante-chamber is back-filled with UHP Ar gas. After immersing, cyclic voltammograms (CV) are obtained by scanning potential with 5 mV/second scan rate. The coverage of adsorbate on the substrate can be obtained by calculating the ratio of [the charge (in μC) of the adsorbate by integrating UPD peak] to [the theoretical charge (in μC) of the adsorbate

to form a monolayer (ML)] [75]. By definition, one ML indicates one adsorbate for each surface atom [7]. After the electrodeposition, the substrate is emersed (withdrawn) from the solution. Upon emersion, the double-layer would lose electrical contact with the bulk electrolyte, but not with the electrode [74]. Thus, the overall charge within the interface must remain neutral. However, this requirement for neutrality would allow the occurrence of spontaneous faradaic reactions within the emersed layer. Such reactions can take place spontaneously provided that they do not result in charge imbalance within the layer, even if they are accompanied by loss of adsorbate [74]. If the solutions constantly flow through the cell, one solution can be exchanged with the next solution without losing potential control [7, 22]. Therefore, the flow cell system in the ante-chamber is currently under construction.

Then, the ante-chamber should be evacuated in order to transfer the substrate to the main chamber for surface analysis. Upon evacuation, there may be precipitates or salts formed on the surface if the solution concentration is too high, or possible surface perturbation or reconstruction may be occurred [74, 75]. To prevent the problems, the solution concentration should as low as ~ mM. After evacuating the ante-chamber, the substrate is transferred from the ante-chamber to the main chamber through a gate valve, without exposing to air, so there would be the least chance for the surface to be oxidized. The surface is then characterized by AES, LEED, and XPS (under construction).

Ultrahigh Vacuum Surface Analysis

The surface analysis requires UHV condition because the electrons ejected from an electron gun should reach at the surface without colliding with gas molecules [76, 77]. Also, UHV prevents the surface from being oxidized and contaminated. The following surface analysis techniques have been used in Stickney’s laboratory.

- Auger Electron Spectroscopy (AES): The surface to be analyzed is irradiated with a beam of electrons of sufficient energy, typically in the range of 2-10 keV, to ionize one or more core levels in surface atoms [5, 6, 74, 75, 77]. In Figure 1.5, after the ionization, the atom can be relaxed by either of the two processes, ejection of a characteristic X-ray photon (fluorescence) or ejection of an Auger electron. The resulting ejected Auger electron has a kinetic energy given by: $E_{kin}\ (KL_1L_{23}) = E_K - E_{L1} - E_{L23} - E_{inter}\ (L_1L_{23}) + E_R - \Phi_S$, where $E_{inter}\ (L_1L_{23})$ is the interaction energy between the holes in the L_1 and L_{23} shell, E_R is the sum of the intra-atomic and extra-atomic relaxation energies, and Φ_S is the work function term. Because no two elements have the same set of atomic binding energies, analysis of Auger energies provides elemental identification.
- Low-Energy Electron Diffraction (LEED): Figure 1.6 shows the schematic diagram of LEED [5, 6, 74, 75, 77]. The incident electron beam, accelerated by the potential V_0, is emitted from the electron gun behind the hemispherical fluorescent glass screen and hits the sample through a hole in the screen. The surface is at the center of the hemisphere so that all back-diffracted electrons travel towards the LEED screen on radial trajectories. Before the electrons hit the screen, they must pass a retarding field energy analyzer, which typically consists of four (or three) hemispherical grids concentric with the screen, each containing a central hole through which the electron gun is inserted. The first grid is connected to the earth ground, and it minimizes undesirable electrostatic deflection of diffracted electrons. The second and third (only second) grids is called suppressor grids, which enable a narrow energy range of elastically scattered electrons to be transmitted to the fluorescent screen. The fourth (third) grid is usually grounded to reduce field penetration of the suppressor grids by the screen voltage to make the diffraction spots visible. Because the fluorescent screen is transparent, the spots can

be observed through a viewport behind the screen without being shadowed by the sample holder. Only the electron gun assembly (diameter < 15 mm) obstructs the view slightly. The usual way of recording the LEED pattern is a light-sensitive digital camera.

- In-situ Electrochemical Scanning Tunneling Microscopy (EC-STM): STM is a fascinating technique for atomic scale surface morphologies. In STM, the probe is a sharp metal tip scanned across a conducting surface at distances of the order of typically 1 nm [6, 77]. A bias voltage of typically a few mV is applied between the tip and the sample leading to a tunneling current of the order of a few nA.

In the Stickney lab, in-situ EC-STM has been used for atomic scale surface morphologies [45-48]. In-situ EC-STM is the combination of electrochemistry and STM, and is opposed to ex-situ STM in air or vacuum. It is the technique in which the current that flows through a very small electrode tip near a conductive, semiconductive, or even a insulating substrate immersed in solution is used to characterized processes and structural features at the substrates as the tip is moved near the surface [78]. Figure 1.7 shows the schematic diagram of in-situ EC-STM. In EC-STM, the working electrode is mounted horizontally at the bottom of a small cell that contains auxiliary and reference electrodes. The scanning tip is held above the working electrode. The potentials of the working electrode (E_w) and the tip (E_t) are controlled independently with a potentiostat, where E_w is selected to produce the reaction of interest and E_t is adjusted to give the desired bias [78]. Because only the tunneling current is of interest in EC-STM, electrode reactions that occur at the tip are undesirable. Thus, in EC-STM, the tip is coated with glass or polymer, with only a very small area at the very bottom portion left exposed [78]. The actual exposed area can be estimated, if necessary, by using the tip as an ultramicroelectrode (UME), noting the magnitude of the limiting current in a known solution.

The tip potential is also chosen to be in a region where electrode reactions do not occur. The thickness of the electrolyte layer over the working electrode must be small, so that only the tip, and not the tip holder or a piezo, contacts the solution [78]. This arrangement makes it difficult to keep the electrolyte solution free of oxygen, unless the whole cell and STM head are kept in an inert atmosphere, such as with a glove bag.

The EC-STM tip interacts with the surface both by interatomic forces and by the tip's electrical field. Thus, the tip can affect the structure of the scanned area, especially at high tunneling currents [78]. This effect can sometimes be recognized after scanning over a given small region by decreasing the set tunneling current, increasing the x-y scan dimensions, and observing whether an image of a square perturbed region, where the earlier scanning took place, is visible [78].

An important limitation of EC-STM is that a quantitative correlation between the tunneling current and useful theoretical equations is not yet possible [78]. Thus, there is little real chemical and analytical information in the EC-STM scans, and one gains mechanistic and structural information mainly from the interpretation of images. However, one can obtain additional information by noting how the EC-STM behavior varies with the substrate potential versus a reference electrode or the tip bias between tip and substrate [78].

References

1. G. Cao, *Nanostructures & Nanomaterials*, Imperial College Press, London, 2004.
2. M. Ohring, *Materials Science of Thin Films*, Academic Press, San Diego, 2002.
3. N. Kanani, *Electroplating*, Elsevier, Oxford, 2004.
4. M.A. Herman, W. Richter, and H. Sitter, *Epitaxy*, Springer, Berlin, 2004.

5. G.A. Somorjai, *Chemistry in Two Dimensions: Surfaces*, Cornell University Press, Ithaca, 1981.

6. G.A. Somorjai, *Introduction to Surface Chemistry and Catalysis*, John Wiley & Sons, Inc., New York, 1994.

7. J.L. Stickney, in *Advances in Electrochemical Science and Engineering*, R.C. Alkire and D.M. Kolb (Eds.), pp. 1 ~ 105, Wiley-VCH, Weinheim, 2002.

8. D.M. Kolb, M. Przasnyski, and H. Gerischer, *J. Electroanal. Chem.*, **54**, 25 (1974).

9. J.L. Stickney, C.B. Ehlers, and B.W. Gregory, in *Electrochemical Surface Science*, M.P. Soriaga (Ed.), ACS Press, Washington, 1988.

10. J.L. Stickney, C.B. Ehlers, and B.W. Gregory, *Langmuir*, **4**, 1368 (1988).

11. C.B. Ehlers, I. Villegas, and J.L. Stickney, *J. Electroanal. Chem.*, **284**, 403 (1990).

12. L.P. Colletti, B.H. Flowers Jr., and J.L. Stickney, *J. Electrochem. Soc.*, **145**, 1442 (1998).

13. T.E. Lister and J.L. Stickney, *Appl. Surf. Sci.*, **107**, 153 (1996).

14. M.K. Mathe, S.M. Cox, B.H. Flowers, R. Vaidyanathan, L. Pham, N. Srisook, U. Happek, and J.L. Stickney, *J. Cryst. Growth*, **271**, 55 (2004).

15. B.W. Gregory and J.L. Stickney, *J. Electroanal. Chem.*, **300**, 543 (1991).

16. D.W. Suggs and J.L. Stickney, *Surf. Sci.*, **290**, 362 (1993).

17. D.W. Suggs and J.L. Stickney, *Surf. Sci.*, **290**, 375 (1993).

18. L.B. Goetting, B.M. Huang, T.E. Lister, and J.L. Stickney, *Electrochim. Acta*, **40**, 143 (1995).

19. H.M. Baoming, T.E. Lister, and J.L. Stickney, in *Handbook of Surface Imaging and Visualization*, A.T. Hubbard (Ed.), CRC Press, Boca Raton, 1995.

20. K. Varazo, M.D. Lay, T.A. Sorenson, and J.L. Stickney, *J. Electroanal. Chem.*, **522**, 104 (2002).

21. B.H. Flowers Jr., T.L. Wade, J.W. Garvey, M. Lay, U. Happek, and J.L. Stickney, *J. Electroanal. Chem.*, **524-525**, 273 (2002).

22. J.L. Stickney, in *Electroanalytical Chemistry*, A.J. Bard and I. Rubinstein (Eds.), Marcel Dekker, New York, 1999.

23. M.K. Mathe, S.M. Cox, V. Venkatasamy, U. Happek, and J.L. Stickney, *J. Electrochem. Soc.*, **152**, C751 (2005).

24. V. Venkatasamy, M.K. Mathe, S.M. Cox, U. Happek, and J.L. Stickney, *Electrochem. Acta*, **51**, 4347 (2005).

25. V. Venkatasamy, N. Jayaraju, S.M. Cox, C. Thambidurai, M.K. Mathe, and J.L. Stickney, *J. Electroanal. Chem.*, **589**, 195 (2006).

26. V. Venkatasamy, N. Jayaraju, S.M. Cox, C. Thambidurai, and J.L. Stickney, *J. Electrochem. Soc*, **154**, H720 (2007).

27. R. Vaidyanathan, J.L. Stickney, and U. Happek, *Electrochim. Acta*, **49**, 1321 (2004).

28. R. Vaidyanathan, S.M. Cox, U. Happek, D. Banga, M.K. Mathe, and J.L. Stickney, *Langmuir*, **22**, 10590 (2006).

29. I. Villegas and J.L. Stickney, *J. Electrochem. Soc.*, **139**, 686 (1992).

30. I. Villegas and J.L. Stickney, *J. Vac. Sci. Technol. A*, **10**, 3032 (1992).

31. T.L. Wade, L.C. Ward, C.B. Maddox, U. Happek, and J.L. Stickney, *Electrochem. Solid State Lett.*, **2**, 616 (1999).

32. T.L. Wade, R. Vaidyanathan, U. Happek, and J.L. Stickney, *J. Electroanal. Chem.*, **500**, 322 (2001).

33. U. Demir and C. Shannon, *Langmuir*, **10**, 2794 (1994).

34. J. Yang, W. Zhu, X. Gao, S. Bao, and X. Fan, *J. Electroanal. Chem.*, **577**, 117 (2005).

35. J.Y. Yang, W. Zhu, X.H. Gao, S.Q. Bao, X.A. Fan, X.K. Duan, and J. Hou, *J. Phys. Chem. B*, **110**, 4599 (2006).

36. J.Y. Yang, W. Zhu, X.H. Gao, X.A. Fan, S.Q. Bao, and X.K. Duan, *Electrochim. Acta*, **52**, 3035 (2007).

37. G. Pezzatini, S. Caporali, M. Innocenti, and M.L. Foresti, *J. Electroanal. Chem.*, **475**, 164 (1999).

38. M. Innocenti, F. Forni, G. Pezzatini, R. Raiteri, F. Loglio, and M.L. Foresti, *J. Electroanal. Chem.*, **514**, 75 (2001).

39. M. Innocenti, G. Pezzatini, F. Forni, and M.L. Foresti, *J. Electrochem. Soc.*, **148**, C357 (2001).

40. D.M. Kolb, in *Advances in Electrochemistry and Electrochemical Engineering*, H. Gerischer and C.W. Tobias (Eds.), Wiley-Interscience, New York, 1978.

41. K. Sieradzki, S.R. Brankovic, and N. Dimitrov, *Science*, **284**, 138 (1999).

42. S.R. Brankovic, J.X. Wang, and R.R. Adzic, *Surf. Sci.*, **474**, L173 (2001).

43. M.F. Mrozek, Y. Xie, and M.J. Weaver, *Anal. Chem.*, **73**, 5953 (2001).

44. J.Y. Kim, Y.-G. Kim, and J.L. Stickney, *Electrochem. Soc. Trans.*, **1**, 41 (2006).

45. Y.-G. Kim, J.Y. Kim, D. Vairavapandian, and J.L. Stickney, *J. Phys. Chem. B*, **110**, 17998 (2006).

46. Y.-G. Kim, J.Y. Kim, C. Thambidurai, and J.L. Stickney, *Langmuir*, **23**, 2539 (2007).

47. J.Y. Kim, Y.-G. Kim, and J.L. Stickney, *J. Electrochem. Soc.*, **154**, D260 (2007).

48. J.Y. Kim, Y.-G. Kim, and J.L. Stickney, *J. Electroanal. Chem.*, in press (2008).

49. P.D. Angnello, *IBM J. Res. Dev.*, **46**, 317 (2002).

50. T. Ohno, *Surf. Sci.*, **255**, 229 (1991).

51. P. Moriarty, B. Murphy, and G. Hughes, *J. Vac. Sci. Technol. A*, **11**, 1099 (1993).

52. M.D. Pashley and D. Li, *J. Vac. Sci. Technol. A*, **12**, 1848 (1994).

53. H. Xia, W.N. Lennard, G.R. Massoumi, J.J.J. van Eck, L.J. Huang, W.M. Lau, and D. Landheer, *Surf. Sci.*, **324**, 159 (1995).

54. Y. Ke, S. Milano, X.W. Wang, N. Tao, and Y. Darici, *Surf. Sci.*, **415**, 29 (1998).

55. D.R.T. Zahn, T.U. Kampen, S. Hohenecker, and W. Braun, *Vacuum*, **57**, 139 (2000).

56. Y. Gobil, J. Cibert, K. Saminadayar, and S. Tatarenko, *Surf. Sci.*, **211**, 969 (1989).

57. W. Faschinger, P. Juza, and H. Sitter, *J. Cryst. Growth*, **115**, 692 (1991).

58. V.H. Etgens, R. Pinchaux, M. Sauvage-Simkin, J. Massies, N. Jedrecy, N. Greiser, and S. Tatarenko, *Surf. Sci.*, **251**, 478 (1991).

59. A. Bourret, P. Fuoss, G. Feuillet, and S. Tatarenko, *Phys. Rev. Lett.*, **70**, 311 (1993).

60. D.W. Tu and A. Kahn, *J. Vac. Sci. Tech. A*, **2**, 511 (1984).

61. D.W. Tu and A. Kahn, *J. Vac. Sci. Technol. A*, **3**, 922 (1985).

62. S. Hohenecker, T.U. Kampen, T. Werninghaus, D.R.T. Zahn, and W. Braun, *Appl. Surf. Sci.*, **142**, 28 (1999).

63. S. Hohenecker, T.U. Kampen, W. Braun, and D.R.T. Zahn, *Surf. Sci.*, **435**, 347 (1999).

64. L. Beaunier, H. Cachet, M. Froment, and G. Maurin, *J. Electrochem. Soc.*, **147**, 1835 (2000).

65. H. Cachet, R. Cortes, M. Froment, and A. Etcheberry, *Thin Solid Films*, **361-362**, 84 (2000).

66. L. Beaunier, H. Cachet, R. Cortes, M. Froment, and A. Etcheberry, *Thin Solid Films*, **387**, 108 (2001).

67. A. Etcheberry, H. Cachet, R. Cortes, and M. Froment, *Surf. Sci.*, **482**, 954 (2001).

68. P. Allongue and E. Souteyrand, *J. Vac. Sci. Tech. B*, **5**, 1644 (1987).

69. P. Allongue and E. Souteyrand, *J. Electroanal. Chem.*, **286**, 217 (1990).

70. P. Allongue and E. Souteyrand, *J. Electroanal. Chem.*, **362**, 79 (1993).

71. P. Allongue, E. Souteyrand, and L. Allemand, *J. Electroanal. Chem.*, **362**, 89 (1993).

72. J.Y. Kim and J.L. Stickney, *J. Phys. Chem. C,* **112**, 5966 (2008).

73. M.D. Lay and J.L. Stickney, *J. Am. Chem. Soc.*, **125**, 1352 (2003).

74. M.P. Soriaga and J.L. Stickney, in *Modern Techniques in Electroanalysis*, P. Vanysek (Ed.), Chemical Analysis Series, 1996.

75. M.P. Soriaga, *Prog. Surf. Sci.*, **39**, 325 (1992).

76. J.H. Moore, C.C. Davis, and M.A. Coplan, *Building Scientific Apparatus: A practical guide to design and construction*, Addision-Wesley Publishing Co., London, 1983.

77. H. Bubert and H. Jenett, *Surface and Thin Film Analysis*, Wiley-VCH, Weinheim, 2002.

78. A.J. Bard and L.R. Faulkner, *Electrochemical Methods Fundamental and Applications*, John Wiley & Sons, Inc., Weinheim, 2001; D. Wang and L.-J. Wan, *J. Phys. Chem. C*, **111**, 16109 (2007).

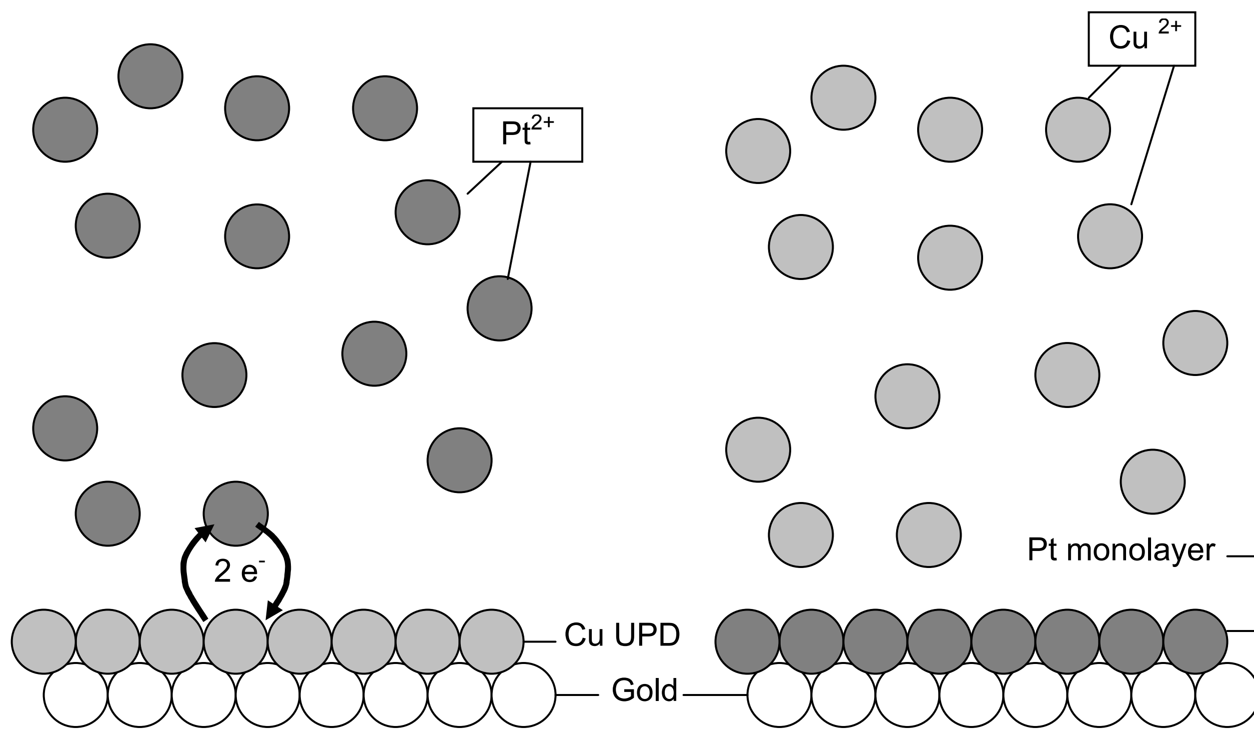

Figure 1.1 The cartoon of Pt surface-limited redox replacement with a Cu sacrificial layer.

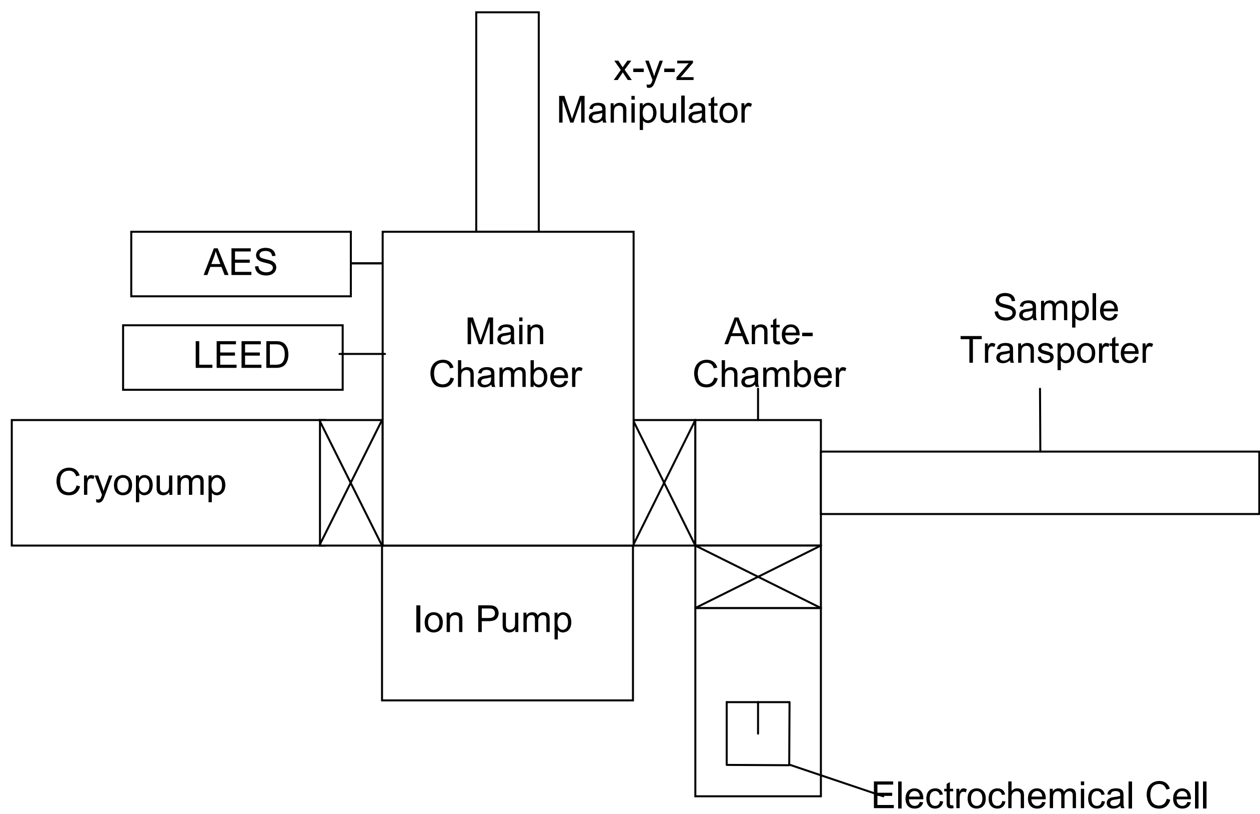

Figure 1.2 The schematic diagram of Stickney ultrahigh vacuum chamber.

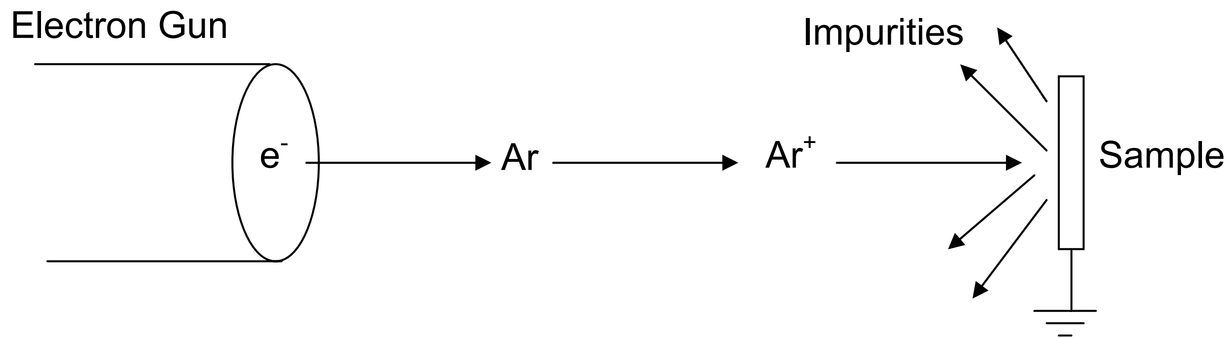

Figure 1.3 The schematic diagram of Ar^+ ion bombardment.

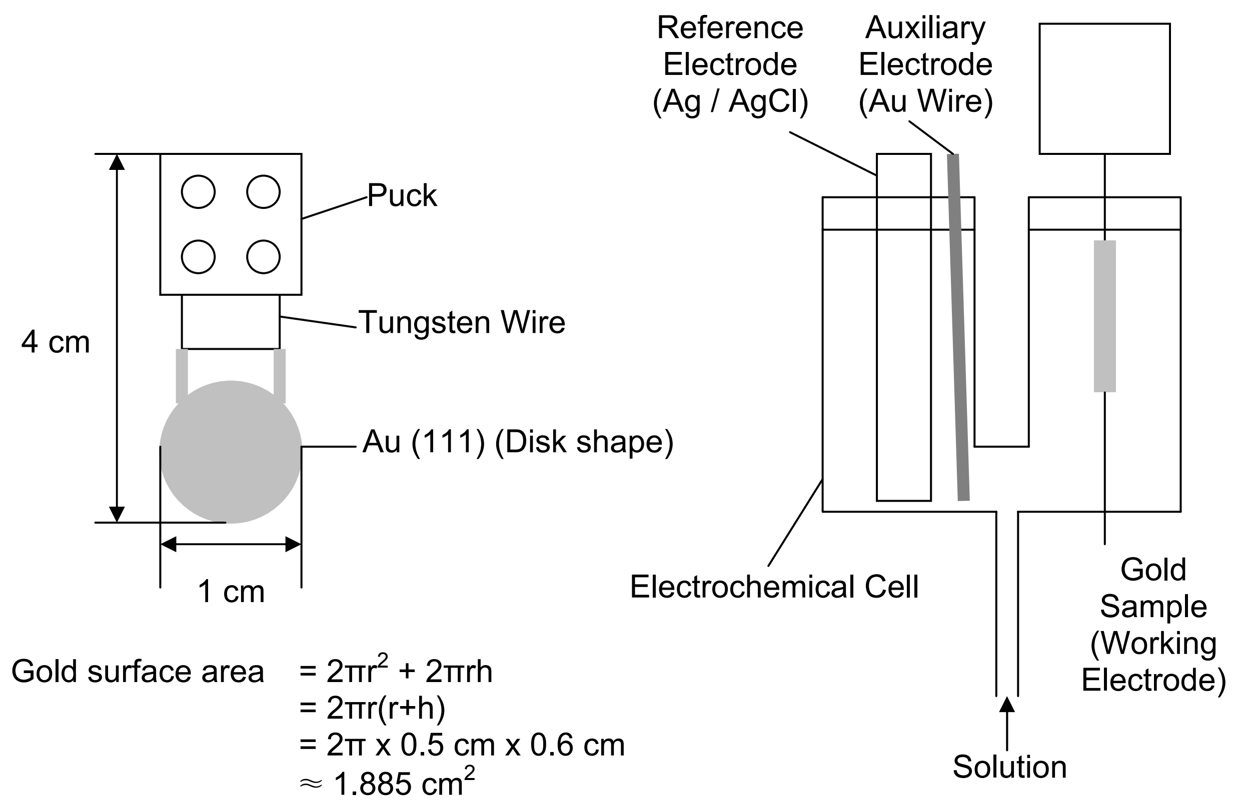

Figure 1.4 The schematic diagram of Au(111) substrate holder and the electrochemical cell.

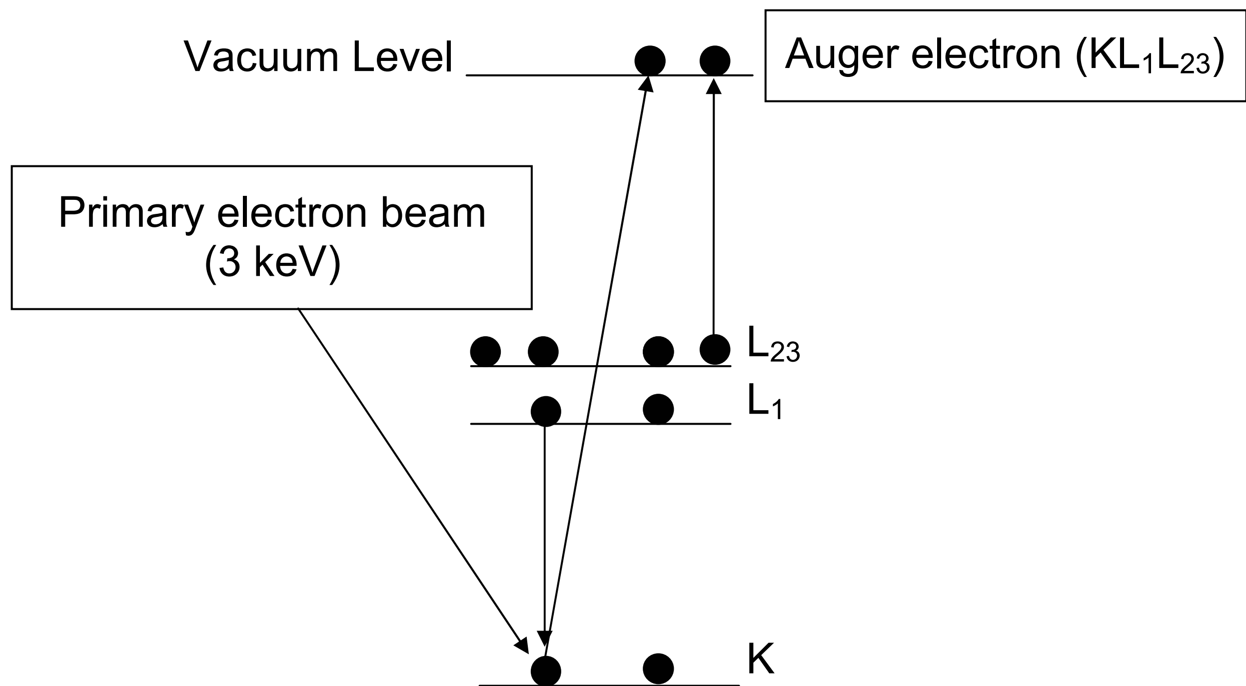

Figure 1.5 The schematic diagram of Auger process.

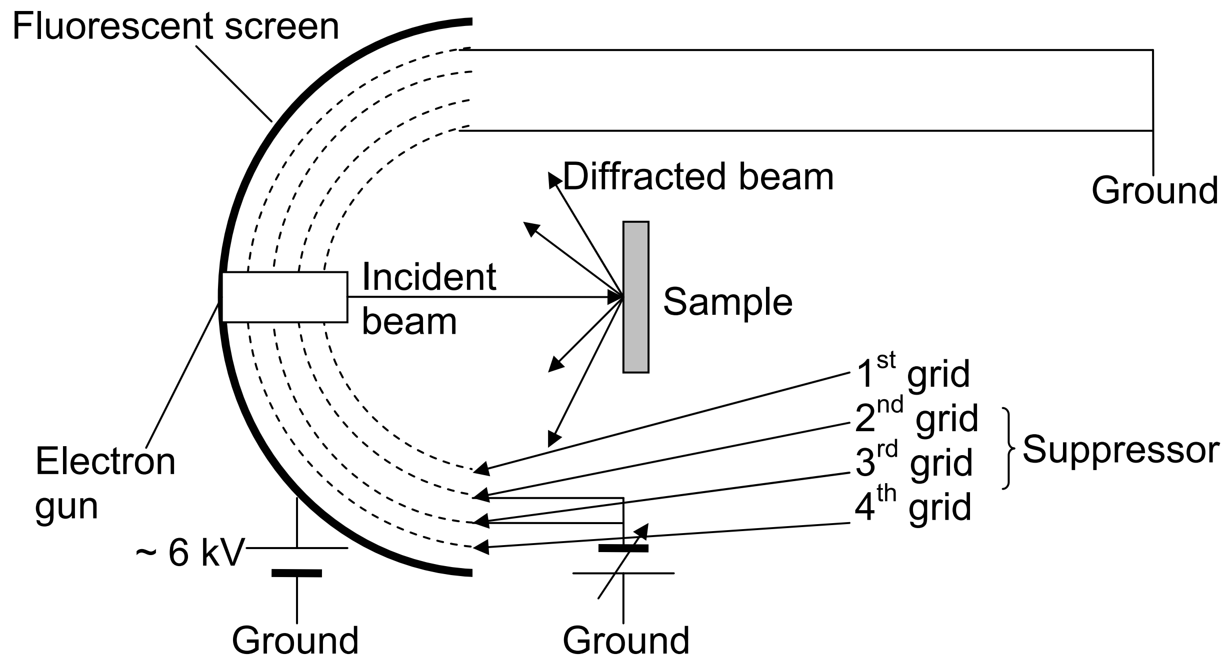

Figure 1.6 The schematic diagram of low-energy electron diffraction (LEED).

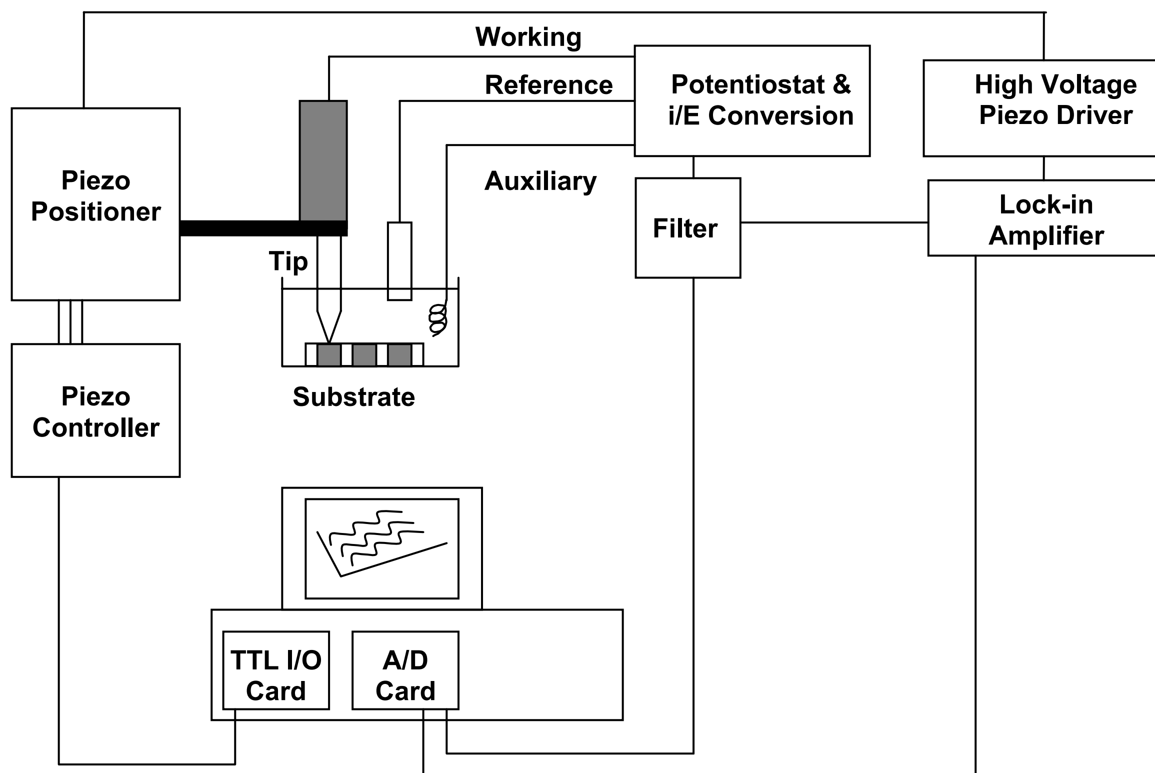

Figure 1.7 The schematic diagram of in-situ EC-STM.

CHAPTER 2

STUDIES OF CU ATOMIC LAYER REPLACEMENT, FORMED BY UNDERPOTENTIAL DEPOSITS, TO FORM PT NANOFILMS USING ELECTROCHEMICAL ATMOIC LAYER EPITAXY (EC-ALE)[1]

[1] J.Y. Kim, Y.-G. Kim, and J.L. Stickney, *Electrochemical Society Transaction*, **1**, 41-48 (2006). Reprinted here with permission of publisher.

Abstract

In this paper, the development of a surface limited redox replacement reaction (SLR^3) for the deposition of Pt is discussed. In the present study, a Au(111) substrate was cleaned using Ar ion bombardment to form a well ordered (1×1) LEED pattern, after annealing. This surface was then transferred from the UHV surface analysis chamber to an antechamber containing an electrochemical cell. A monolayer of Cu was deposited on the Au substrate from a $CuSO_4$ solution, at an underpotential. The Au substrate, with Cu UPD, was then immersed in a Pt(IV) solution at open circuit, spontaneously replacing the Cu UPD with Pt. The resulting Pt atomic layer coated Au substrate was then transferred back to the analysis chamber, and the surface characterized using LEED and Auger electron spectroscopy (AES). This paper describes the first attempt by this group to grow Pt films by metal EC-ALE.

Introduction

The growth of 2D metal nanofilms electrochemically is an important and difficult area. The majority of electrodeposited metal films follow a nucleation and growth mechanism, resulting in surface roughening. Recently, there has been progress in the development of methodologies for promotion of 2D growth. Sieradzki and co-workers have developed an electrochemical technique using surfactant metals to significantly enhance the ambient temperature nucleation of 2D islands, which he called defect-mediated growth (DMG) [1]. The mediator was periodically deposited and stripped from the surface by appropriate cycling of the electrochemical potential. A monolayer was completed as the growing 2D clusters eventually merged. Adzic and co-workers proposed that a UPD adlayer can be replaced by a nobler metal cation in what they refer to as a surface limited redox replacement reaction (SLR^3), and examples

were performed by replacing Cu UPD with Pt, Pd or Ag [2]. This reaction can be described by equation (2.1):

$$M^0_{UPD} + (m/z)\, P^{z+} \rightarrow M^{m+} + (m/z)\, P^0 \qquad (2.1)$$

where M^0_{UPD} represents a UPD metal adatom on the electrode surface and P^{z+} is a noble metal cation with positive charge z+. They reported that this novel procedure produces a nearly-uniform Pd monolayer on Au(111) by the spontaneous redox replacement of a previously prepared Cu UPD layer by a Pd(II) solute, and confirmed by scanning tunneling microscope (STM) [2]. However, in the case of Cu replacement by Pt(IV), a Pt atomic layer with half the coverage of the original Cu UPD layer should be formed, given the stoichiometry: $2Cu^0 + Pt^{4+} \rightarrow 2Cu^{2+} + Pt^0$. Weaver and co-workers reported the preparation of Pt-group metal films on roughened gold electrodes by utilizing spontaneous redox replacement of a Cu UPD layer by a Pt-group metal cation solute. The resulting films displayed surface-enhanced Raman scattering (SERS) for adsorbates bound to the overlayer and free from substrate interferences [3]. Dimitrov et al. recently published deposition of 25 cycles of Ag deposition, using Pb UPD as a sacrificial layer, which they referred to as "monolayer restricted galvanic displacement" [4].

In the present study iodine atomic layers were used to improve surface mobility of deposited Pt atoms. In previous studies by Adzic [2], Pt atoms deposited using the SLR[3] resulted in a surface composed of nanoclusters. The intent here is to promote electrochemical annealing, where the surface atoms increase in mobility by complexing with the halide atoms, and using potentials close to the oxidation potential.

Experimental

Figure 2.1 shows a schematic diagram of the ultrahigh vacuum (UHV) system used for these studies with the attached electrochemical ante-chamber where the UHV-EC studies were performed [5]. The cryopump and ion pump are attached to the main chamber, as indicated in Figure 1, resulting in a base pressure of ~ 10^{-9} Torr. Sorption pumping was used for roughing. Ar ion bombardment was used to clean the Au(111) substrate, and a tungsten wire, used to mount the crystal, was also used for annealing the sample, by passing a current. Electrochemical experiments were performed in the antechamber attached to the main chamber via a gate valve, and solutions were passed to the electrochemical cell and drained to the waste bottle through Teflon tubes. The electrochemical cell contained a reference electrode (Ag/AgCl) and an auxiliary electrode (gold wire), and was controlled by an in house designed potentiostat. Deposits were transferred to and from the analysis chamber without exposure to air, where they were characterized by AES (Perkin-Elmer) and LEED (Princeton Research Instruments, Inc.).

Prior to insertion into the UHV-EC chamber, the Au substrate was immersed in hot concentrated nitric acid for about 30 minutes and then annealed in a hydrogen flame for about 10 minutes [6]. The Au substrate was then cleaned by Ar^+ ion bombardment, in UHV, prior to each electrochemical experiment [7]. Ion bombardment was performed by first filling the chamber, with the pumps off, to 10^{-5} Torr with ultrahigh pure Ar. Ar atoms were then ionized by electron bombardment, and accelerated towards the crystal with an energy of 200 eV. The Ar ions sputtered the Au substrate, removing the last traces of impurities. However, the surface during ion bombardment became roughened, requiring annealing at ~350 ºC, before the clean surface LEED pattern was resolved [7].

A solution of 1 mM $CuSO_4$ and 0.05 M H_2SO_4 was prepared with anhydrous $CuSO_4$ (Aldrich Co.) and concentrated H_2SO_4 (Aldrich Co.) in 18 MΩ-cm distilled water. After cleaning the Au substrate by the method described above, confirming surface cleanliness and order via AES and LEED, the sample was transferred to the ante-chamber. The Au substrate was then modified with an atomic layer of I atoms by exposure to a solution of 0.1 mM KI, and then rinsed in blank solution (1 mM $HClO_4$ solution). The electrochemical cell was then rinsed twice with the Cu solution, and the Au substrate was immersed in the Cu solution at the open circuit. The potential was then scanned negatively from the open circuit potential (OCP) to just after the second Cu UPD peak (Figure 2.2), where the potential was held, while the sample was emersed (withdrawn) from solution. The resulting I modified Au substrate, with Cu UPD, was then transferred to the analysis chamber.

From cyclic voltammetry, the presence of Cu UPD was evident at 0.05 V, which was confirmed with AES and LEED. The resulting deposit was then transferred back, and immersed in the Pt(IV) solution for two minutes at open circuit, where a final OCP of 0.75 V was observed. The Pt(IV) solution was prepared with H_2PtCl_6 (Fisher Scientific Co.) and $HClO_4$ (Aldrich Co.) in 18 MΩ-cm distilled water.

Result and discussion

Cyclic Voltammetry

In Figure 2.2a, the solid line shows the Cu CV on bare Au(111) and the dashed line shows the Cu CV on an I modified Au(111). The shapes of the Cu CVs on bare Au and I modified Au agreed well with the previous literature [8-10]. The first Cu UPD peak on bare Au was at 0.22 V, while the main UPD peak on the I modified Au was at 0.15 V, suggesting that it

was slightly harder to deposit Cu on I modified Au. The 2nd Cu UPD peaks on bare Au and on I modified Au were evident at 0.08 V and 0.05 V, respectively. The calculated charges for the 1st Cu UPD on bare Au and on I modified Au were 0.67 ML and 0.85 ML, respectively. As seen in figure 2.2b, the LEED pattern observed after the 1st Cu UPD peak on the I modified Au, at 0.2 V, was a (√3×√3)R30°-I, while the pattern shown in Figure 2.2c was observed after scanning to 0.05 V, and suggests a (3×3).

Figure 2.3 shows two CVs in the blank solution after four Pt replacement cycles with the I atom layer present. The solid line is the first CV cycle, and the dashed line the second. The CV was started negatively from 0.5 V, and the direction reversed at −0.3 V. It was then scanned to 1.4 V, and reversed again, stopping at 0 V. The inset is the CV of clean and annealed Au(111). At negative potentials, there is little evidence of the hydrogen waves, as expected, given the presence of the I atom layer which blocks hydrogen adsorption. However, the reversibility of the hydrogen reduction oxidation reactions is evident from the oxidation peak at −0.25 V indicating the presences of Pt on the surface. The oxidation peak (a) results from the oxidation of adsorbed I as indicated in Equation (2.2) [11]:

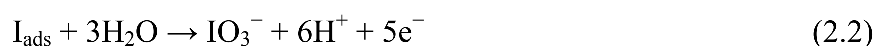

$$I_{ads} + 3H_2O \rightarrow IO_3^- + 6H^+ + 5e^- \qquad (2.2)$$

In addition, peak (a) contains charge for the oxidation of both Pt and Au surface atoms. The reduction peaks (b) and (c) were for reduction of Au and Pt surface oxides, respectively. Pt coverage might be estimated from the relative sizes of the Pt and Au oxide reduction features, as was done by Weaver et al [3]. However, electrochemical oxidation of Pt and Au is known to disrupt nanoscale structure, possibly resulting in mixing of the surface atoms, place exchange. Coulometric measurement of the Pt coverage by stripping is not an option, given that the surface forms the passive oxide layer, rather than a soluble Pt species. In the second cycle, the dashed

curve, some charge for hydrogen adsorption is evident, the hydrogen waves, after the oxidative removal of the adsorbed I atom layer. Quantification of hydrogen adsorption should also provide a measure of the Pt surface atom coverage, as the hydrogen waves are generally felt to be the adsorption of protons: one H atom for every Pt surface atom [3]. However, as the electrode was first oxidized, the resulting surface structure and coverage are questionable. Future studies will involve an initial reduction step to remove the adsorbed halide layer, prior to use of cyclic voltammetry to study the hydrogen waves, and determine the Pt surface coverage.

Auger Electron Spectroscopy (AES)

Figure 2.4 shows AES spectra for (a) the clean Au(111), (b) after two cycles of Pt replacement, and (c) four cycles of Pt replacement. The peak height of the principle Au Auger peak (~ 69 eV) decreased as the replacement cycle increased, while the peak height of the satellite Au Auger peak (~ 240 eV) remained almost the same regardless of the replacement cycles. The lower energy Auger electrons are more easily scattered by the deposit, than the higher energy electrons. The absence of a Cu Auger signal (~ 930 eV) in 2.4b and 2.4c and the fact that the OCP during the Pt replacement shifted from 0.05 V to 0.75 V, suggested that Cu was completely replaced by Pt. The doublet I Auger peak (~ 510 eV) shows that the deposits are underneath the I adlayer, as the number of cycles performed does not effect its intensity. The similarity of the Au Auger peak (~ 69 eV) and the Pt Auger peak (~ 67 eV) made it impossible to differentiate the signals for Pt and Au, and thus to quantify the increasing Pt coverage.

Low-Energy Electron Diffractions (LEEDs)

Figure 2.5 shows LEED patterns: (a) for the clean Au(111), (b) the I modified Au, and (c) after two Pt replacement cycle. The beam energies of (a), (b) and (c) LEED patterns were 52 eV, 48 eV and 52 eV, respectively. The LEED pattern corresponding to the clean and well-

ordered Au is a (1×1), prior to an electrochemical experiment. After adsorption of a I atom layer, the sharp ($\sqrt{3}\times\sqrt{3}$)R30°-I LEED pattern was evident (Figure 2.5b). ($\sqrt{7}\times\sqrt{7}$)R19.1° or (3×3) LEED patterns are expected for Pt in the presence of an I atom layer, according to the literature [11]. However, a diffuse ($\sqrt{3}\times\sqrt{3}$)R30°-I LEED pattern was observed after two Pt replacement cycles, for a Pt coverage of 0.8 ML. The LEED pattern after four Pt replacements on Au showed a diffuse (1×1), not shown. The diffused LEED patterns after the Pt replacement cycles on Au may be the result of the formation of a surface Pt-Au alloy, which will be discussed in a subsequent paper. Clearly, more LEED studies of these deposits are required.

STM studies, by this group, resulted in distinct images of the surfaces help in understanding much of the result presented here, and will be published [12]. After one and two Pt replacements on I modified Au(111), high resolution STM images suggested the presences of disordered hexagonal shaped nano islands, and the five atom cluster and chains after various numbers of cycles.

Conclusion

Surface limited redox replacement reactions (SLR^3) of Pt for Cu UPD were studied using UHV-EC methodologies. The possibility of Pt layer-by-layer growth was investigated. The Au substrate was cleaned by Ar ion bombardment and annealed. The Au substrate was then modified with an I atom layer, and Cu UPD was formed. This surface was then exposed to a Pt(IV) solution at the open circuit, where the Cu UPD was exchanged for Pt over two minutes. The OCP during the Pt replacement shifted from 0.05 V to 0.75 V.

CV in the blank solution after four Pt replacements on Au showed the oxidation of adsorbed I, and the formation of Au and Pt oxides. On the subsequent negative going scan,

separate peaks for reduction of Au and Pt oxides were observed. After removal of the I atom layer by oxidation, hydrogen waves were also observed. Estimation of the Pt coverage, from the Pt reduction peak in the CV suggests that about 0.35 ML of Pt were deposited each cycle; however, this was just a preliminary study, and 0.35 is a crude approximation. Studies to better characterize these amounts are underway. The intensity of the I Auger peak suggested that I remained on top of the deposited Pt. While the LEED pattern of the I modified Au showed a $(\sqrt{3}\times\sqrt{3})R30°$-I, the LEED patterns after two and four Pt replacement cycles showed diffuse $(\sqrt{3}\times\sqrt{3})R30°$ and (1×1) patterns, respectively.

Acknowledgements

The support from Nation Science Foundation, Divisions of Materials and Chemistry, and the Department of Energy is gratefully acknowledged.

References

1. K. Sieradzki, S. R. Brankovic, and N. Dimitrov, *Science*, **284**, 138 (1999).
2. S. R. Brankovic, J. X. Wang, and R. R. Adzic, *Surf. Sci.*, **474**, L173 (2001).
3. M. F. Mrozek, Y. Xie, and M. J. Weaver, *Anal. Chem.*, **73**, 5953 (2001).
4. R. Vasilic and N. Dimitrov, *Electrochem. Solid-State Lett.*, **8**, C173 (2005).
5. M. P. Soriaga and J. L. Stickney, *Modern Techniques in Electroanalytical Chemistry*, p. 1~58, Wiley & Sons, New York (1996).
6. M. D. Lay and J. L. Stickney, *J. Am. Chem. Soc.*, **125**, 1352 (2003).
7. K. Varazo, M. D. Lay, T. A. Sorenson, and J. L. Stickney, *J. Electroanal. Chem.*, **522**, 104 (2002).

8. M. F. Toney, J. N. Howard, J. Richer, G. L. Borges, J. G. Gordon, O. R. Melroy, D. Yee, and L. B. Sorensen, *Phys. Rev. Lett.*, **75**, 4472 (1995).

9. A. Martinez-Ruiz, J. Valenzuela-Benavides, L. Morales de la Garza, and N. Batina, *Surf. Sci.*, **476**, 139 (2001).

10. A. Martinez-Ruiz, M. Palomar-Pardave, J. Valenzuela-Benavides, M. H. Farias, and N. Batina, *J. Phys. Chem. B*, **107**, 11660 (2003).

11. J. L. Stickney, S. D. Rosasco, and A. T. Hubbard, *J. Electrochem. Soc.*, **131**, 260 (1984).

12. Y. -G. Kim, J. Y. Kim, and J. L. Stickney, *manuscript in preparation*.

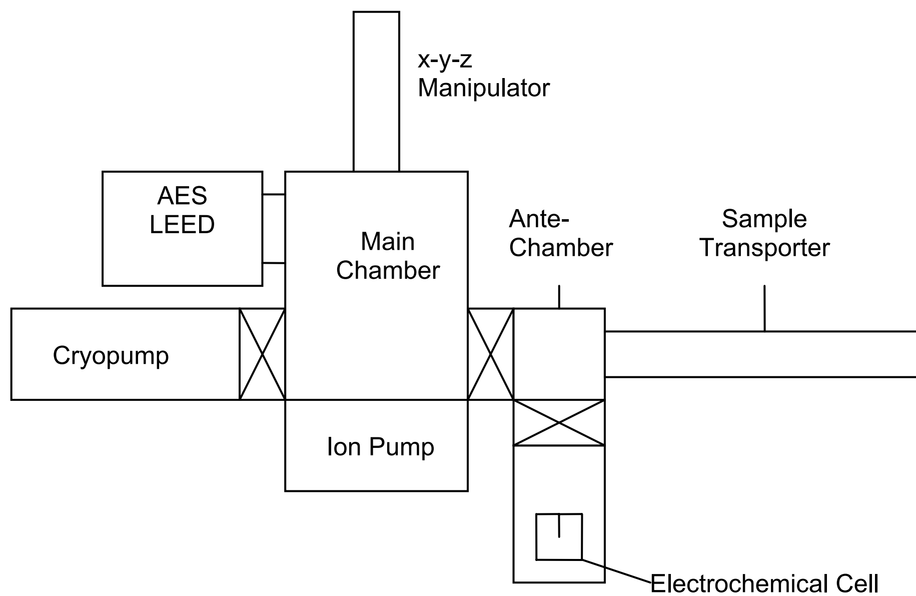

Figure 2.1 The Schematic diagram of UHV-EC system.

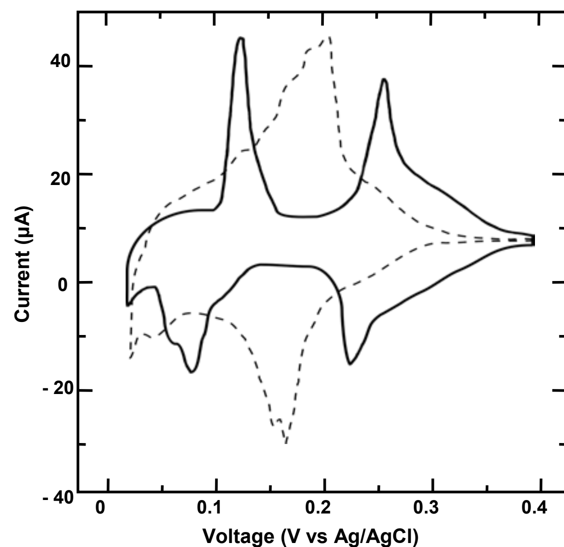

(a)

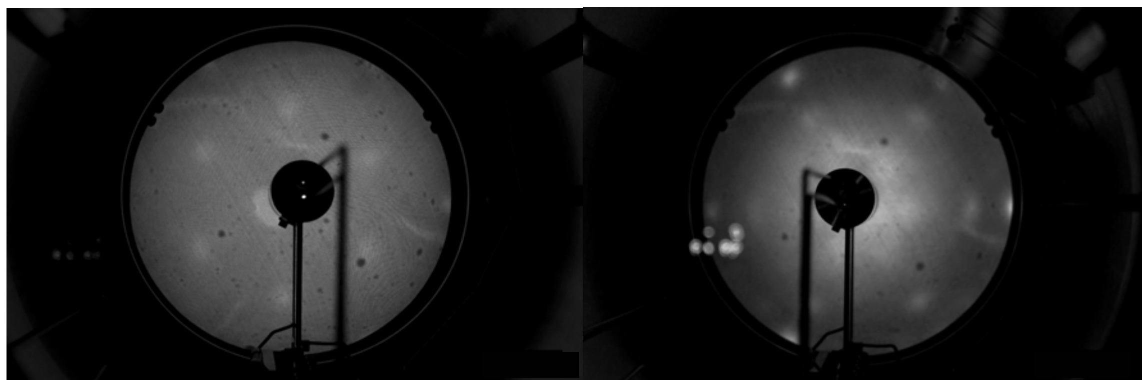

(b) (c)

Figure 2.2 (a) CVs of Cu on bare Au(111) (solid line) and Cu on I modified Au(111) (dashed line), (b) LEED pattern of 1st Cu UPD on I modified Au and (c) LEED pattern of Cu UPD at 0.05 V on I modified Au. Beam energies were 42 eV for (b) and 45 eV for (c).

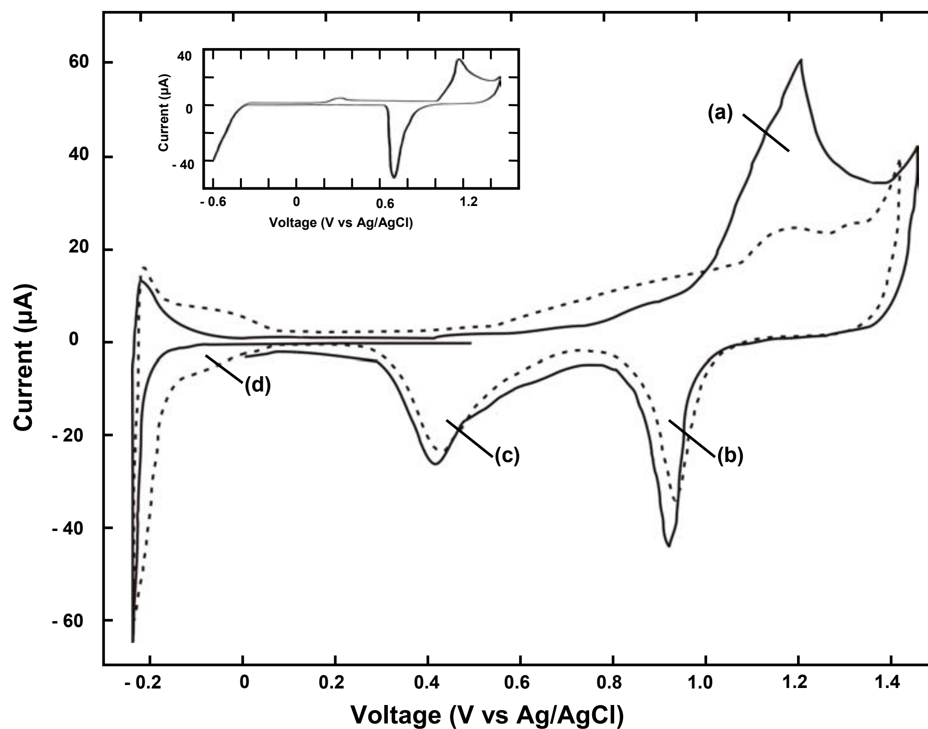

Figure 2.3 1st CV cycle (solid line) and 2nd CV cycle (dashed line) after four Cu UPD replacements by Pt on Au (111). The CV was performed in the blank solution. (a) oxidation of adsorbed I on Pt, (b) Au reduction from Au oxide, (c) Pt reduction from Pt oxide, and (d) hydrogen waves (Inset : the CV of clean and annealed Au(111)).

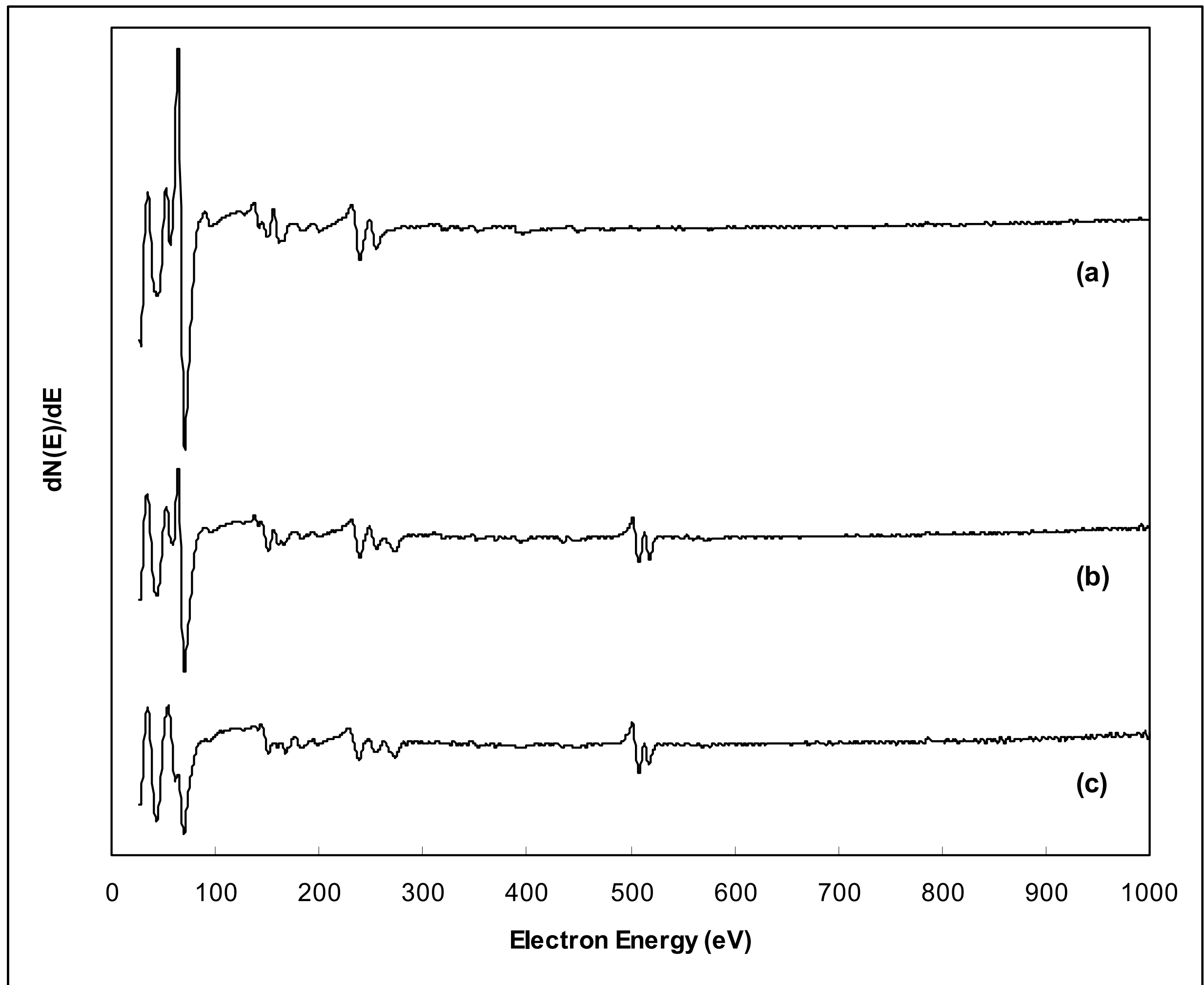

Figure 2.4 Auger electron spectroscopies of (a) clean Au (111), (b) two cycles of Pt replacements, and (c) four cycles of Pt replacements.

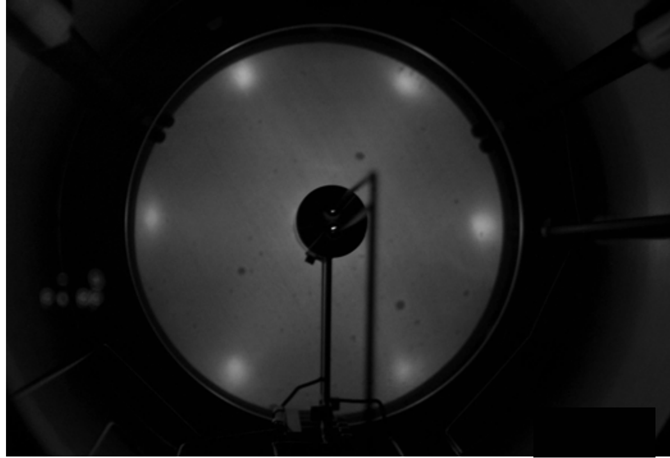

(a)

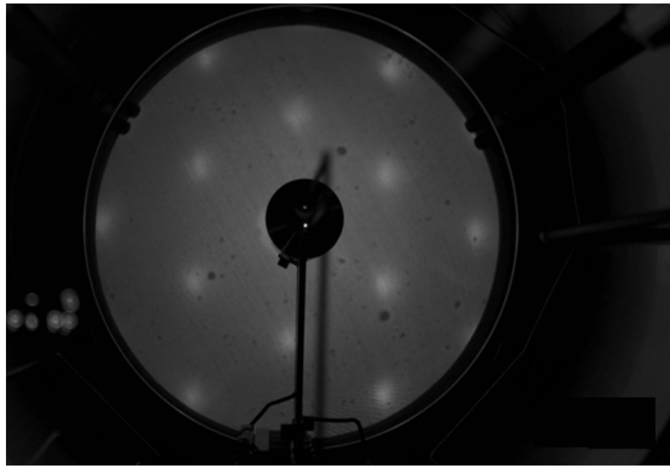

(b)

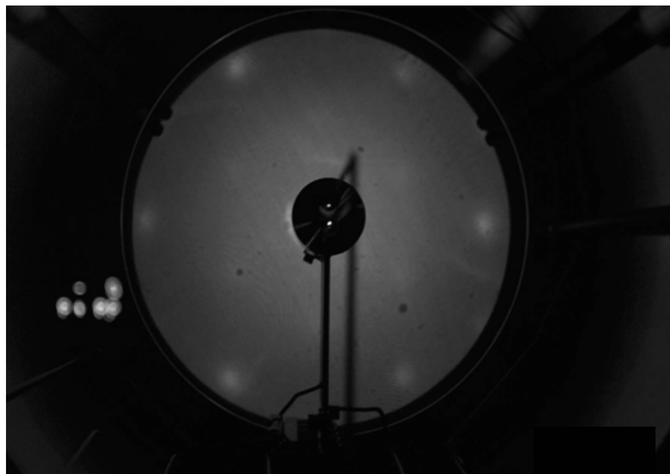

(c)

Figure 2.5 LEED patterns of (a) clean Au (111) (beam energy: 52 eV), (b) I modified Au (111) (beam energy : 48 eV), and (c) two replacements Pt on Au (111) (beam energy : 52 eV).

CHAPTER 3

COPPER NANOFILM FORMATION BY ELECTROCHEMICAL ATOMIC LAYER DEPOSITION (ALD) : UHV-EC AND IN-SITU STM STUDIES[2]

[2] J.Y. Kim, Y.-G. Kim, and J.L. Stickney, *J. Electrochem. Soc.*, **154**, D260-D266 (2007). Reprinted here with permission of publisher.

Abstract

Au(111) single crystal substrates were used in studies of Cu nanofilm formation by electrochemical ALD. Cu UPD was used to deposit the first Cu atomic layer on a Au(111) substrate, modified with an atomic layer of I atoms. By definition, Cu UPD results in the formation of an atomic layer, thus, to deposit subsequent Cu, surface-limited redox replacement (SLRR) was used. The SLRR involved initial formation of Pb UPD on the Cu coated surface just described. This Pb UPD coated surface was then exposed to $CuSO_4$ at OCP, where the Pb atoms were exchanged for Cu. In the UHV-EC studies presented here, two Pb UPD potentials were investigated: −0.400 V and −0.440 V. UHV-EC studies involved use of a surface analysis instrument with optics for LEED and Auger, and to which was attached an ante-chamber containing a Pyrex glass electrochemical H-cell. In this way, surface analysis was performed without transfer of the deposit through air and the contamination which would result. In addition, studies of the first few cycles of redox replacement were investigated using electrochemical in-situ scanning tunneling microscopy (STM), with a flow cell for solution exchange to prevent loss of potential control.

Introduction

In general, the electrochemical formation of metals occurs by nucleation and growth, resulting in surface roughening [1], which increases as the deposit grows, similar to most vapor deposition processes [2]. Development of 2D growth methodologies for nanofilm formation is an important task, given that 2D growth modes should result in lower roughness, control of deposit thickness, and increased crystallinity, as well as promoting epitaxy. The areas of atomic layer epitaxy (ALE) and atomic layer deposition (ALD) are known to promote 2D growth, and

are based on the use of surface limited reactions. By application of surface-limited reactions in a cycle, layer-by-layer growth of nanofilms results. The focus of this group has been the application of ALD methodologies to the formation of semiconductor and metal nanofilms using electrochemical versions of ALE or ALD [3].

Most electrochemical versions of ALD involve underpotential deposition (UPD), an electrochemical surface-limited reaction. UPD is a phenomenon where an atomic layer of one element deposits on a second at a potential prior to (under) that needed to deposit the element on itself, the result of the thermodynamics of compound formation [3].

Historically, electrochemical forms of ALD have been applied in the formation of compound semiconductors as UPD is defined for the formation of a single atomic layer of one element on a second. In the case of compounds, UPD of the component elements might be alternated to grow a deposit one atomic layer at a time; UPD of one element deposits on a second and vice versa.

In order to electrodeposit pure metals layer-by-layer, in a 2D ALD mode, a novel technique involving surface-limited redox replacement (SLRR) has been adopted. The method is an outgrowth of work by Brankovic and Adzic [4], Weaver [5], Dimitrov [6], and Stickney [7]. Initial studies involved the desire to grow an atomic layer of a metal not readily formed via UPD, such as Pt [4, 5]. The principle was that an atomic layer of a less noble metal could first be deposited using UPD, and that surface would be exposed to a solution containing ions of a more noble element, resulting in redox replacement of the less noble metal (sacrificial metal) for an atomic layer of the more noble metal. Use of UPD limits deposition of the sacrificial element to an atomic layer, which then serves to limit deposition of the more noble metal. The next step was the realization that multiple cycles could be performed to create thicker films of these metals,

more than the atomic layer usually resulting from UPD [5]. Multiple cycles of Pt were performed, but a number of questions resulted concerning quality and structure of the Pt films formed. It was not clear that the deposits were growing strictly in a layer-by-layer format. It appeared that some areas of the substrate may not have been covered, and the deposit morphology appeared to quickly roughen in some cases. This is consistent with the history of Pt electrodeposition, where the highly convoluted surface known as Pt black was generally formed. Work by this group showed that the use of halides could improve the distribution of the depositing Pt when combined with SLRR reactions, and that structures consistent with the formation of a Pt surface were formed [7]. This use of an adsorbed halide has been referred to as electrochemical annealing [8, 9].

The next step has been to show that this form of electrochemical ALD is a more general method and can form other metals. In the initial studies of this process, single atomic layers of Ag and Pd were both deposited [4]. Questions were then: can nanofilms be formed, with what quality, how efficient is the exchange process, and can even less noble metals be deposited?

Which metals can be deposited to form nanofilms will depend on whether the sacrificial metal can be underpotentially deposited on top of the more noble metal. It is in this way that multiple atomic layers of a metal can be formed, repeating UPD of the sacrificial metal, and exchange for the more noble metal in a cycle: electrochemical ALD. Adzic et al. replaced Cu UPD with Pt(IV), Pd and Ag, and studied their deposits with scanning tunneling microscopy (STM) [4]. Weaver et al. performed two, four, and eight replacement cycles using Cu UPD as sacrificial layers, with Pt(II) and Pt(IV) and followed their results with cyclic voltammetry and surface-enhanced Raman spectroscopy (SERS) [5]. Dimitrov et al. recently produced quasi-

perfect 2D growth of up to 35 layers of Ag on Au(111) using the SLRR reactions, using Pb UPD as the sacrificial layers [6].

In this article, studies of the growth of Cu films, using Pb UPD as sacrificial layers, are reported. Investigations were based on the use of ultrahigh vacuum (UHV) surface analytical techniques directly with electrochemical experiments (UHV-EC) [10]. In addition, in-situ scanning tunneling microscopy (STM) was used to follow the growth of the first few Cu layers using a unique flow system [11]. Cu is more noble than Pb, and therefore should replace Pb UPD spontaneously: $Pb^{0}_{UPD} + Cu^{2+} \rightarrow Pb^{2+} + Cu^{0}$. The resulting Cu atomic layers were studied using Auger electron spectroscopy (AES) for surface composition and low-energy electron diffraction (LEED) for surface order and the deposit unit cell. In-situ STM was used to follow surface morphology and the structure of the I coated Cu deposits. The Pb replacement efficiencies were determined using coulometry by following the amount of Pb deposited, and then stripping the resulting Cu deposits.

In these studies, the surface of the substrate was coated with I atoms, in order to promote electrochemical annealing. That is, an atomic layer of I atoms was formed spontaneously on the Cu surfaces, yet did not significantly interfere with the exchange process. Adsorbed halides were felt by the authors to provide extra mobility to the metal surface atoms, under certain potential conditions. This was anticipated to allow deposited metal atoms to form a more perfect adlayer, somewhat analogous to the effect of annealing, and thus the description as "electrochemical annealing". In addition, the adsorbed I atomic layers protected the Cu surface from oxidation during emersion (withdrawal of the substrate from solution) and carbon contamination which might have resulted. Finally, the structures of the halide layers on Cu are

well characterized [12], and relatively easy to image with STM, allowing monitoring of the surface composition and structure.

Experimental

A disk-shaped Au(111) substrate, 1-cm in diameter and 1-mm thick, was used for the UHV-EC studies. It was cleaned with hot concentrated HNO_3, annealed in a hydrogen flame, and then inserted into the UHV (~ 10^{-9} Torr) chamber. The Au(111) substrate was then cleaned by Ar^+ ion bombardment, and thermally annealed, in a cleaning procedures described elsewhere [13]. It was then transferred to an ante-chamber, directly attached to the UHV system and containing an electrochemical cell, where it was immersed for 2 min at open circuit in a 0.1 mM solution of KI (J. T. Baker Chemical Co.), with 0.1 M $HClO_4$ (Aldrich Co.), resulting in adsorption of an atomic layer of I.

The KI solution was then exchanged for 1 mM $CuSO_4$ (Aldrich Co.), with 5 mM H_2SO_4 (Aldrich Co.), and Cu UPD was formed at 0.050 V. All potentials are reported *vs.* Ag/AgCl (3 M KCl) (BioAnal). Pb UPD was then performed on the initial Cu UPD layer at −0.400 V or −0.440 V, for 2 minutes. The Pb solution consisted of 0.5 mM $Pb(ClO_4)_2$ (Aldrich Co.), 0.25 mM KI, and 0.05 M $HClO_4$ (Aldrich Co.). The resulting surfaces were then immersed in the Cu solution for 10 seconds at open circuit, where the sacrificial Pb layer was exchanged Cu.

The above process, Pb UPD followed by exchange for Cu, was repeated between 1 and 10 times, followed by transfer to the UHV surface analysis chamber for analysis using AES (Perkin-Elmer) and LEED (Princeton Research Instruments, Inc.). As a last step, the sample was transferred back to the electrochemical cell in the ante-chamber, and the Cu was anodically stripped to determine the Cu replacement efficiency (%). The efficiency was determined as a

function of the total charge for the initial Cu UPD, summed with the charges for each of the Pb UPD steps in a particular experiment, and was thus a function of the number of cycles performed.

In-situ STM studies were performed using a Nanoscope III. The electrodes used were Au single crystal beads made in house using the Clavilier methodology. Imaging was performed on one of the resulting large (111) planes, clearly visible to the eye [7]. The electrochemical cell was designed to allow solution to pass over the electrode, and through the cell. In this way, solutions were exchanged without loss of potential control [11].

Results

Figure 3.1 displays CVs for Cu UPD on the clean Au(111) (solid line), and on an I-atom-modified substrate (dashed line), both from the $CuSO_4$ solution. In addition, a CV for Pb UPD on an I-atom-modified Au(111) substrate, on which Cu UPD was present, is shown as the dot-dashed curve at lower potentials in Figure 3.1. All three CVs were performed using the UHV-EC instrument. The whole Au(111) slice was immersed in solution, so the voltammetry represents the two main (111) faces, as well as the polycrystalline sides, and some polycrystalline character is expected in the CVs. The scan rate was 5 mV/sec.

Comparing the solid and the dashed lines, in Figure 3.1, indicates that modification of the Au(111) crystal with I atoms has shifted the first Cu UPD peak (clean Au(111)) negatively, indicating that it is initially more difficult to deposit Cu on the I-coated surface [14]. On the other hand, the second UPD peak for Cu on the clean substrate (solid line) is shifted positively for deposition on the I-coated surface, so that in the case of the I-coated surface (dashed), both peaks combined to form a large doublet for Cu UPD at 0.150 V. The net Cu UPD coverages for depositions at 0.050 V were similar for both the clean and I-coated Au(111) substrate, very close

to a full monolayer (where a monolayer, ML, is defined as the deposition of one atom for every surface Au atom). The CV for Cu UPD on the clean Au(111) surface is consistent with the literature for Cu UPD from a sulfate solution [15, 16], while the dashed line for UPD on the I-coated Au(111) is very similar to the work of Batina et al. [14], and reminiscent of Cu UPD on I-coated Pt(111) [17].

The CV for Pb UPD on clean Au(111) displays two features: at −0.200 V and −0.250 V [18]. In Figure 3.1, the dot-dashed curve corresponds to deposition of Pb UPD on the surface resulting from Cu UPD on the I atom-modified Au(111). This CV suggests that Pb UPD (dot dashed) was shifted from −200 mV to −0.440 V (Figure 3.1), indicating a much lower Pb underpotential, compared with clean Au(111). Under the conditions used (Figure 3.1) the charge for Pb UPD formed at −0.440 V (~1 ML), on the initial Cu UPD, was nearly twice that for Pb UPD formed at −0.400 V (~½ ML). Two sets of SLRR experiments were performed in this study, both involving exchanging of a sacrificial Pb UPD layer for Cu. The first set involved Pb UPD at −0.400 V, and the second set involved Pb UPD at −0.440 V. Given the nature of SLRR, the more Pb UPD formed, the more Cu that should result.

Open circuit potentials (OCP) during exchange of Pb UPD for Cu were observed after each replacement. The OCP for the first exchange, Pb UPD formed on the initial Cu UPD, stabilized at 0.060 V. During subsequent exchanges, the OCP stabilized closer to 0.030 V. This OCP (0.030 V) was consistent with the formal potential for the Cu^{2+}/Cu couple: the presence of bulk Cu. The high OCP for the first cycle (0.060 V) indicates the Cu deposit still resembled a high coverage UPD rather than bulk Cu deposit, or that the surface was not completely covered, and a mixed potential resulted.

Figure 3.2a displays the AES spectrum for Cu UPD at 0.050 V on I-modified Au(111), where the ratio of the Cu (920 eV) to Au (240 eV) Auger peaks was about 1. The I doublet (peaks at 511 and 518 eV) indicates the presence of an I atom layer on top. It is known that Cu can be electrodeposited under an adsorbed I atom layer on some metals [17]. Given the reactivity of Cu with oxygen, even the traces found in the UHP Ar used as the back fill gas in these UHV-EC studies, an oxygen signal would have been expected if the Cu was not protected by the I atom layer [19]. Figures 3.2b and 3.2c are AES spectra after Pb UPD at −0.400 V and −0.440 V, respectively, on Cu UPD formed at 0.050 V, which was coated with I atoms. A Pb peak is present at 95 eV, while the signals for both Au and Cu appear to decrease, their being covered by Pb atomic layers. The Cu/Au ratio was greater than one, as expected, given that both Pb and Cu were on top of the Au, and would scatter the Au Auger electrons. In addition, the doublet for I at about 500 eV was gone, having been replaced by a peak for O (511 eV). Although I-atoms adsorb strongly to Au and Cu, they do not strongly adsorb to Pb [18]. Thus, Pb UPD can result in the loss of an I atom layer, so that the Pb surface oxidizes upon emersion from solution, in the O_2 traces found in the antechamber [20]. The Cl peak at 180 eV corresponds to a very low coverage, also picked up in the antechamber upon emersion. The Cl signal may, alternatively, indicate a small amount of emersed perchlorate electrolyte, which would also account for some of the oxygen present, though not all of it.

Figure 3.3 shows AES spectra for (a) a clean Au(111), (b) after ten Cu replacement cycles formed via Pb UPD at −0.400 V, and (c) after ten Cu replacement cycles formed via Pb UPD at −0.440 V. The Auger ratio of the Cu peak (920 eV) to the Au peak (240 eV) in Figure 3.3b was Cu/Au = 6.4, significantly smaller than that in Figure 3.3c, Cu/Au = 17. This increase in the Cu/Au ratio between 3.3b and 3.3c is consistent with each replacement of Pb UPD at

−0.400 V resulted in close to a ½ ML, while replacement of Pb UPD at −0.440 V was closer to 1 ML/cycle. The net result is that 10 cycles with Pb UPD at −0.400 V resulted in about 5 ML of Cu deposited, while 10 cycles with Pb UPD at −0.440 V results in closer to 10 ML (Figure 3.4).

It is clear that the Cu/Au Auger ratios in Figures 3.3b (6.4) and 3.3c (17), are not 1:2, for the deposits formed with Pb UPD potentials of −0.400 V and −0.440 V, respectively, as might be expected. The use of Auger peak height ratios in this way is only linear for the first ML or so. In the present study, although the coverages of Cu were increasing with each cycle, and thus the Auger peak height for Cu, at the same time the Au peak height was decreasing, as Au Auger electrons were increasingly scattered by the Cu over layer. Thus the relative ratio for deposits formed at −0.400 V and −0.440 V was 6.4/17 (0.38) rather than the expected 0.5, based on coverages. It is not clear that a Au signal should even be present after deposition of 10 ML of Cu on the surface, given the limited mean free path of the Au electrons through the Cu film. The presence of the Au signal may be an indication of the presence of some degree of surface roughness.

Another difference between the Auger spectra in Figures 3.3b and 3.3c is that the electrode surface in 3.3b was coated by I, the doublet near 500 eV, while the electrode in Figure 3.2c was coated by O, the singlet near 500 eV, suggesting an oxidized surface. Given that the same procedures were used for each experiment, it is difficult to explain the presence of I atoms in one case, and O in the other. The explanation probably involves the affinity of Pb for I atoms. From previous studies of Pb UPD on I-coated Au, it is known that I does not bind strongly to Pb under these conditions [18]. However, at lower Pb UPD coverages on Au, Pb and I can coexist adsorbed on the surface. Given the affinity of Au and Cu for I atoms, Pb and I on Cu probably behave similarly. In the present study the Pb solution contained KI, so that after Pb UPD at

−0.400 V, some I atoms may have remained adsorbed on the surface during transfer to the Cu solution. Upon redox replacement of the Pb with Cu, I atoms would strongly adsorb on the Cu surface. In the case where Pb UPD was performed at −0.440 V, no I atoms would have remained adsorbed due to the high Pb coverage, and thus no I atoms were transferred with the deposit and immersed in the Cu^{2+} solution. The resulting Cu surface was thus unprotected by I atoms upon emersion from the Cu solution and transfer to the analysis chamber. As noted above, unprotected Cu oxidizes upon emersion and transfer (Figure 3.3c).

Figure 3.4 shows stripping charges for all deposited Cu, as a function of the number of cycles performed and the Pb UPD potential used. The squares are for Pb UPD at −0.440 V, while the diamonds are for Pb UPD at −0.400 V. Charges are reported as ML, relative to the Au surface. The linear changes in coverage with the number of cycles are characteristic of an ALD process.

Figure 3.5a displays LEED patterns for the clean substrate, a Au(111)(1×1), while Figure 3.5b is the pattern for an I-modified Au(111) surface, a Au(111)($\sqrt{3}\times\sqrt{3}$)R30º-I, corresponding to 1/3 ML coverage of I [21]. In Figure 3.5c and 3.5d are the observed LEED patterns for Cu UPD on I-coated Au at 0.050 V and Cu UPD with the addition of one Cu replacement, using Pb UPD at −0.400 V, respectively. Both images showed diffuse and somewhat distorted (3×3) patterns. No pattern was evident, just diffuse intensity, for the surface resulting from Cu replacement of Pb UPD deposited at −0.440 V. This was expected given that the Auger spectrum in Figure 3.3c showed an oxidized surface, which generally result in a disordered surface. However, if a similar surface (Cu UPD and one redox replacement of Pb UPD with Cu at −0.440 V) was then immersed in the KI solution, at open circuit, the diffused (3×3)-I LEED pattern shown in Figure

3.6a was observed. After five replacements of Pb UPD (at −0.440 V), and immersion into the KI solution, a diffuse (√3×√3)R30°-I pattern was observed (Figure 3.6b).

Images from in-situ STM studies, by this group, are displayed in Figure 3.7. The first image is of a (3×3)-I structure formed on the Au(111) surface, modified with an atomic layer of I atoms, during Cu UPD. Similar images were observed at potentials corresponding to the UPD doublet, shown in Figure 3.1 (dashed). Figure 3.7b is the image of a large scan, showing large terraces after Cu UPD on the I-coated Au surface. Figures 3.7c and 3.7d are larger area images of the surface after UPD and one redox replacement. Figure 3.7c was first, followed three minutes latter with 3.7d. It is evident from these images that the more cycles performed, the more monoatomic pits and islands present on the surface. However, the annealing process was relatively fast, showing that the atoms were mobile: the islands disappeared and pits filled in. In addition, there was growth at step edges, in some cases taking the form of single atom high fingers protruding out from the step edge, Figures 3.7c and 3.7d. Figure 3.7e shows the surface after Cu UPD and two cycles of Pb UPD replacement by Cu which displays more pits and islands. Again this morphology anneals with time. After Cu UPD and three replacements, the images in Figures 3.7f and 3.7g were obtained. Note that some of the pits were two monolayers deep. Figures 3.7g is a close up, showing the presence of a well ordered (√3×√3)R30°-I lattice on the Cu surface, as well as a look in the pits that may penetrate to the first Cu UPD layer on Au.

Figure 3.8 shows the replacement efficiency (RE), versus the number of Cu replacement cycles for Pb UPD at −0.400 V and at −0.440 V. The efficiencies were calculated as %: [[(total Cu Q) − (initial Cu UPD Q)] / (Σ Pb UPD Qs)] × 100 = % RE. Total Cu charge was calculated from anodic stripping voltammetry after deposit formation. The initial Cu UPD charge and Pb UPD charges were the integrated deposition currents. Efficiencies for deposits formed using Pb

UPD at −0.400 V are displayed as diamonds, while those for deposits formed using Pb UPD at −0.440 V are displayed as squares. For deposits formed with Pb UPD at −0.400 V, the efficiency decreased from near 100% to 60% as the number of Cu redox replacement cycles increased. On the other hand, the efficiencies for Cu redox replacement of Pb UPD at −0.440 V showed significant variability, but averaged about 84%.

Discussion

In general, the unit cells of deposits formed in this study were in agreement with those observed for Cu UPD on I-coated Au(111) or I-coated Cu(111), found in the literature [12, 14, 22]. That is, in detailed studies of the UPD of Cu on I-coated Au(111), Batina et al. observed a (3×3)-I unit cell [14], and a ($\sqrt{3}\times\sqrt{3}$)R30º-I structure was observed for I atoms adsorbed on bulk Cu(111) [12]. However, Batina et al., using in-situ STM, only observed the (3×3)-I structure for very low coverages of Cu. They concluded that the Cu coverages were so low as to not account for the (3×3), but that the Cu merely served to stress the I atom layer, and converted it to the (3×3)-I structure. This does not appear to account for all the (3×3) LEED patterns observed in the present study (Figures 3.5 and 3.6) or coincide with all the in-situ STM results obtained by this group.

Possible explanations for these discrepancies include: some domains in the present studies involved low coverages of Cu, while others may have had multiple Cu layers. In other words, there was a mixture of domains on the surface. It is believed that between ½ and 2 ML of Cu were present on the surface when the (3×3)-I LEED patterns were observed (Figures 3.5c and 3.5d, as well as Figure 3.6), depending on the number of ALD cycles, and the potential used for Pb UPD. It is evident from the STM images (Figure 3.7) that the surface was not

homogeneously covered after a given number of cycles, but displayed both islands and pits. In addition, given the OCP observed for these deposits, at least a ½ ML of Cu UPD would thermodynamically be required in any domains on the surface not covered with multiple Cu layers, the pit bottoms for example.

It is also possible that some Cu was lost during the emersion and re-immersion steps between solutions. This may account for exchange efficiencies less than 100 %, and possibly the presence of areas on the surface with lower Cu coverages, where the (3×3)-I LEED patterns originated. The emersion and evacuation process could change the surface structure observed, but halide coated metal surfaces, such as I on Pt, Au and Cu, are well known to show similar structures in UHV and via in-situ STM. No emersion etc. was used in the in-situ STM studies, were the (3×3)-I structures were observed, and where the potentials prevented loss of UPD Cu from the surface. Although, in this study, STM images of the (3×3)-I structure was not observed for Cu coverages in excess of about 0.6 ML, as in the work of Batina et al. [14]. It is noteworthy that in other Cu nanofilm growth studies by this group, using a flow deposition system so no emersions and immersions were involved, efficiencies very close to 100% were observed in some cases.

Conclusions drawn by the Authors were that even with Cu UPD coverages above ½ ML on the surface of I-coated Au(111), domains with a (3×3)-I unit cell did exist. During UHV-EC studies of Cu ALD, where the deposit was emersed and immersed, some Cu may have been lost. However, from Auger studies, as well as the efficiency studies, only a small % of the Cu was lost, possibly from isolated domains, dropping the Cu coverage, and thus accounting for the (3×3)-I LEED patterns observed even when the overall coverage was higher. To avoid such issues in

future studies, a flow cell is being constructed so that solutions can be exchanged in the UHV-EC studies without emersion, or loss of potential control, until transfer to UHV for analysis.

It is encouraging that the LEED patterns seen at higher coverages of Cu did display the expected $(\sqrt{3}\times\sqrt{3})R30^{o}$-I, previously observed on Cu(111) [12, 22], via in-situ STM. It would have been good to be able to determine at what coverage the structure converts from (3×3) to $(\sqrt{3}\times\sqrt{3})R30^{o}$-I, but results from this group and the literature suggest that there is some ill defined structure which grows in after the (3×3)-I in Cu UPD studies on I-coated Au(111) [14]. The $(\sqrt{3}\times\sqrt{3})R30^{o}$-I, on the other hand, does appear at coverages between 2 and 3 ML, in both STM and UHV-EC studies.

Conclusions

Surface-limited redox replacement of Pb UPD to form atomic layers of Cu has been studied. Pb UPD as sacrificial layers, to deposit Cu atomic layers, has been used in an ALD cycle to grow smooth nanofilms of Cu. UHV-EC and in-situ STM were used to follow the composition, structure and morphology of Cu film growth. The extent of film growth at the monolayer level was controlled by the number of cycles performed and the Pb UPD potential. However, deposit surface morphology was rougher than anticipated. Given sufficient time, the atomic layers do anneal out, and it is anticipated that by optimizing times, potentials and halide introduction, deposit morphology will improve. It is important to keep in mind that the morphology which would result from standard electrodeposition methodologies at room temperature would likely result in nucleation growth and the associated morphology. With such as a comparison, these films had excellent morphology.

The surface structures observed were consistent with the literature, except that the (3×3)-I structure observed for Cu deposition on I-coated Au(111) appeared at higher Cu coverages than expected from the literature. There are a number of plausible explanations, including that domains supporting different structures were present simultaneously on the surface, or that during UHV-EC studies some Cu may have been lost from the surface, resulting in lower replacement efficiencies and possibly accounting for the domain variability suggested. Use of a flow through cell during UHV-EC studies should provide more consistency, as well as higher exchange efficiencies.

Acknowledgements

The financial support from National Science Foundation, Divisions of Materials and Chemistry and the Department of Energy, is gratefully acknowledged.

References

1. M. Fleischmann and H.R. Thirsk, in *Advances in electrochemistry and electrochemical engineering*, P. Delahay and C.W. Tobias (Eds.), Interscience Publishers, John Wiley and Sons, Inc., New York, 1963.
2. H.O. Pierson, *Handbook of chemical vapor deposition*, Noyes Publications, Park Ridge, NJ, 1992.
3. J.L. Stickney, in *Advances in Electrochemical Science and Engineering*, R.C. Alkire and D.M. Kolb (Eds.), Wiley-VCH, Weinheim, 2002.
4. S.R. Brankovic, J.X. Wang, and R.R. Adzic, *Surf. Sci.*, **474**, L173 (2001).
5. M.F. Mrozek, Y. Xie, and M.J. Weaver, *Anal. Chem.*, **73**, 5953 (2001).

6. R. Vasilic and N. Dimitrov, *Electrochem. Solid-State Lett.*, **8**, C173 (2005).
7. Y.-G. Kim, J.Y. Kim, D. Vairavapandian, and J.L. Stickney, *J. Phys. Chem. B*, **110**, 17998 (2006).
8. I. Villegas, C.B. Ehlers, and J.L. Stickney, *J. Electrochem. Soc.*, **137**, 3143 (1990).
9. J.L. Stickney, I. Villegas, and C.B. Ehlers, *J. Am. Chem. Soc.*, **111**, 6473 (1989).
10. M.P. Soriaga and J.L. Stickney, *Chemical Analysis (New York)*, **139**, 1 (1996).
11. M.D. Lay, T.A. Sorenson, and J.L. Stickney, *J. Phys. Chem. B*, **107**, 10598 (2003).
12. J. Inukai, Y. Osawa, and K. Itaya, *J. Phys. Chem. B*, **102**, 10034 (1998).
13. J.Y. Kim, Y.-G. Kim, and J.L. Stickney, *Electrochem. Soc. Trans.*, **1**, 41 (2006).
14. A. Martinez-Ruiz, J. Valenzuela-Benavides, L.M. de la Garza, and N. Batina, *Surf. Sci.*, **476**, 139 (2001).
15. M.F. Toney, J.N. Howard, J. Richer, G.L. Borges, J.G. Gordon, and O.R. Melroy, *Phys. Rev. Lett.*, **75**, 4472 (1995).
16. M. Dietterle, T. Will, and D.M. Kolb, *Surf. Sci.*, **342**, 29 (1995).
17. J.L. Stickney, S.D. Rosasco, B.C. Schardt, and A.T. Hubbard, *J. Phys. Chem.*, **88**, 251 (1984).
18. Y.-G. Kim, J.Y. Kim, C. Thambidurai, and J.L. Stickney, *in preparation*, (2006).
19. C.B. Ehlers and J.L. Stickney, *Surf. Sci.*, **239**, 85 (1990).
20. B.C. Schardt, J.L. Stickney, D.A. Stern, A. Wieckowski, D.C. Zapien, and A.T. Hubbard, *Surf. Sci.*, **175**, 520 (1986).
21. J.E. Harris, M.E. Bothwell, J.F. Rodriguez, M.P. Soriaga, and J.L. Stickney, *J. Phys. Chem.*, **93**, 2610 (1989).
22. R. Randler, M. Dietterle, and D.M. Kolb, *Z. Phys. Chem.*, **208**, 43 (1999).

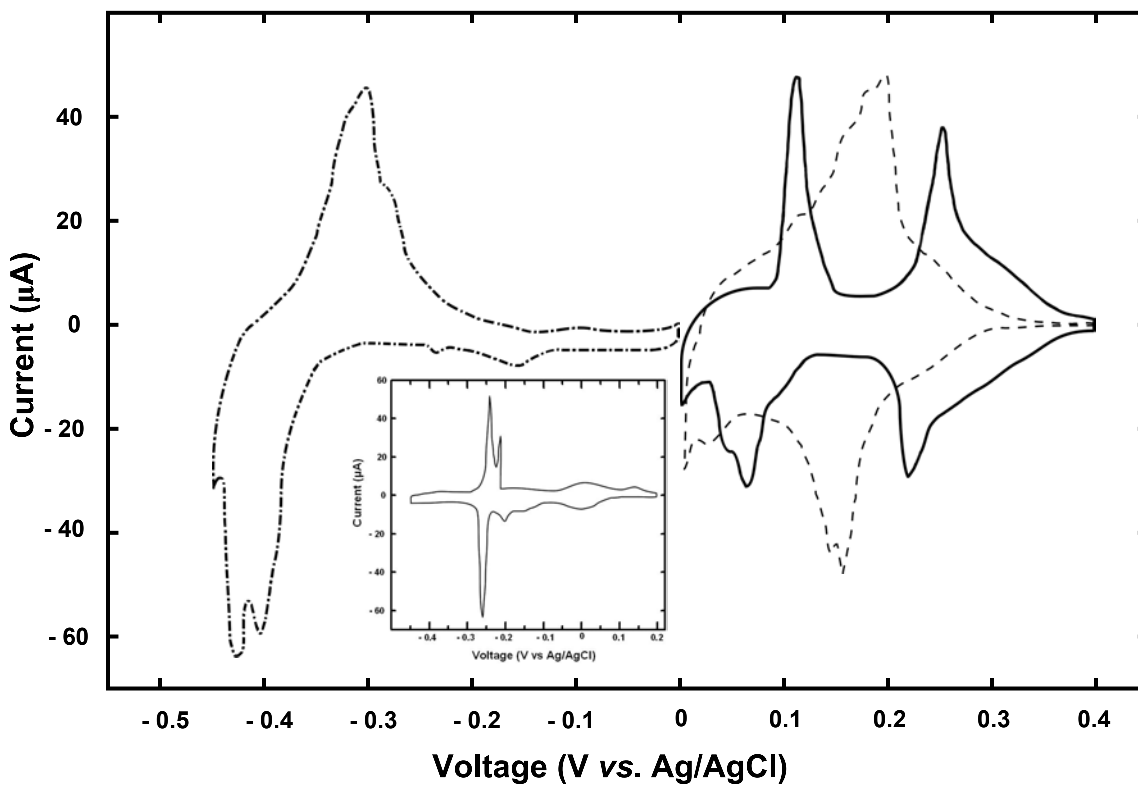

Figure 3.1 Cyclic voltammetries of Cu on bare Au(111) (solid line), Cu on I-modified Au(111) (dashed line), and Pb on Cu UPD (dot-dashed line). Scan rate = 5 mV/sec. Inset: Pb CV on bare Au(111).

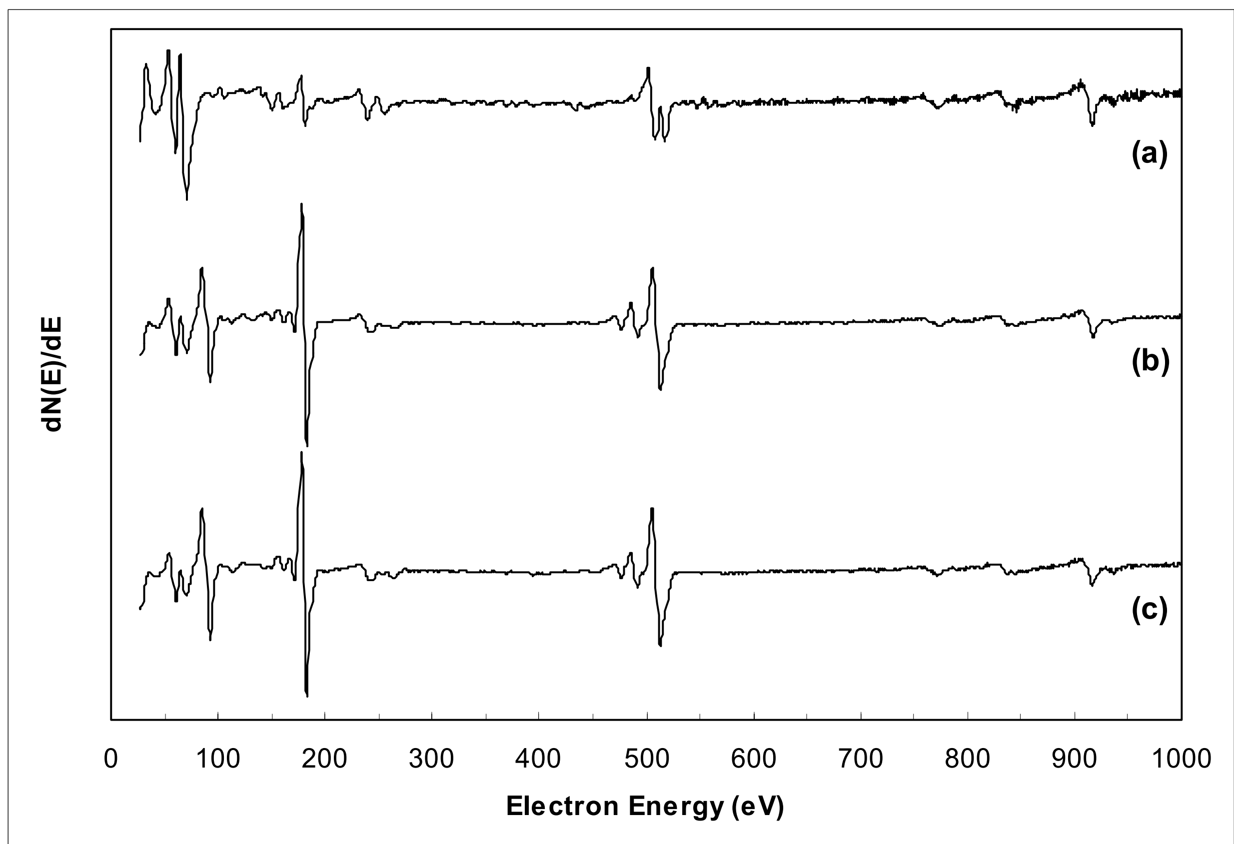

Figure 3.2 AES spectra of (a) the initial Cu UPD at 0.050 V on I-modified Au(111), (b) after Pb UPD at −0.400 V on the initial Cu UPD, and (c) after Pb UPD at −0.440 V on the initial Cu UPD.

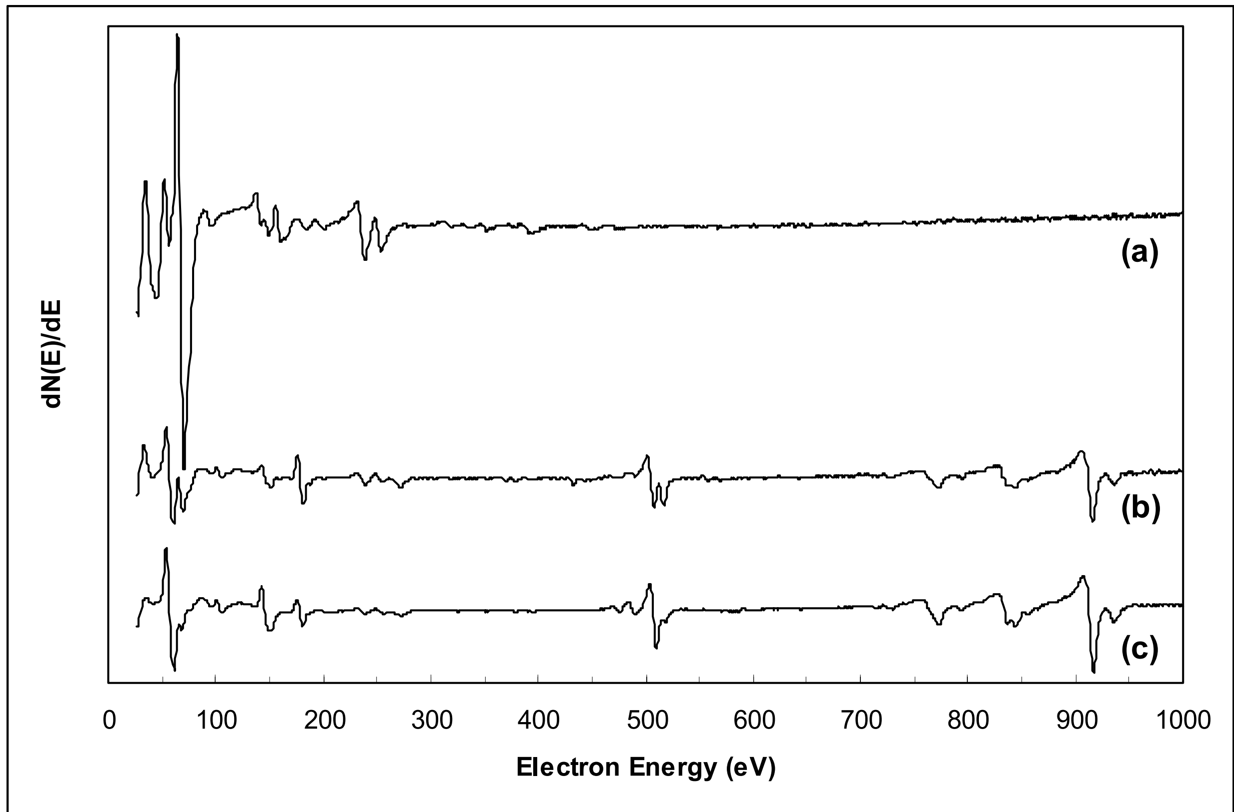

Figure 3.3 AES spectra of (a) clean Au(111), (b) after ten Cu replacements with Pb UPD at −0.400 V, and (c) after ten Cu replacements with Pb UPD at −0.440 V.

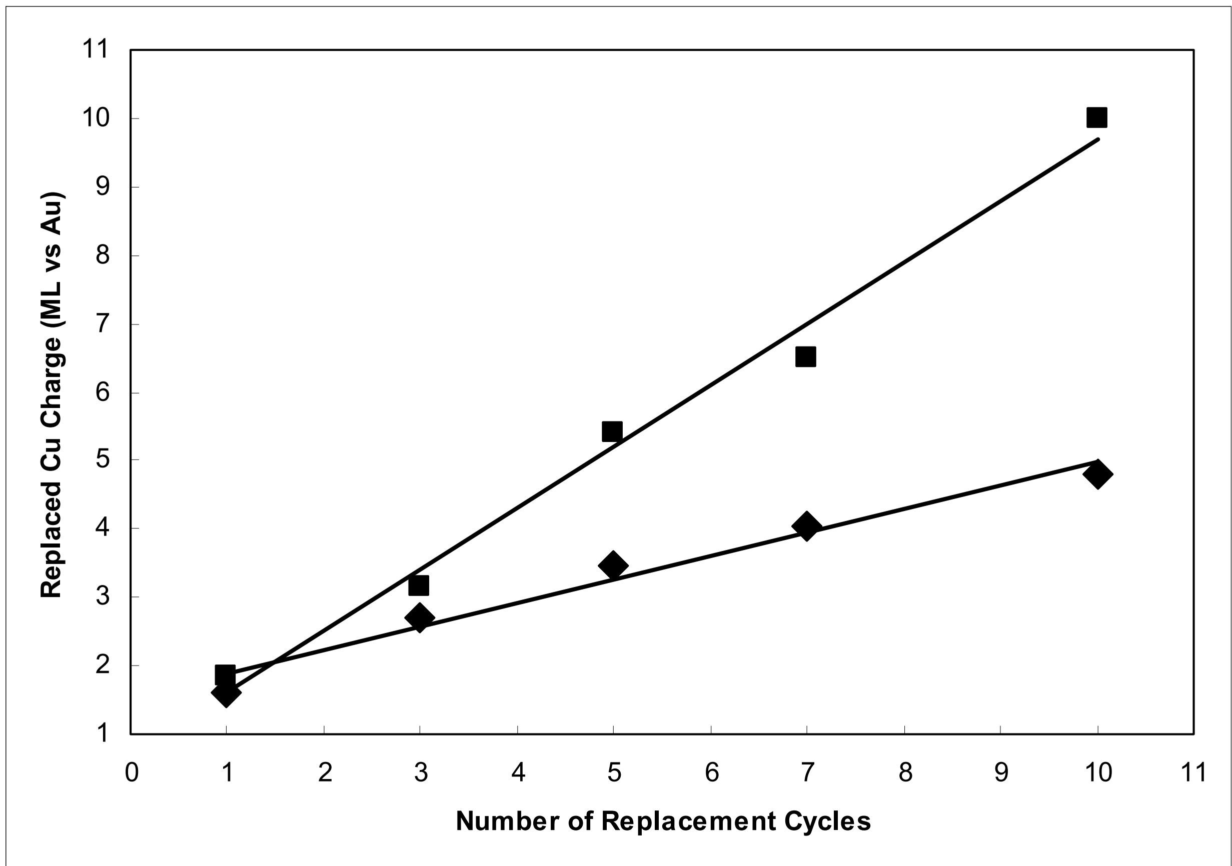

Figure 3.4 Replaced Cu anodic stripping charge (ML vs Au) versus the number of replacement cycles; Squares: Cu replacements with Pb UPD at −0.440 V; Diamonds: Cu Replacements with Pb UPD at −0.400 V; Solid lines: the best-fit lines.

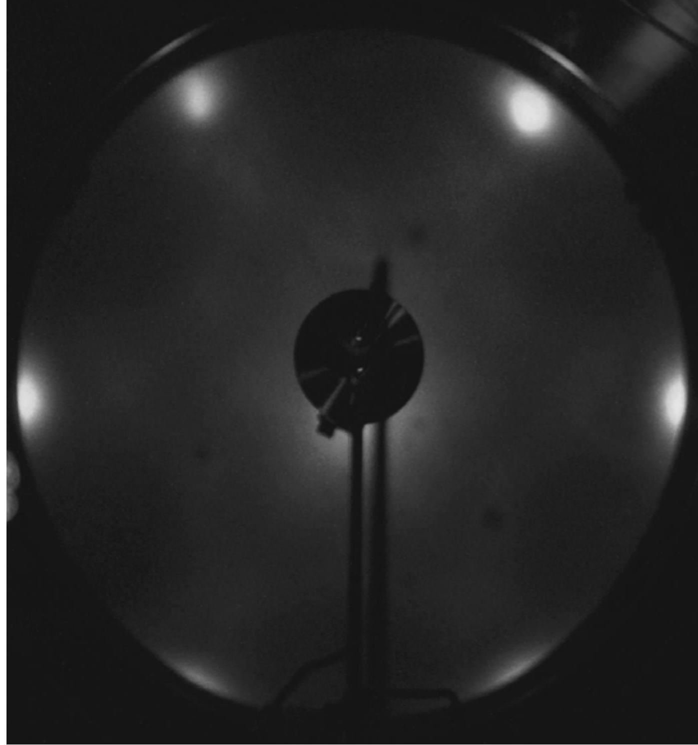

(a)

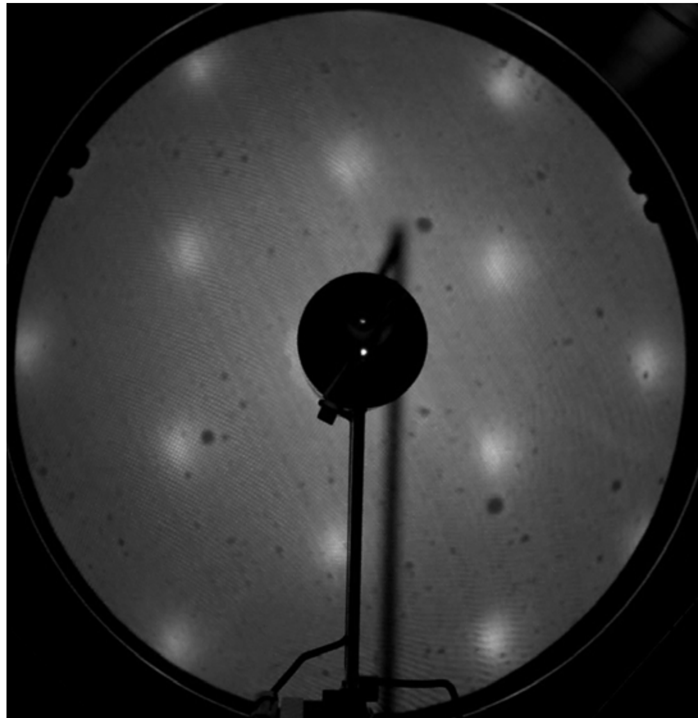

(b)

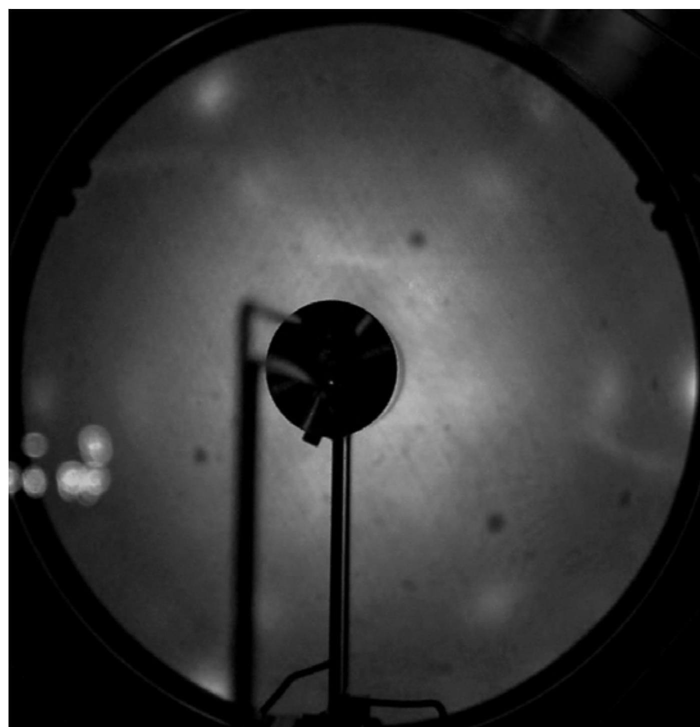

(c)

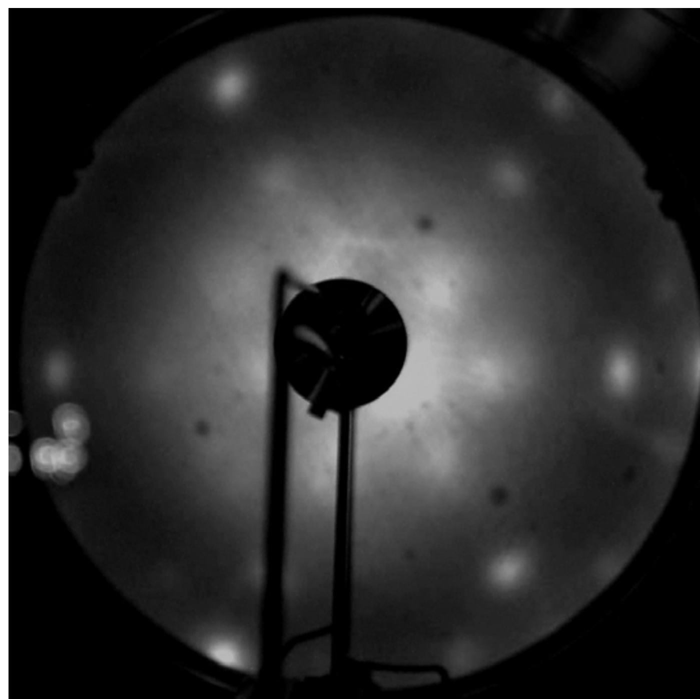

(d)

Figure 3.5 LEED patterns of (a) clean Au(111) (beam energy = 45.0 eV), (b) I-modified Au(111) (beam energy = 48.0 eV), (c) Cu UPD at 0.050 V on I-modified Au(111) (beam energy = 45.0 eV), and (d) after one Cu replacement with Pb UPD at −0.400 V (beam energy = 45.0 eV).

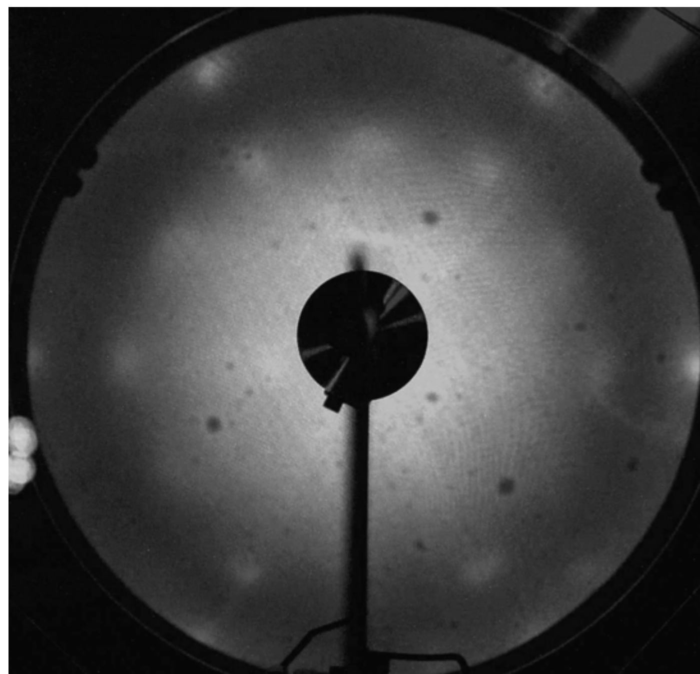

(a)

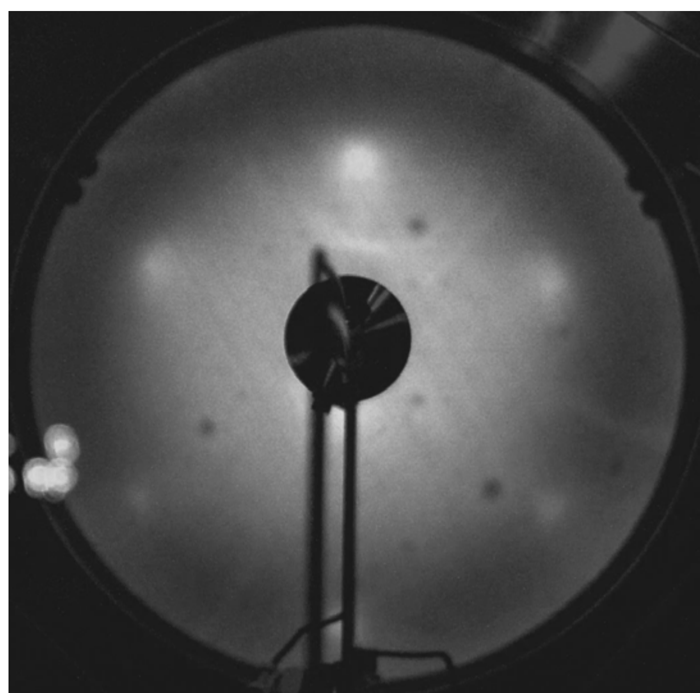

(b)

Figure 3.6 LEED patterns of (a) I modification of one Cu replacement with Pb UPD at −0.440 V (beam energy = 43.0 eV) and (b) I modification of five Cu replacements with Pb UPD at −0.440 V (beam energy = 45.0 eV).

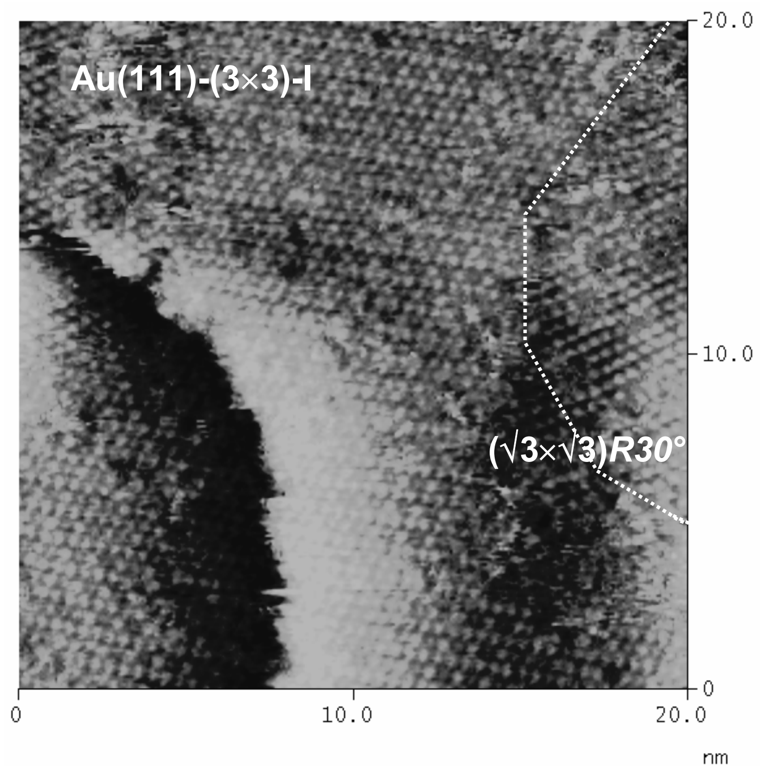

(a)

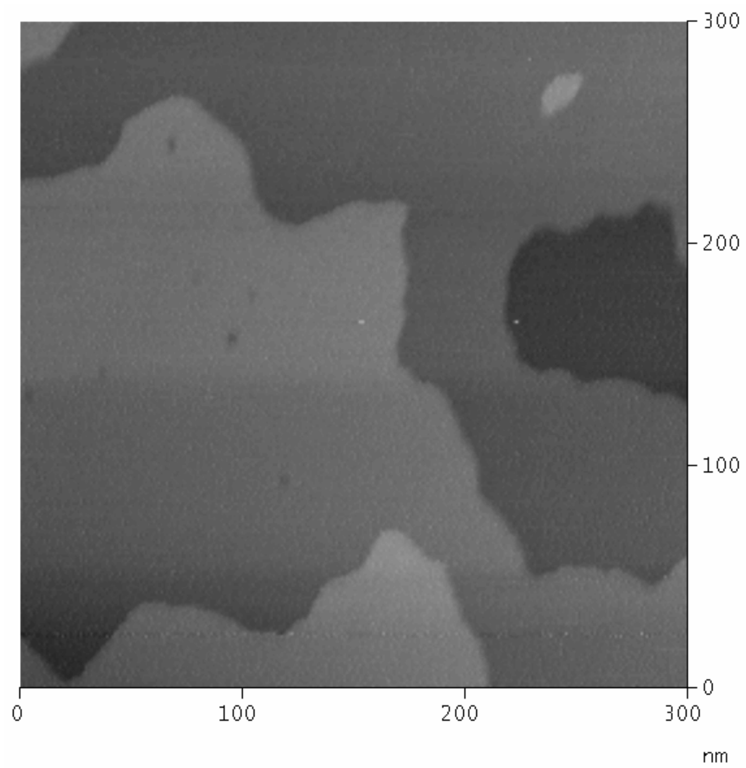

(b)

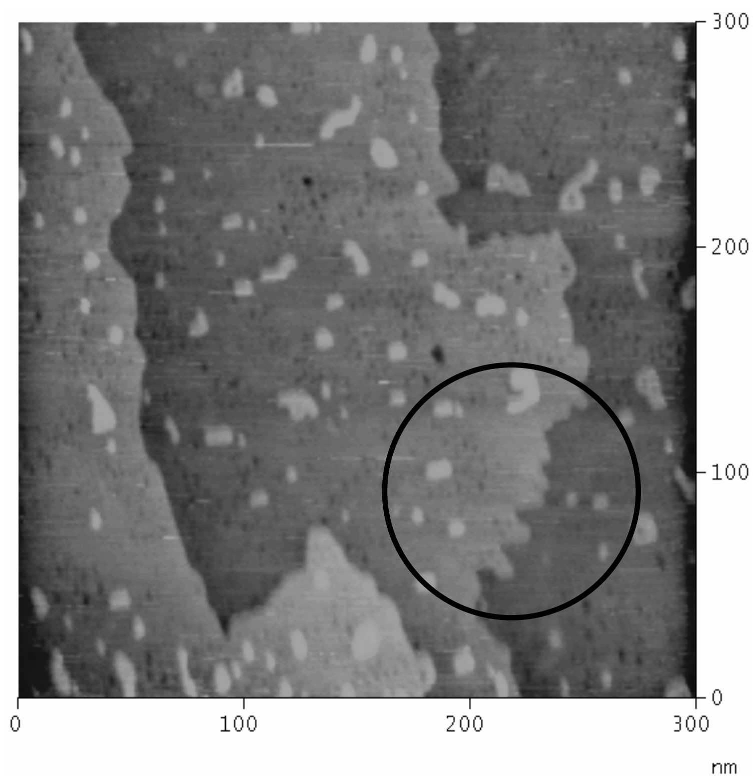

(c)

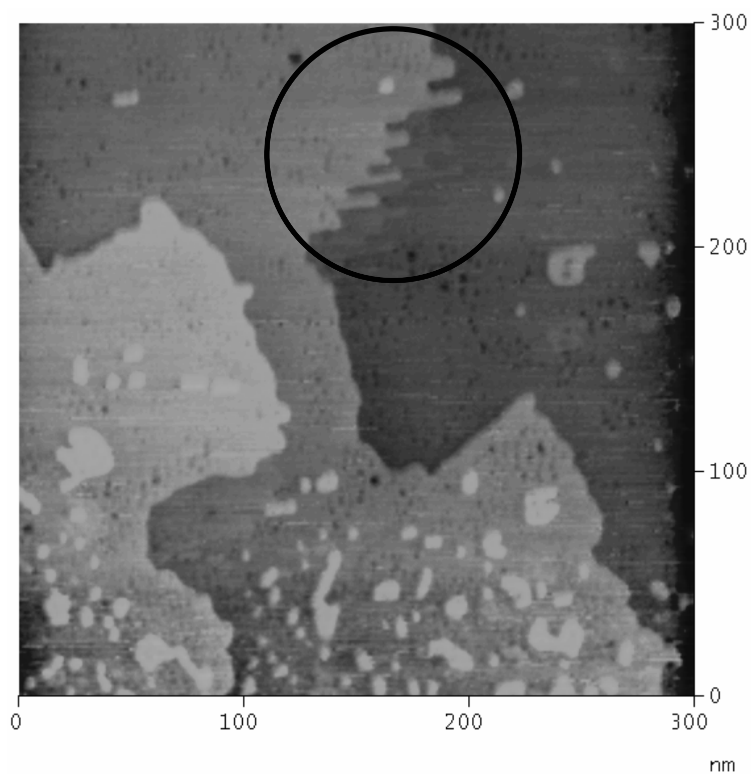

(d)

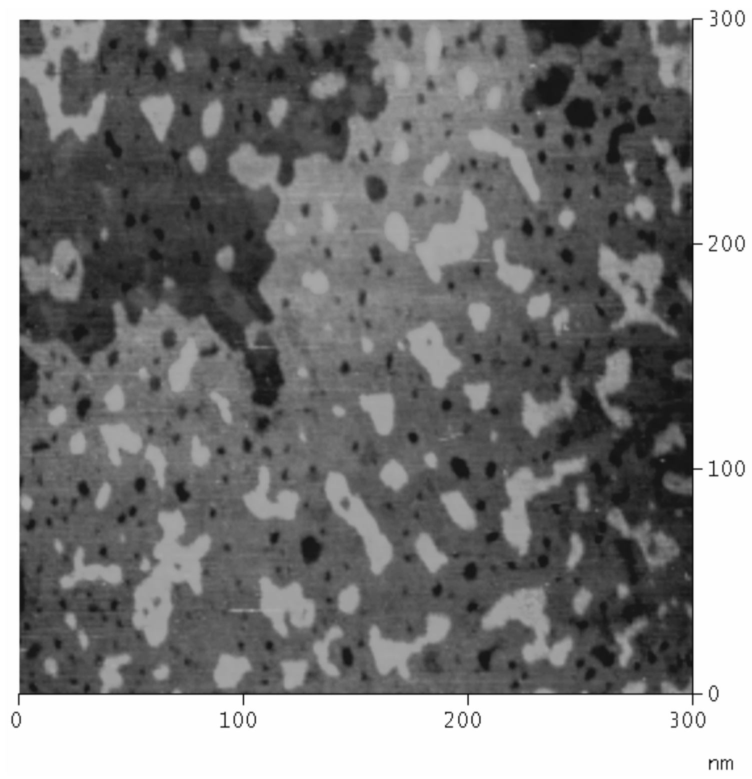

(e)

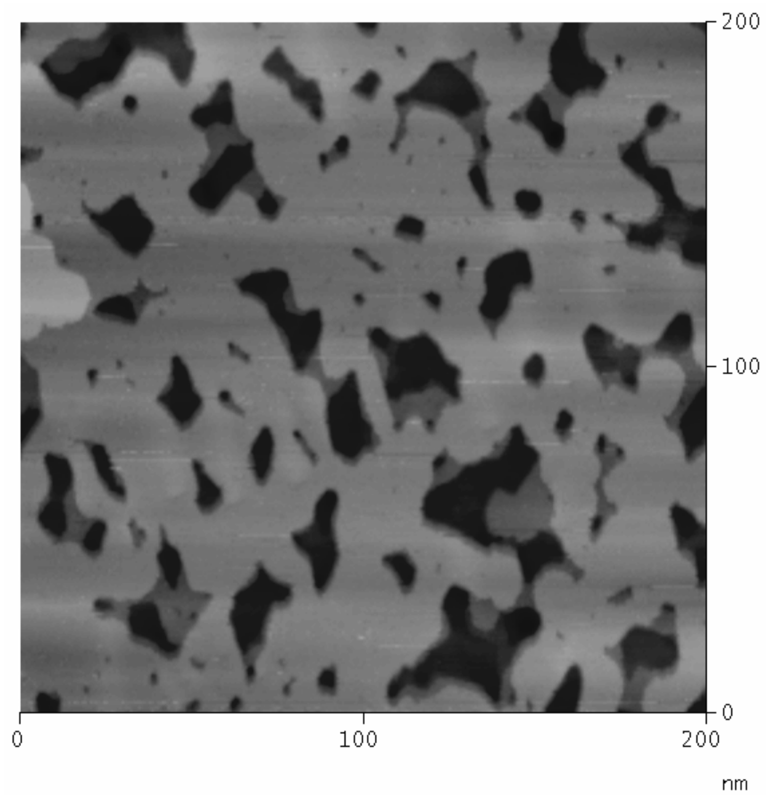

(f)

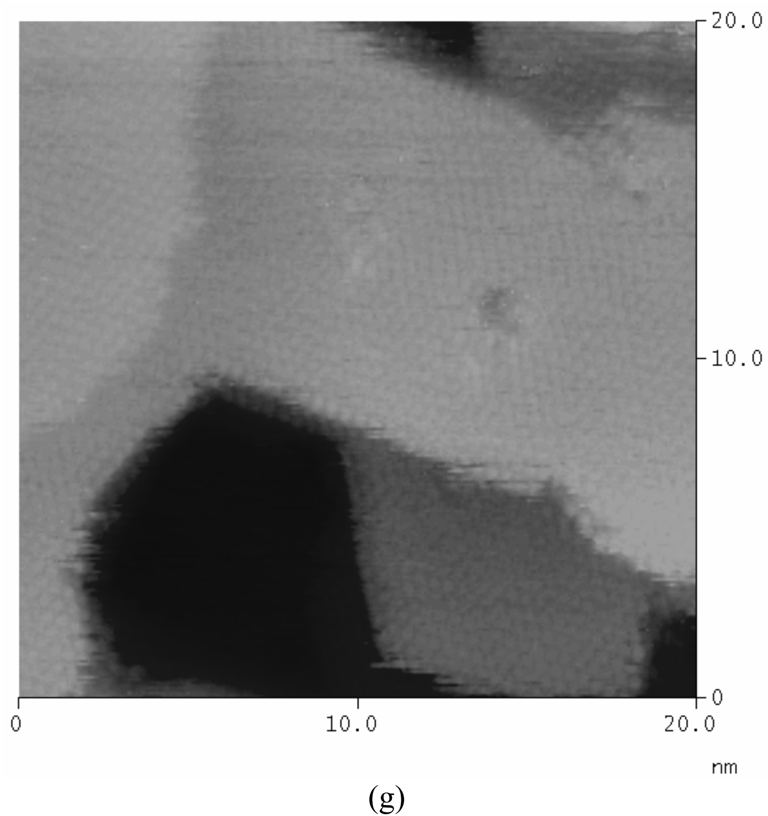

(g)

Figure 3.7 In-situ STM images of (a) after Cu UPD on I-modified Au(111) (20×20 nm^2), (b) after Cu UPD on I-modified Au(111) (300×300 nm^2), (c) after Cu UPD and one Cu replacement (300×300 nm^2), (d) three minutes after (c) (300×300 nm^2), (e) after Cu UPD and two Cu replacements (300×300 nm^2), (f) after Cu UPD and three Cu replacements (200×200 nm^2), and (g) after Cu UPD and three Cu replacements (20×20 nm^2).

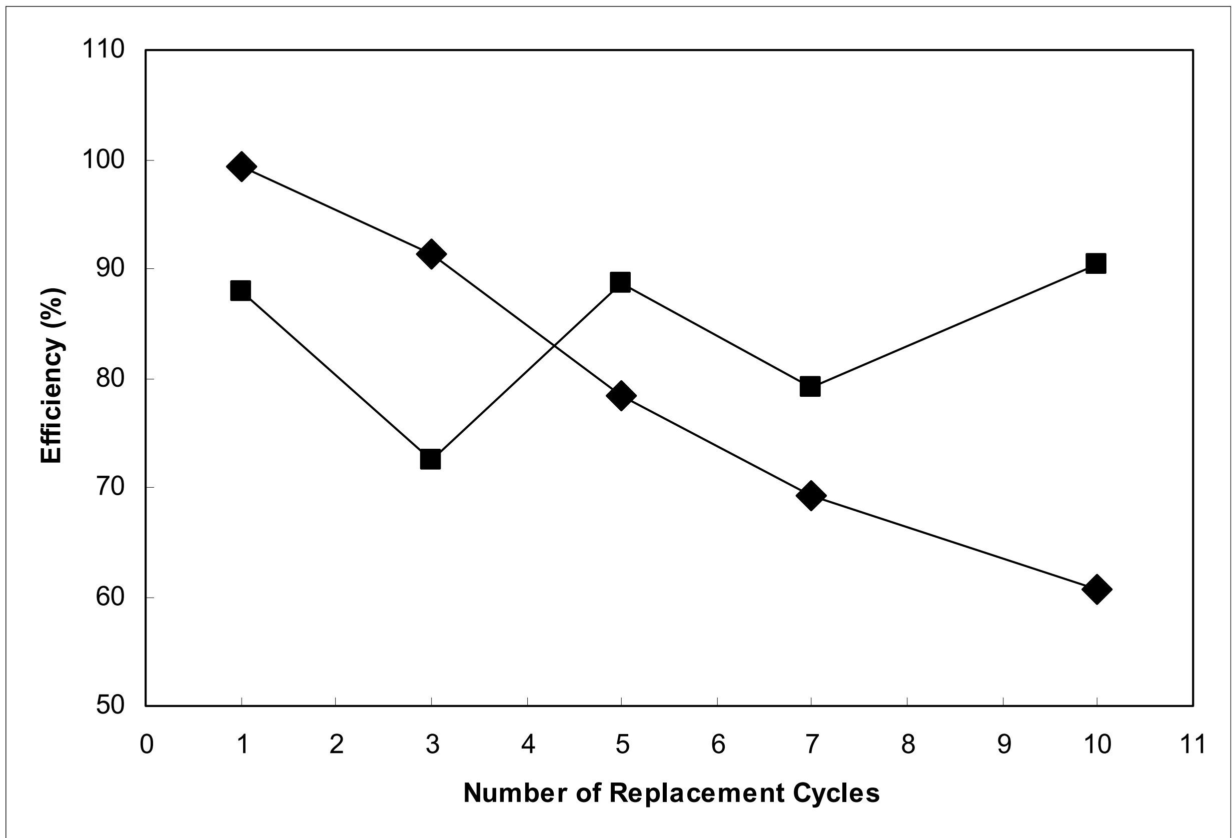

Figure 3.8 Replacement efficiency (%) versus the number of replacement cycles; Square: Cu replacements with Pb UPD at −0.440 V; Diamond: Cu replacements with Pb UPD at −0.400 V.

CHAPTER 4

Cu NANOFILM FORMATION BY ELECTROCHEMICAL ATOMIC LAYER DEPOSITION (ALD) IN THE PRESENCE OF CHLORIDE IONS[3]

[3] J.Y. Kim, Y.-G. Kim, and J.L. Stickney, Accepted by *J. Electroanal. Chem.* (2007). Reprinted here with permission of publisher.

Abstract

The effect of Cl^- on the structure of Cu nanofilms deposited with electrochemical ALD, using surface limited redox replacement (SLRR), is described. These investigations involved ultrahigh vacuum analytical methodologies coupled directly with electrochemical studies (UHV-EC), as well as in-situ scanning tunneling microscopic (STM) studies. Pb was chosen as the sacrificial metal as it forms atomic layers on Cu via underpotential deposition (UPD). In addition, it is significantly more reactive than Cu, less noble, and thus undergoes redox replacement by Cu. Pb UPD was formed at −0.44 V versus Ag/AgCl, for 20 seconds. The substrates used in these studies were Ar^+ ion bombarded and annealed Au(111) single crystal substrates. The resulting Pb UPD coated Au(111) was immersed in a Cu^{2+} ion solution at open circuit for 10 seconds, allowing redox replacement of the Pb UPD by Cu. Nanofilms were then formed by repeating this process of Pb UPD followed by exchange for Cu. The resulting Cu nanofilms were characterized using low-energy electron diffraction (LEED), Auger electron spectroscopy (AES), and in-situ STM. The total Cu in a deposit was estimated by anodic stripping. Up to five cycles of Pb replacement by Cu were performed in these studies. The structures formed displayed a (5×5) unit cell, consisting of a 4 by 4 arrangement of Cl atoms on the Cu surface. The degree of surface order appeared to decrease gradually as the number of replacement cycles was increased, though a relatively clear LEED pattern was still observed after 5 replacement cycles.

Keywords: Electrochemical ALD; Surface-Limited Redox Replacement (SLRR); UHV; UPD; LEED; EC-STM; Electrochemical Annealing (EA)

Introduction

Besides halide anions (F^-, Cl^-, Br^-, and I^-) being common components of supporting electrolytes, they are known to act as surfactants on metal surfaces, and have been used in what is referred to here as electrochemical annealing (EA) [1, 2]. EA describes a process where the surface of a metal is smoothed at the atomic scale by a combination of the adsorption of a surfactant species and adjustment of the electrochemical potential to near that required to oxidize the metal [3, 4]. This combination appears to promote surface mobility, and thus ordering. Most EA studies have involved adsorbed halides as surfactants on some of the more noble metal substrate surfaces, such as Au [1], Cu [5] and Pd [6], although CO has also been suggested as a surfactant which promotes EA [7]. The idea is that by complexing the surface atoms with an adsorbate, and using relatively positive potentials, allowing extra surface mobility, and thus surface smoothing. This appears to result from a weakening of the metallic bonding between the first and second metal layers [8]. Adsorbed halides are also known to protect Pt surfaces from contamination, as they are well known to form ordered atomic layers epitaxially on metal substrate surfaces [9]. I^- is especially well known for this, as these anions spontaneously adsorb as layers of neutral I atoms, oxidative adsorption, even at open circuit [1]. In addition, in ultrahigh vacuum electrochemical studies (UHV-EC), adsorbed halide layers have been known to prevent surface reconstructions [10], or upon adsorption, to lift reconstructions.

Underpotential deposition (UPD) is a phenomenon where an atomic layer of a less noble element is deposited on a second, more noble, element. Deposition stops after formation of an atomic layer, as the surface area is limited, and the depositing element no longer has access to the substrate element. It is the result of the free energy of formation of a surface compound or alloy [11]. There are numerous studies of metal UPD on surfaces supporting adsorbed halide

layers [9, 12-15]. Such atomic layer formation occurs at a potential prior to (under) that needed to deposit the element on itself (bulk deposition) and thus is referred to as UPD. Behm et al. and Kolb et al. presented in-situ scanning tunneling microscopy (STM) images to demonstrate the influence of a trace of Cl^- (10^{-4} M) on the UPD of Cu on Au(100) [16] and Au(111) [17]. They suggested that coadsorbed Cl^- anions stabilize the Cu adlayer, resulting in a sharp adsorption peak in the I−V curve at 0.295 V, versus a saturated calomel electrode (SCE), and that the anions effectively lead to strongly attractive interactions between the Cu adatoms, indicated by the observation of (n × 2) islands, in a trace of Cl^-. Matsumoto et al. also used traces of Cl^-, Br^-, or I^-, in Cu solutions (50 mM H_2SO_4 + 1 mM $CuSO_4$) to investigate the coadsorption of Cu and halide anions on Pt(111), Pt(100), and Au(111) [15]. Their STM images of coadsorbed Cu and halide structures on Au(111) revealed a (5 × 5) structures for Cu + Cl, after the first cathodic UPD peak (0.450 V vs. SHE), as well as after the second (0.310 V). Structures formed by the deposition of Cu in the presence of Br^- displayed ($\sqrt{7} \times \sqrt{7}$)R19.1° and (4 × 4) structures after the first (0.450 V) and second (0.375 V) UPD deposition peaks, respectively, and a (3 × 3) structure for Cu deposition in the presences of I^- (0.380 V). Lipkowski et al. proposed models surface structures for Cl^- coadsorbed with Cu UPD, from studies combining electrochemical methodologies and polarization-resolved X-ray absorption spectra (XAS) [18]. The electrodeposited copper atoms were packed between the outer Au surface layer and under the chloride capping layer, resulting in a (5 × 5) surface unit cell.

The present report involved UHV-EC [19] and in-situ STM studies of the formation of Cu nanofilms formed using electrochemical ALD, in the presence of Cl^-. ALD stands for atomic layer deposition, a thin film formation methodology based on the layer-by-layer growth of thin films using surface limited reactions. UPD is a prominent example of an electrochemical surface

limited reaction; however, it results only in the formation of a single atomic layer. To form more than one atomic layer, a cycle is needed, with each resulting in the formation of an atomic layer. Repeating the cycle linearly increases the deposit thickness. As noted, there must be more to the cycle than UPD, as by itself, UPD only results in formation of a single atomic layer. To form metal nanofilms, cycles have been developed using surface limited redox replacement (SLRR) [20]. The principle developed by Brankovic and Adzic was that if the metal you desire to deposit does not form an atomic layer, take a more reactive metal (the sacrificial metal) that will form an atomic layer by UPD and exchange it in a solution of an ionic precursor for the metal you want. The amount exchanged will be limited by the electrons available in the sacrificial atomic layer, as when it has been dissolved, no more deposition will take place.

This process was first used in a cycle by the late Mike Weaver [21] to grow Pt nanofilms. Electrochemical ALD nanofilms of Pt have also been reported by Kim et al. [1]. Formation of Cu nanofilms using electrochemical ALD has been recently reported by both the authors [2] and Dimitrov et al. [22].

Experimental

A 1.0 cm diameter Au(111) single crystal disk, 1-mm thick, was used as the substrate for the UHV-EC studies. It was cleaned in vacuum using Ar^+ ion bombardment (IBB), 1 $\mu A/cm^2$, and annealing by resistance heating. Figure 4.1a shows the (1×1) LEED pattern, 50 eV, of the clean Au(111) surface after IBB and annealing. The clean substrate was transferred to the ante-chamber, without exposing to air. The ante-chamber was then back-filled with ultrahigh purity (UHP) Ar gas and the electrochemical cell was inserted. Solutions were pumped into the cell using pressurized Pyrex bottles. All potentials noted in this article are reported with respect to a

Ag/AgCl (3M KCl) reference electrode. The solutions used were de-aerated with UHP Ar gas for about 30 minutes prior to each electrochemical experiment.

The Pb^{2+} ion solution, 0.25 mM $Pb(ClO_4)_2$ (Aldrich Co.) + 50 mM HCl (Aldrich Co.), was introduced into the electrochemical cell, before the Au(111) crystal lowered in, and underpotential deposition was performed at −0.44 V for 20 seconds. The resulting sacrificial metal Pb UPD layer was then immersed into the Cu^{2+} solution, where it was replaced at open circuit for 10 seconds**:**

$$Pb_{UPD} + Cu^{2+} \rightarrow Pb^{2+} + Cu_{bulk} \tag{4.1}$$

This process was repeated to grow thicker films. After the desired number of Cu replacement cycles, the electrochemical cell was removed, the ante-chamber pumped down, and the substrate transferred back to the main chamber for characterization with LEED (Princeton Research Instrument, Inc.) and Auger Electron Spectroscopy (AES) (Perkin-Elmer). Finally, the sample was transferred back to the ante-chamber for anodic stripping of the deposited Cu in the blank, 1 mM HCl, to estimate the total Cu coverage in monolayers (ML). A ML was defined in the present study as one atom for every Au surface atom (1.35×10^{15} atoms/cm^2 for a smooth (111) surface). After the anodic stripping of Cu, the replacement efficiency was determined as follows:

$$\text{Cu Replacement Efficiency} = (\text{Charge for stripping Cu})/\Sigma(\text{Pb UPD charges}) \tag{4.2}$$

Both processes involved two electrons, so ideally one Cu atom should result from each Pb atom deposited. The total Cu charge was determined by anodic stripping voltammetry, while Pb UPD charges were determined from the current-time traces for deposition.

In the UHV-EC studies, Cu^{2+} solutions of two HCl concentrations were investigated: 1 mM $Cu(ClO_4)_2$ (Aldrich Co.) + 50 mM HCl; and 1 mM $Cu(ClO_4)_2$ + 2.5 mM HCl. In UHV-EC

studies it is well known that aqueous solutions with electrolyte concentrations of 10 mM or above are generally problematic, as the emersion layer (that layer of solution dragged with the crystal when it is removed from solution) contains sufficient salts which, upon evaporation, crystallize on the surface, degrading LEED patterns, and raising questions concerning the nature of Auger peaks present in the spectrum. One way around this problem is to rinse the sample with a dilute solution, after emersion (removal) of the substrate from a solution, to decrease the electrolyte concentration in the emersion layer. This can be performed at open circuit, or controlled potential. In the present case, deposits formed using the 50 mM HCl solution were rinsed with 1 mM HCl blank solution prior to transfer to the analysis chamber, while those from the 2.5 mM HCl solution were simply emersed and transferred, without the rinse. After characterization with LEED and AES, the deposits were transferred back to the ante-chamber for coulometric stripping of the deposited Cu.

In-situ STM studies, performed using a Nanoscope III (Digital Instruments, Santa Barbara, CA), were used to confirm the surface structures in-situ. For the STM studies, Au single crystal beads were formed using the method developed by Clavilier [23], and imaging was performed on one of the resulting large (111) planes of the single crystal bead. The electrochemical cell was designed to allow solution to pass over the electrode so that the solutions could be exchanged without loss of potential control during imaging [24].

Results and Discussion

The solid line, Figure 4.2, corresponds to the voltammetry for Pb^{2+} UPD on bare Au(111) from the Pb solution described above. Note, although the front and back of the crystal were polished to [111] orientations, the sides were still polycrystalline. Since the whole crystal was

immersed in solution, to perform electrochemical experiments, the voltammetry displayed in this article retains some polycrystalline features. The scan rate used for Figure 4.2 was 5 mV/sec. Of note in this voltammetry is the relative reversibility of Pb UPD on the clean surface (solid line). The first Pb UPD features were observed at about −0.1 V, a low broad hump with a few sharp spikes. The second grouping of UPD peaks began closer to −0.2 V, and consisted of at least three large sharp peaks. In total, the Pb UPD charge after scanning to −0.44 V was equivalent to the deposition of about 0.95 ML, consistent with the literatures [25-27]. These large UPD features suggest the majority of the Pb experiences an underpotential of about 200 mV. AES spectra obtained after Pb UPD below −0.3 V indicated the presence of Pb (90 eV), with a Pb/Au (240 eV) Auger peak ratio of about 4, and the presence of small amounts of O (510 eV) and Cl (180eV). It has been shown in studies of Pb UPD on Pt that some Pb tends to oxidize upon emersion from various lead halide solutions [28-30] during the transfer process in UHV-EC studies, probably accounting for the small oxygen Auger signal. The studies of Pb deposition from Cl and Br solutions on Pt surfaces suggested that at lower coverages of Pb, less than 0.5 ML, halides were co-adsorbed with Pb [28, 30]. The Cl signal may thus be from Cl atoms adsorbed in areas where some Pb was lost during the transfer, where the Pb coverage was lower. Previous studies with I^- adsorption on Pb UPD on Au(111) indicated that I co-adsorbed with Pb only up to a coverage of 0.44 ML, and desorbed in the presences of higher Pb coverages [31], suggesting other halides, Cl for instance, may desorb in the presences of high Pb coverages. The Cl signal was not very significant, corresponding to much less than 5 % of a monolayer.

The dotted and dashed lines in Figure 4.2 are Pb CVs for surfaces after one cycle of Cu deposition. The dashed curve was the surface resulting from exchange of Pb for Cu in the 2.5 mM HCl solution, while the dotted curve was for the surface resulting from exchange of Pb for

Cu in the 50 mM HCl solution. After replacing Pb UPD with Cu, and before the dotted and dashed Pb CVs shown in Figure 4.2, the Cu surfaces were emersed and examined in UHV with LEED and Auger. It must be pointed out, as noted in the last section, that Cu solution with the high HCl concentration, 50 mM, required a rinse step before emersion and analysis in UHV. That is, the probability of an emersed electrolyte layer invalidating the resulting Auger and LEED data was too high not to rinse the surface before transfer to the analysis chamber. Thus an open circuit rinse step in 1 mM HCl was performed after exchange in the Cu solution with 50 mM HCl, but not for the Cu solution with 2.5 mM HCl.

During the course of this study, it became apparent that the open circuit rinse step with 1 mM HCl resulted in some loss of Cu from the surface. From Figure 4.2, the dotted curve represents Pb UPD on the substrate coated with Cu after exchange in the 50 mM HCl Cu solution, followed by the 1 mM HCl rinse. It shows two major peaks, at −0.32 V and −0.38 V. On the other hand, the dashed curve represents Pb UPD on the substrate coated with Cu after exchange in the 2.5 mM HCl Cu solution, with no rinse, and shows one major peak at −0.41 V. It is proposed here that Pb deposition on a fully Cu coated substrate results in the dashed curve, and the one peak at a very low underpotential. After the rinse, and some loss from the Cu atomic layer, two peaks were evident in the dotted curve. Apparently, some Pb initially deposits on areas where the Cu atomic layer has been somewhat depleted, −0.32 V, and more closely resembles the Au surface, while the rest of the Pb deposits on the full Cu atomic layer, −0.38 V.

It is noteworthy that with the Cu on the surface, in both cases, the Pb UPD voltammetry was more irreversible than on clean Au, and that the underpotentials were significantly reduced. As will be noted below, the Cu surfaces were coated with adsorbed Cl, and the presence of this Cl appears to impede Pb UPD, as evidenced by the irreversibility in the voltammetry. For the

surface with a slightly higher Cu coverage, the dashed curve, the UPD features are closer to bulk deposition, as the surface has a more complete coating of Cl.

Figure 4.1b shows the LEED pattern after Pb UPD at −0.44 V on the bare Au(111) surface. The pattern consists of a ring of twelve spots, with another ring of twelve inside, rotated by 15 degrees, one third of the way in from the integral beams. Some disorder in the structure is indicated by the diffuse intensity of the pattern. The rings suggest that the structure has multiple domains, rotated from each other on the surface. Previous studies in the deposition of Pb on Au(111) indicated a Moiré pattern structure [31]. The uniqueness of the LEED pattern does not appear inconsistent with the presence of a Moiré structure, however, at present the unit cell and relationship of the pattern with respect to the Moiré is not clear.

Figure 4.3a shows Cu UPD CVs on bare Au(111) using the 50 mM HCl Cu solution (solid line) and the 2.5 mM HCl Cu solution (dotted line), both at 5 mV/sec. Similar CVs have been published by other workers [12, 32]. The main Cu UPD peak, in the 50 mM HCl solution, occurred at about 0.325 V, and showed strong reversibility, while that for the 2.5 mM HCl solution was at 0.3 V, and showed significant splitting in the peaks, some irreversibility. It is interesting that for the higher HCl concentration, the deposition peak was sharper and more reversible, suggesting the deposition mechanism fundamentally involved chloride. The dashed curve in Figure 4.3a was for Cu UPD in a "chloride free" solution (1 mM $Cu(ClO_4)_2$ + 50 mM $HClO_4$), where no sharp deposition feature was evident, although there were two prominent peaks in the oxidation scan at 0.15 V. It should be noted, that previous studies with Cu surfaces have clearly shown that "chloride free" electrolyte is hard to come by, given the tenacity of Cl^- adsorption on Cu surfaces [5, 33, 34]. Even traces of Cl^- from the glassware, the supporting electrolyte, the water or the reference electrode, are sufficient to form an adsorbed Cl monolayer,

given time. It is suggested here that the oxidation peak shown in the dashed curve (0.15 V), may result from a surface containing some Cl, resulting from adsorption of these traces of Cl^- in solution, which have accumulated during the CV, while Cu was present on the surface.

Figure 4.3b shows the average open circuit potential (OCP), observed after successive Cu replacement cycles in the 2.5 mM HCl Cu solution. The first OCP is near that corresponding to the Cu UPD stripping peaks. After the second and subsequent Cu replacement cycles, the potentials shifted negative to those corresponding more closely with bulk Cu deposition. These results are consistent with the second cycle resulting in a second Cu ML, and a surface more closely resembled bulk Cu, than UPD. Auger spectra recorded for these Cu nanofilms displayed only peaks for Au, Cl, and Cu (920 eV). No Auger peaks were observed for Pb and O, indicating complete replacement of the sacrificial Pb UPD by Cu. In addition, the absences of O demonstrates that the surface was completely covered with Cl, as Cu has a sticking coefficient for O_2 of 1 [35], and even traces of O_2 in the antechamber would have oxidized any Cu not protected by the Cl adsorbed atomic layer.

Figure 4.4 shows Auger peak ratios of (a) Cu to Cl and (b) Cu to Au. The Cu/Cl Auger ratio shows the steady increase expected, as the amount of Cl is constant, one adsorbed atomic layer, while the number of layer of Cu goes up steadily with each replacement. The Cl signal acts as a kind of internal standard, with the coverage remaining constant, and with nothing adsorbing on top of the Cl to scatter the Auger electrons. Similarly, the Au can be used as the internal standard, as in Figure 4.4b, and again, the Cu/Au ratio remains linear with increasing numbers of replacement cycles. The Cu/Cl ratios (Figure 4.4a) should provide a better measure of the increase in Cu signal, as the Au substrate Auger electrons become scattered by the depositing Cu, theoretically resulting in an upturn in the Cu/Au ratio as the coverage of Cu

increases. However, self scattering of the Cu layers will counter act scattering of the Au by the growing Cu film, to some extent, result in wider linear range. The steady increases of the Cu Auger ratios in Figure 4.4a and 4.4b is consistent with layer by layer growth of the Cu nanofilm, and an ALD process.

Figure 4.5 shows the LEED pattern (50 eV) observed after Cu UPD from the Cu solution containing 50 mM HCl. The pattern shows significant diffuse intensity, indicating disorder in the surface structure, but the presence of a (4 × 4) unit cell is clearly indicated (note the three fractional order beams between the integral beams at 3:00 and 5:00). More fractional beams were observed using beam energies less than 50 eV, and all were consistent with the presences of a (4 × 4) surface unit cell. Given the use of 50 mM HCl, an open circuit rinse in 1 mM HCl was used prior to transfer to the analysis system. Some researchers have observed (4 × 4) surface structure by STM and LEED under similar conditions [36, 37]. Related patterns were observed after multiple cycles of SLRR of Pb for Cu, using the 50 mM HCl solution, followed by OC rinses in 1 mM HCl. After five replacement cycles, the (4 × 4) was still present, but a gradual increase in diffuse intensity and loss of clarity for the fractional order beams indicated an increase in surface disorder.

By using the Cu solution containing only 2.5 mM HCl, and avoiding the OC rinse before analysis, the LEED patterns shown in Figure 4.6 were obtained. Figure 6a was observed after Cu UPD from the chloride solution, and displays a very well defined (5 × 5) unit cell (note the four fractional order beams between the integral beams at 3:00 and 5:00). The integral beams are those closest to the edge, however, the beams next in towards the center were clearly brighter. Generally, for LEED patterns from adsorbate structures, the integral beams are the brightest, and are associated with the substrate surface. That the next in fractional order beams, the (0, 4/5)

beam for instance, were brighter is partially the result of the having at least two atomic layer on top of the substrate, Cu and the Cl atomic layers, so that fewer of the electrons in the 50 eV beam are influenced by the underlying Au substrate.

The two LEED patterns shown in Figure 4.6 are for after Cu UPD at 0.2 V (Figure 4.6a) and after one Cu replacement cycle (Figure 4.6b), and both clearly show the (5 × 5) unit cell. These patterns are both distinctly sharper than the patterns shown in Figure 4.5, after the OC rinse. From the sharpness and reversibility of voltammetry in Figure 4.3a (solid line) for Cu UPD with the 50 mM HCl, it might be expected that a more ordered surface structure was formed, relative to that in the Cu solution containing 2.5 mM HCl, Figure 4.3a (dotted curve). This is probably true, and it is just the need for the rinse before transfer to the analysis chamber which degrades the quality of the surface structure formed using the Cu solution with 50 mM HCl. This points out one of the limitations of UHV-EC work, in that it may be desirable to use high electrolyte or reactant concentrations in a study, however if the total concentration of species present in the solution exceeds the mM level, emersed layers tend to contain sufficient species to crystallize out on the surface, and obscure the data. These emersed layers can thus be rinsed away, but under the open circuit conditions used here, they appear to have resulted in some loss of Cu and Cl, and an increase in surface disorder. On the other hand, without the rinse, and using a 2.5 mM HCl, the high degree of surface order is clearly evident.

The LEED patterns, after UPD (Figure 4.6a) and that after the addition of a Cu replacement cycle, are well defined, though the second pattern does show a small increase in diffuse intensity, and thus an increase in surfaced disorder. The same (5 × 5) was evident after each replacement cycle, though the disorder increased with each cycle, and Figure 4.6c is the pattern observed after five Cu replacement cycles. Experience has shown that electrodeposition

of more than one or two atomic layers of an element generally results in a strong increase in disorder as observed by LEED, in most cases, no LEED beams are observed. The degree of ordered evident after five replacement cycles, Figure 4.6c, is very encouraging, and supports the contention that the growth process is layer by layer.

Figure 4.7a displays an in-situ STM image of Cu UPD in HCl, on Au(111). The atoms imaged are the adsorbed Cl atoms, rather than the underlying Cu. The deposit shows a very well ordered surface, with a distinct unit cell. The high resolution image, Figure 4.7b, clearly shows that the surface structure formed by the Cu UPD and adsorbed Cl has the dimensions of a (5 × 5) unit cell (a = 1.44 nm), and that the chloride atoms in the basis form a 4 by 4 array, for a coverage of 16/25 of Cl. The nature of the underlying Cu atoms in the basis is not clear, however. Previous studies by other workers have reported a similar (5 × 5) unit cell [15, 32, 38]. Several reasonable structures have been proposed to account for the (5 × 5) by Lipkowski et al. [14, 18], from their work with X-ray adsorption fine structure. Figure 4.7c is an STM image after the addition of a Cu replacement cycle to the Cu UPD structure, and again shows the (5 × 5) cell, which resembles a Moiré pattern. High quality STM images showing a structure similar in appearance was reported by Dimitrov et al. for ALD of Cu with Pb as the sacrificial metal, but without Cl^-, and after deposition of Pb UPD, the sacrificial layer [39].

Figure 4.8 shows the total coverages of Cu, as a function of the number of replacement cycles. Coverages were determined by integration of the anodic stripping voltammetry, after the stated number of Cu replacement cycles [2]. The graph is essentially linear, but does appear to role off after 4 cycles. The subsequent Pb UPD charges were similar from the first to the fifth, with the variation of ~5 %. As only one experiment was performed for each point, it is not clear if the roll off was the result of operator error for the 5th cycle or a trend. Studies in this group of

Cu electrochemical ALD using sulfate solutions have demonstrated linear increases, with each cycle, for 200 cycles. However, in studies of Pt deposition by electrochemical ALD, where adsorbed layers of I atoms were present, resulted in difficulties in exchanging the Cu UPD sacrificial layers for Pt, after a few cycles. That is, the Pt studies indicated that the halides may interfere with the SLRR after a few cycles, though this issue is presently under study.

Conclusion

The nature of Cu deposits formed by electrochemical ALD, via surface limited redox replacement, from chloride solutions were investigated using UHV-EC techniques as well as in-situ STM. An attempt to investigate the dependence on Cl concentration proved problematic, as the higher concentration HCl solutions required a rinse, where some Cu appeared to be desorbed. However, it was shown that the higher the HCl concentration, the sharper and more reversible the voltammetry, suggesting that chloride was directly involved in the Cu UPD mechanism. Previous studies of the two dimensional phase changes which accompany UPD on single crystal surfaces, have suggested that the sharper the peaks, the more likely the deposit will be well ordered, and that some surface compound has been formed, such as the Cu-Cl surface layer formed in the present study.

As far as the deposition cycles were concerned, Auger showed the increases in signal expected for an element depositing layer by layer, as well as the decrease in the substrate intensity expected for being covered layer by layer. Well ordered LEED patterns were observed, indicating the formation of a structure with a (4×4) unit cell, when some Cu had been lost due to the rinse. On the other hand, a well ordered structure, with a (5×5) unit cell, was observed when no rinse was used. In-situ STM also indicated the presences of a very well ordered (5×5)

structure, with a 4 by 4 arrangement of Cl atoms in the top layer, for 16/25 coverage of Cl. The (5 × 5) had been previously observed in studies of the UPD of Cu from chloride media, and reasonable structures were proposed. However, these are the first studies to show that this structure remained after as many as five cycles of Cu ALD. Finally, coulometric stripping of the deposited Cu displayed the expected linear relationship between coverage and the number of deposition cycles.

Acknowledgements

The financial support from National Science Foundation, Divisions of Materials and the Department of Energy, is gratefully acknowledged.

References

1. Y.-G. Kim, J.Y. Kim, D. Vairavapandian, and J.L. Stickney, *J. Phys. Chem. B*, **110**, 17998 (2006).
2. J.Y. Kim, Y.-G. Kim, and J.L. Stickney, *J. Electrochem. Soc.*, **154**, D260 (2007).
3. E. Pichardo-Pedrero, G.L. Beltramo, and M. Giesen, *Applied Physics A*, **87**, 461 (2007).
4. M. Giesen, G. Beltramo, S. Dieluweit, J. Muller, H. Ibach, and W. Schmickler, *Surf. Sci.*, **595**, 127 (2005).
5. J.L. Stickney, C.B. Ehlers, and B.W. Gregory, *Langmuir*, **4**, 1368 (1988).
6. Y.-G. Kim, J.H. Baricuatro, M.P. Soriaga, D.W. Suggs, *J. Electroanal. Chem.*, **509**, 170 (2001); Y.-G. Kim and M.P. Soriaga, *J. Phys. Chem. B*, **102**, 6188 (1998).
7. V. Komanicky, A. Menzel, K.C. Chang, and H. You, *J. Phys. Chem. B*, **109**, 23543 (2005).

8. S. Huemann, N.T.M. Hai, P. Broekmann, K. Wandelt, H. Zajonz, H. Dosch, and F. Renner, *J. Phys. Chem. B*, **110**, 24955 (2006).

9. O.M. Magnussen, *Chem. Rev.*, **102**, 679 (2002).

10. M.P. Soriaga, *Prog. Surf. Sci.*, **39**, 325 (1992).

11. J.L. Stickney, in *Advances in Electrochemical Science and Engineering*, R.C. Alkire and D.M. Kolb (Eds.), Wiley-VCH, Weinheim, 2002.

12. D.M. Kolb, in *Advances in Electrochemical Science and Engineering*, R.C. Alkire and D.M. Kolb (Eds.), Wiley-VCH, Weinheim, 2002.

13. A. Martinez-Ruiz, J. Valenzuela-Benavides, L.M. de la Garza, and N. Batina, *Surf. Sci.*, **476**, 139 (2001).

14. Z.C. Shi, S.J. Wu, and J. Lipkowski, *J. Electroanal. Chem.*, **384**, 171 (1995).

15. H. Matsumoto, J. Inukai, and M. Ito, *J. Electroanal. Chem.*, **379**, 223 (1994).

16. F.A. Moller, O.M. Magnussen, and R.J. Behm, *Phys. Rev. B*, **51**, 2484 (1995).

17. N. Batina, T. Will, and D.M. Kolb, *Faraday Discussions*, **94**, 93 (1992).

18. S. Wu, Z. Shi, J. Lipkowski, A.P. Hitchcock, and T. Tyliszczak, *J. Phys. Chem. B*, **101**, 10310 (1997).

19. M.P. Soriaga and J.L. Stickney, *Chemical Analysis (New York)*, **139**, 1 (1996).

20. S.R. Brankovic, J.X. Wang, and R.R. Adzic, *Surf. Sci.*, **474**, L173 (2001).

21. M.F. Mrozek, Y. Xie, and M.J. Weaver, *Anal. Chem.*, **73**, 5953 (2001).

22. L.T. Viyannalage, R. Vasilic, and N. Dimitrov, *J. Phys. Chem. C*, **111**, 4036 (2007).

23. J. Clavilier, R. Faure, G. Guinet, and R. Durand, *J. Electroanal. Chem.*, **107**, 205 (1980).

24. M.D. Lay, T.A. Sorenson, and J.L. Stickney, *J. Phys. Chem. B*, **107**, 10598 (2003).

25. K. Engelsmann, W.J. Lorenz, and E. Schmidt, *J. Electroanal. Chem.*, **114**, 1 (1980).

26. A. Hamelin and J. Lipkowski, *J. Electroanal. Chem.*, **171**, 317 (1984).

27. S.J. Hsieh and A.A. Gewirth, *Surf. Sci.*, **498**, 147 (2002).

28. B.C. Schardt, J.L. Stickney, D.A. Stern, A. Wieckowski, D.C. Zapien, and A.T. Hubbard, *Langmuir*, **3**, 239 (1987).

29. J.L. Stickney, D.A. Stern, B.C. Schardt, D.C. Zapien, A. Wieckowski, and A.T. Hubbard, *J. Electroanal. Chem.*, **213**, 293 (1986).

30. B.C. Schardt, J.L. Stickney, D.A. Stern, A. Wieckowski, D.C. Zapien, and A.T. Hubbard, *Surf. Sci.*, **175**, 520 (1986).

31. Y.-G. Kim, J.Y. Kim, C. Thambidurai, and J.L. Stickney, *Langmuir*, **23**, 2539 (2007).

32. E. Herrero, L.J. Buller, and H.D. Abruna, *Chem. Rev.*, **101**, 1897 (2001).

33. J.L. Stickney, B.W. Gregory, and C. Ehlers, *J. Electrochem. Soc.*, **135**, C158 (1988).

34. C.B. Ehlers, I. Villegas, and J.L. Stickney, *J. Electroanal. Chem.*, **284**, 403 (1990).

35. J.L. Stickney, C.B. Ehlers, and B.W. Gregory, *ACS Symposium Series*, **378**, 99 (1988).

36. D. Friebel, T. Mangen, B. Obliers, C. Schlaup, P. Broekmann, and K. Wandelt, *Langmuir*, **20**, 2803 (2004).

37. H. Bludau, K. Wu, M.S. Zei, M. Eiswirth, H. Over, and G. Ertl, *Surf. Sci.*, **404**, 786 (1998).

38. J. Hotlos, O.M. Magnussen, and R.J. Behm, *Surf. Sci.*, **335**, 129 (1995).

39. L.T. Viyannalage, R. Vasilic, and N. Dimitrov, *ECS Transaction*, **2**, 307 (2007).

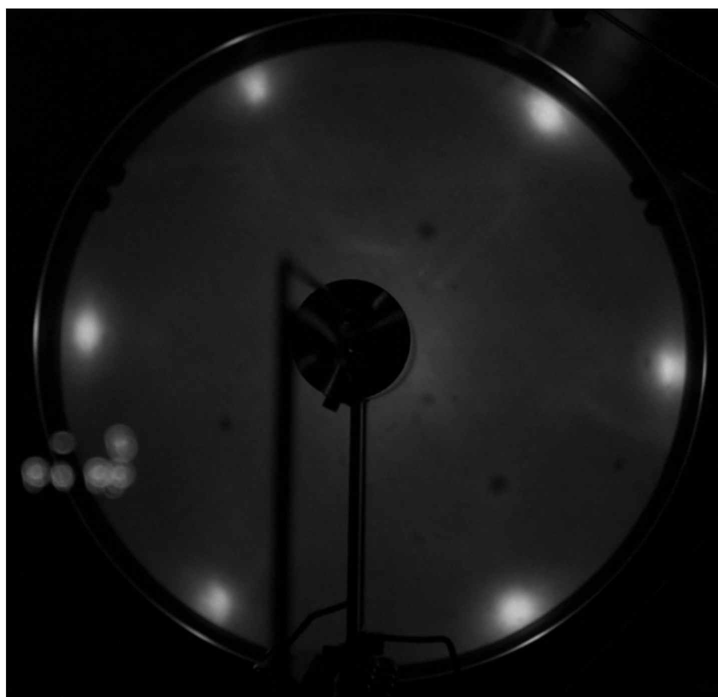

(a)

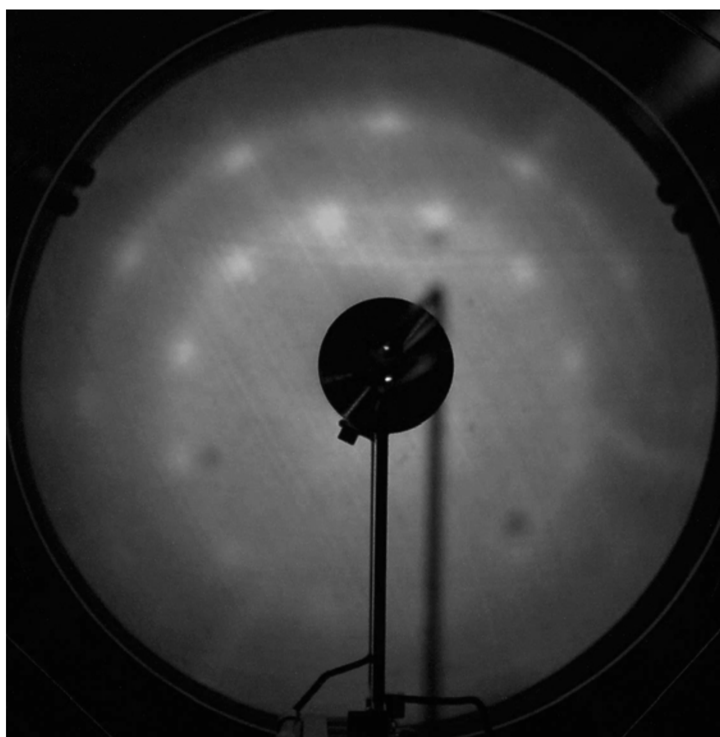

(b)

Figure 4.1 The LEED pattern (a) after cleaning with Ar^+ ion bombardment and annealing (Beam energy = 50 eV), and (b) after Pb UPD at −0.44 V on bare Au(111) (Beam energy = 50 eV).

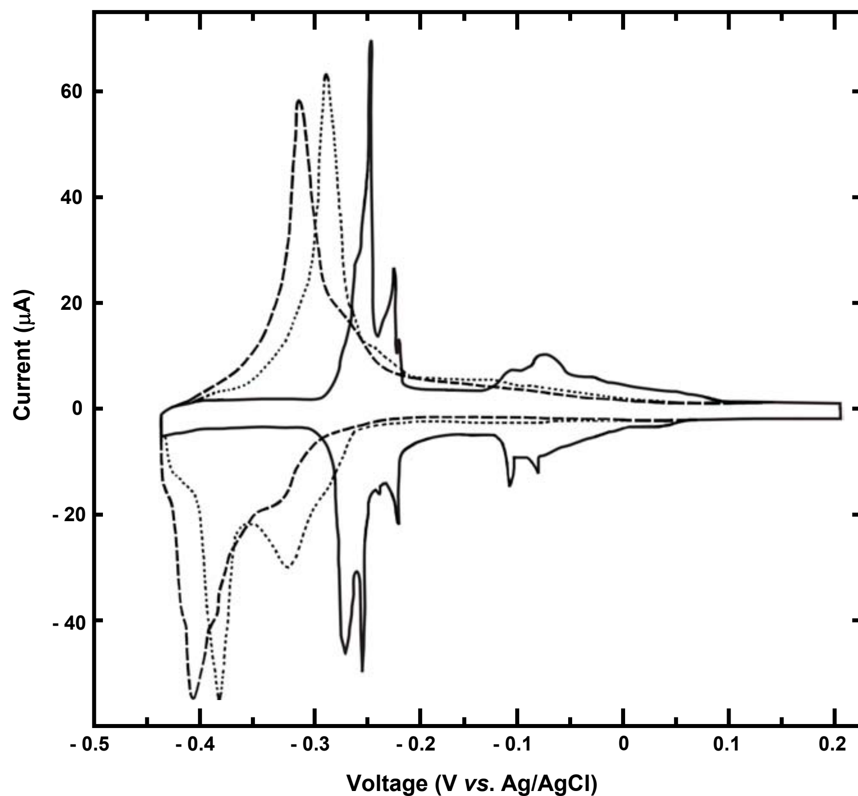

Figure 4.2 Pb CVs on bare Au(111) (solid line), on one replaced Cu nanofilm with using high chloride Cu solution (rinsing after the replacement involved) (dotted line), and on one replaced Cu nanofilm with using low chloride Cu solution (rinsing after the replacement not involved) (dashed line) (Scan rate = 5 mV/sec).

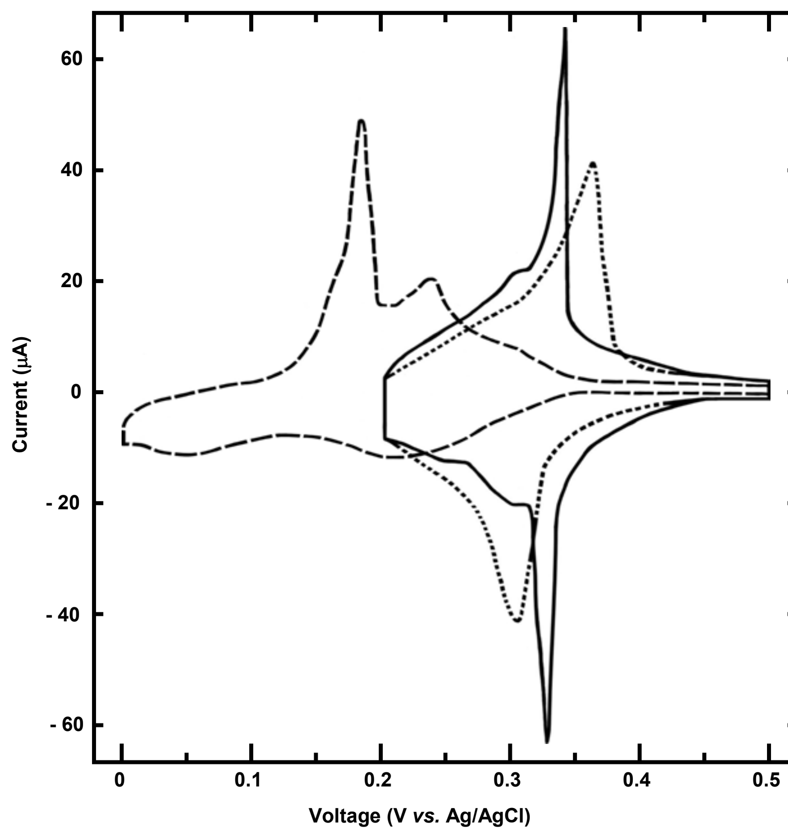

(a)

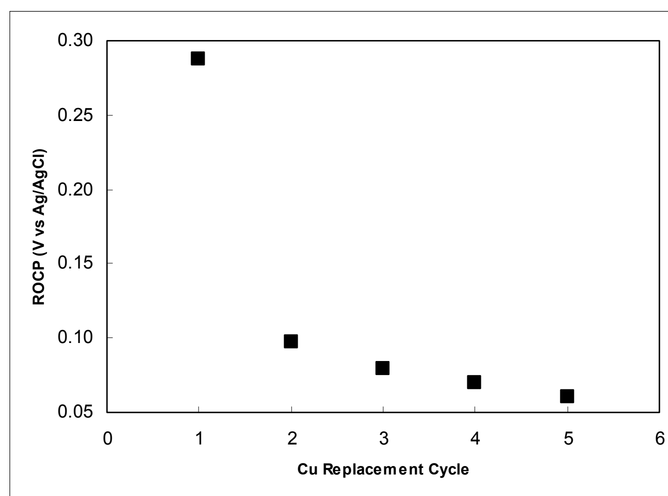

(b)

Figure 4.3 (a) Cu CVs on bare Au(111) using high chloride Cu solution (solid line), low chloride Cu solution (dotted line), and chloride-free Cu solution (dashed line) (Scan rate = 5 mV/sec). (b) Average replacement open circuit potentials (OCPs, V versus Ag/AgCl) versus each Cu replacement cycle in case of Cu SLRR with low chloride Cu solution.

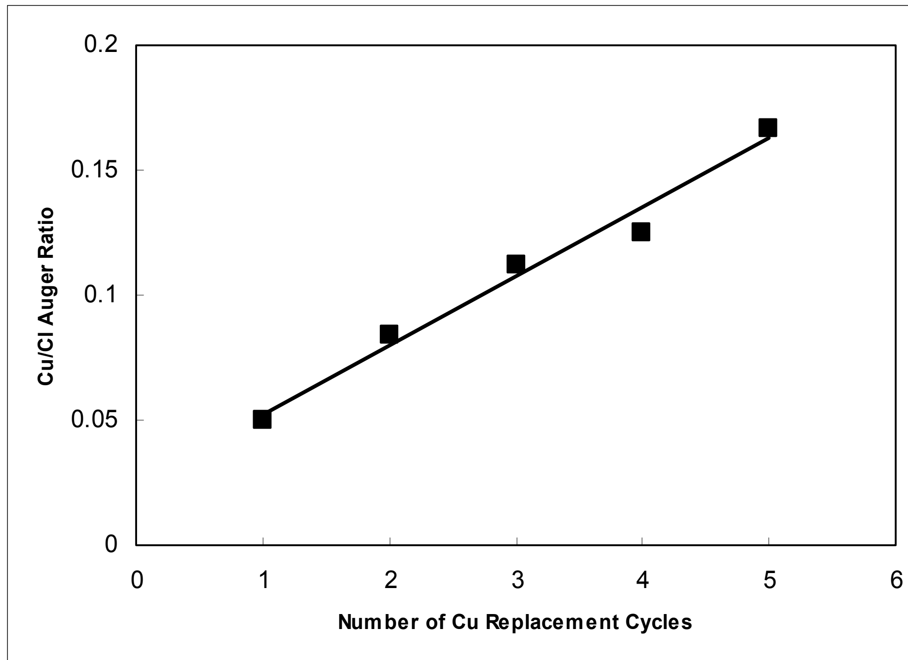

(a)

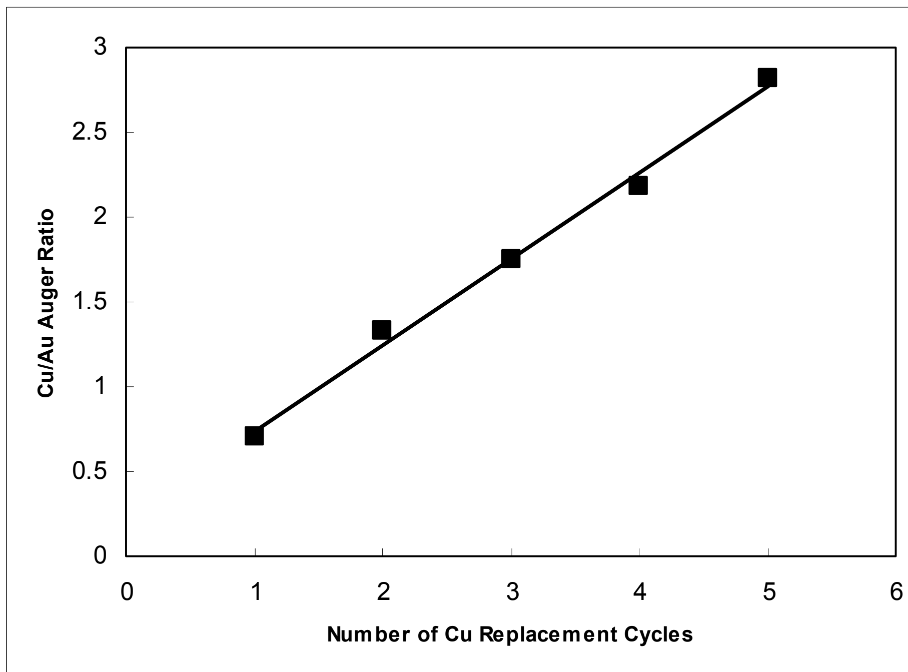

(b)

Figure 4.4 (a) Cu (920 eV) to Cl (180 eV) and (b) Cu to Au (240 eV) Auger peak ratios versus the number of Cu replacement cycles in case of Cu SLRR with low chloride Cu solution; Solid lines: the best-fit lines.

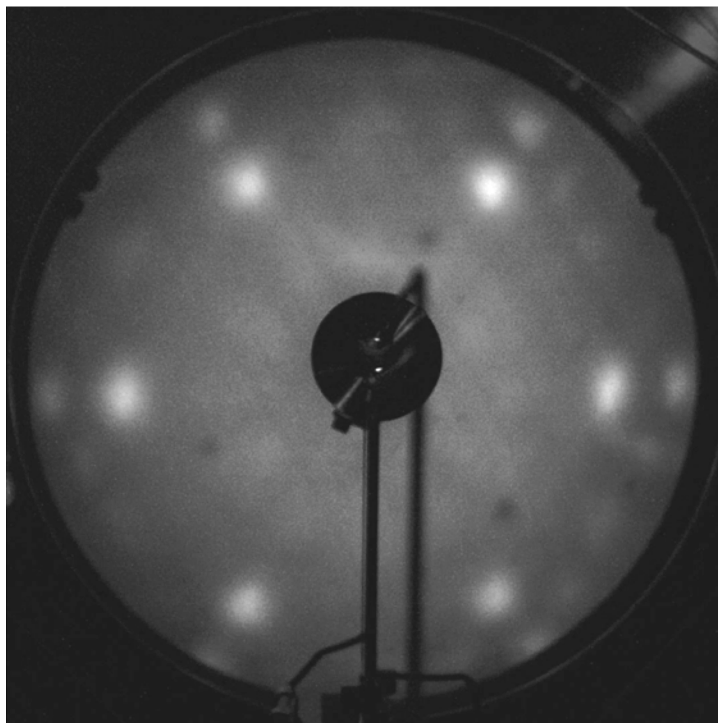

Figure 4.5 LEED patterns after Cu UPD at 0.2 V, using high chloride Cu solution and open circuit rinse (Beam energy = 50 eV).

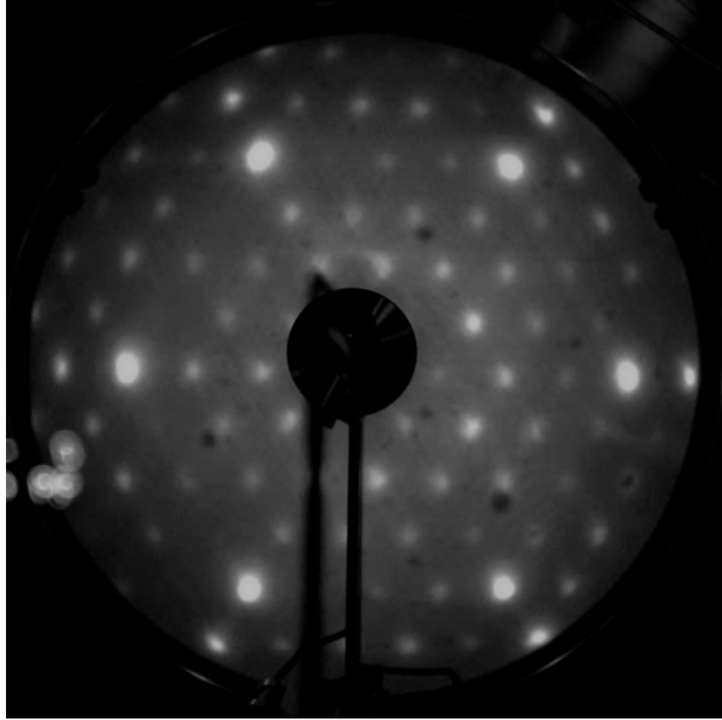

(a)

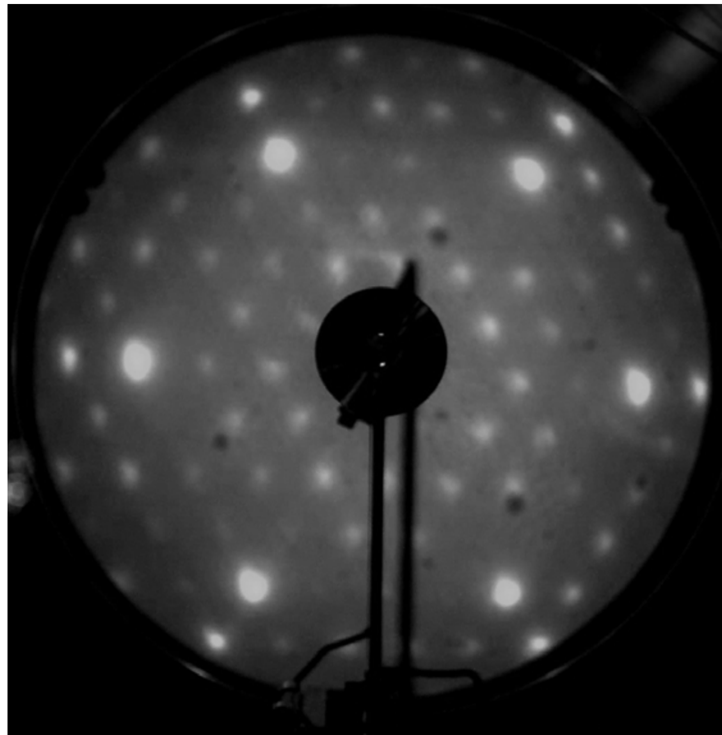

(b)

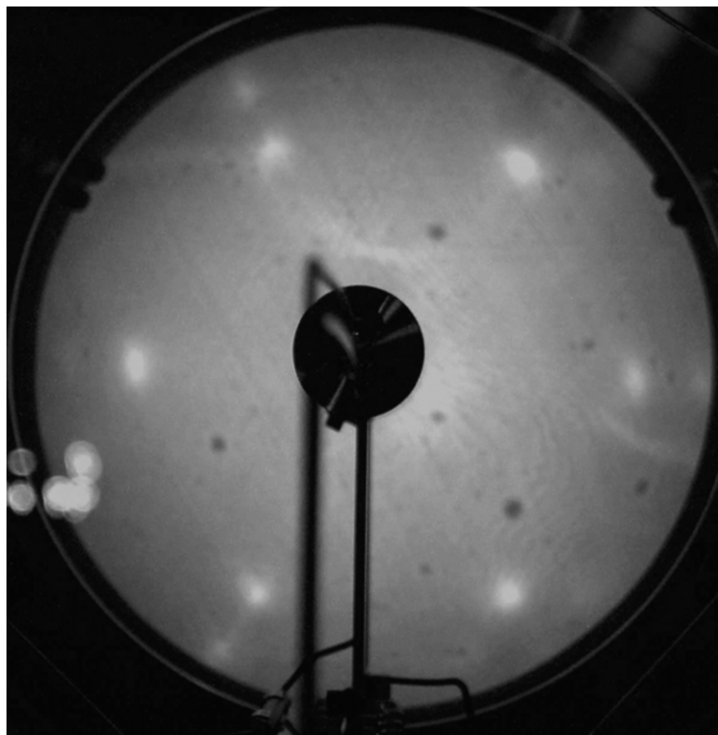

(c)

Figure 4.6 LEED patterns after (a) Cu UPD at 0.2 V, (b) one Cu replacement, and (c) five Cu replacements, using low chloride Cu solution and no open circuit rinse (Beam energy = 50 eV).

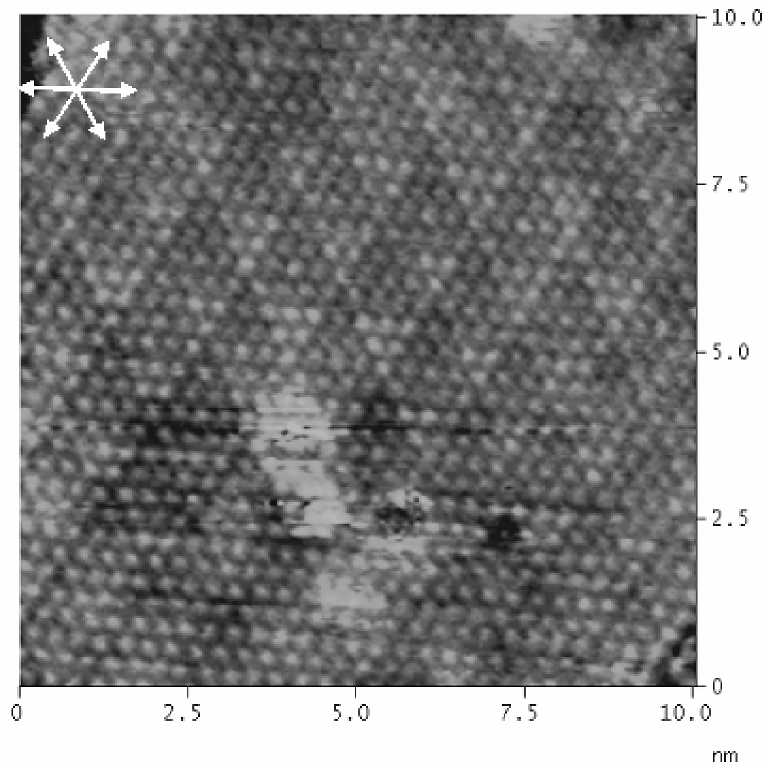

(a)

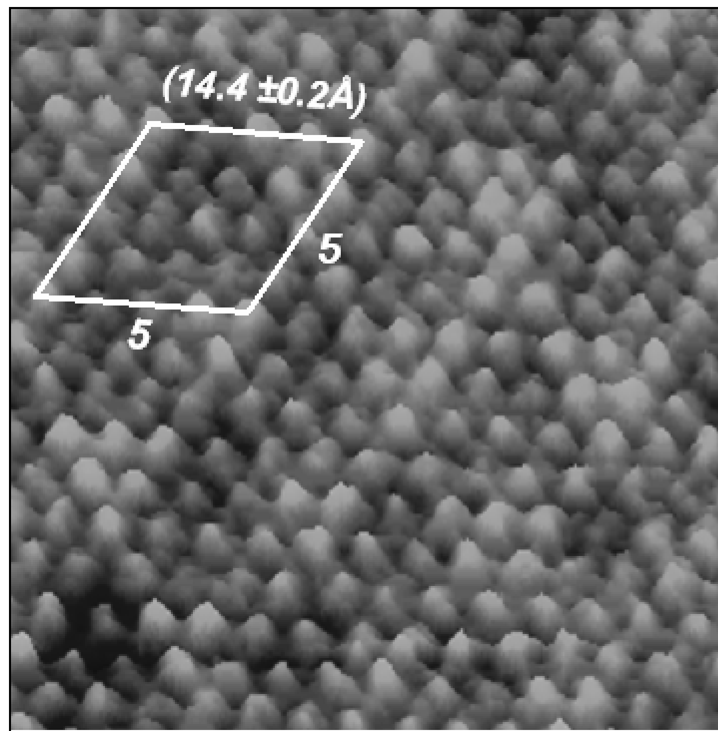

(b)

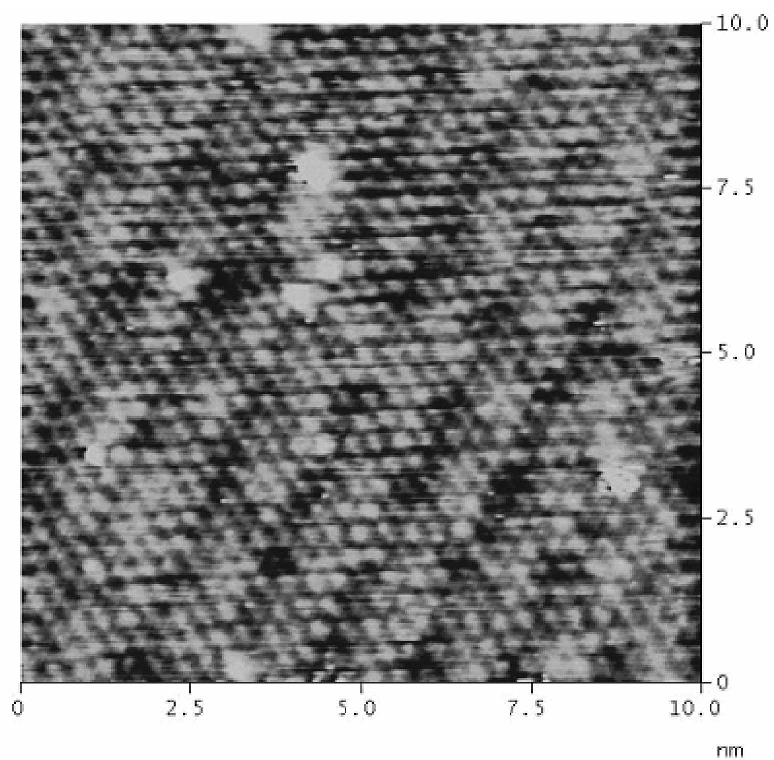

(c)

Figure 4.7 In-situ STM images of (a) Cu UPD on Au(111), 10 × 10 nm^2, (b) zoom-in image of (a), and (c) after first Cu replacement with Pb UPD on Cu UPD on Au(111), 10 × 10 nm^2.

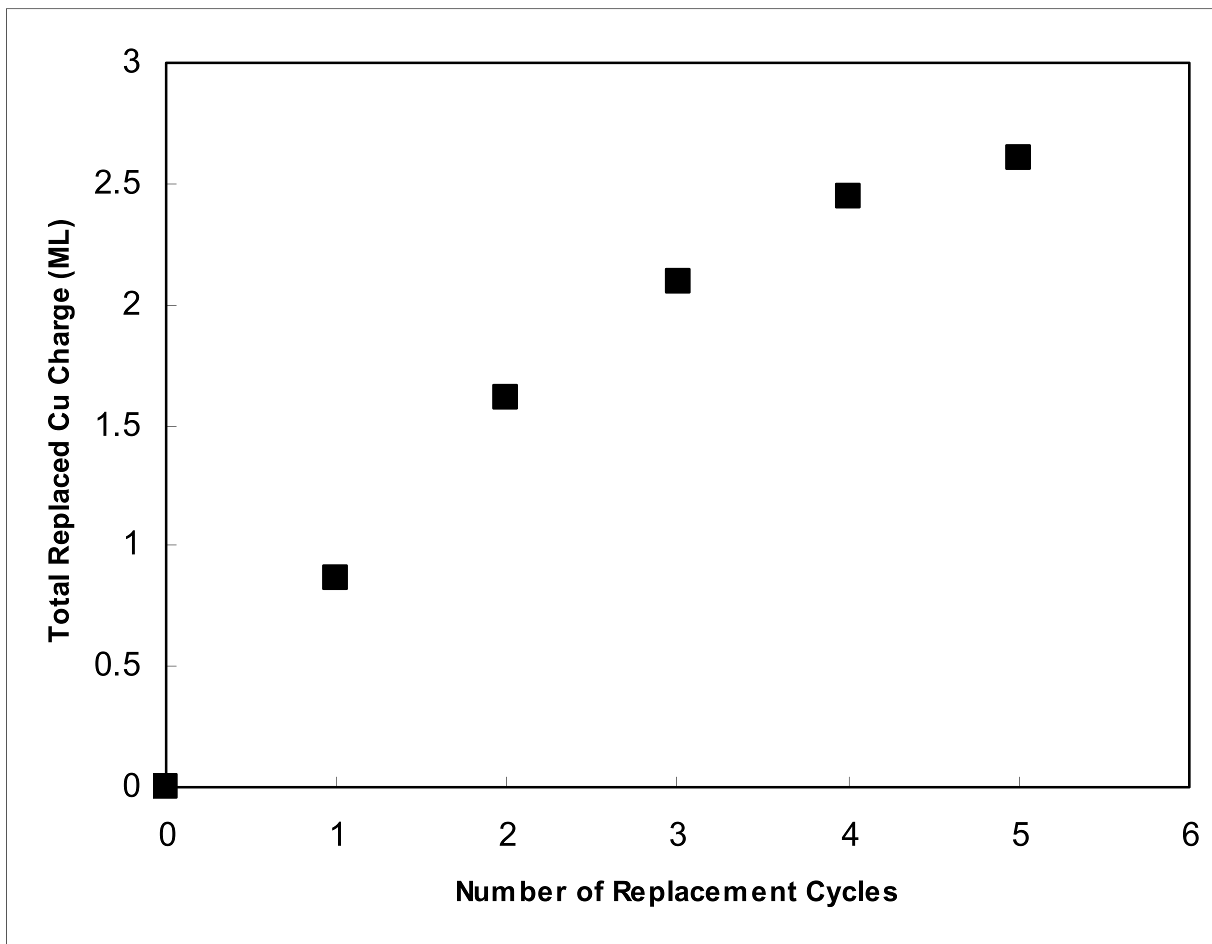

Figure 4.8 Total replaced Cu charge (ML) calculated from anodic stripping voltammetries versus the number of Cu replacement cycles in case of Cu SLRR with low chloride Cu solution.

CHAPTER 5

SURFACE STRUCTURES OF CLEAN N-GE(111) AND N-GAAS(100) SUBSTRATES : UHV-EC AND IN-SITU EC-STM STUDIES[4]

[4] J.Y. Kim, Y.-G. Kim, and J.L. Stickney, To be submitted to *Chem. Mater.* (2008).

Abstract

This article shows the surface structures of clean semiconductor substrates, n-type Ge(111) and n-type GaAs(100), by Auger electron spectra and low energy electron diffraction patterns, and their stabilities in some aqueous solutions. Hydroxylated n-Ge(111) surface formed between −0.3 V and −0.1 V in 0.1 M $HClO_4$, and hydrided surface formed between −0.4 V and −0.8 V. n-Ge(111) substrate was cleaned by UV ozone cleaning, and the Ar^+ ion bombardment. n-GaAs(100) substrate was cleaned by 10 % HF, UV ozone cleaning, and the Ar^+ ion bombardment. The hot ion bombardment and the subsequent annealing resulted in (2 × 1) n-Ge(111) and c(2 × 2) n-GaAs(100) surface structures. In-situ scanning tunneling microscopy images were also obtained in 50 mM H_2SO_4 solution. The stabilities of n-GaAs(100) were studied in pH 2, 5, and 11 solutions with cyclic voltammograms and Auger spectra.

Keywords: Semiconductor, Ion bombardment, Annealing, Auger electron spectroscopy, Low-energy electron diffraction, Scanning tunneling microscopy

Introduction

The surface structures of some semiconductor substrates, such as silicon (Si), germanium (Ge), gallium arsenide (GaAs), or indium phosphide (InP), have been intensely studied, by Auger electron spectra (AES), low-energy electron diffraction (LEED), or scanning tunneling microscopy (STM), for about a half century [1, 2]. Unlike some noble metals, such as gold, platinum, copper, or palladium, those semiconductor substrates are well-known to be vulnerable to heat. In other words, applying heat to those semiconductor substrates would lead their surfaces to reconstructions [3-5]. The cleavage face of silicon, Si(111), is a (2 × 1) structure at a room

temperature, and its reconstructed structure is well-known to be (5 × 5) and (7 × 7) at 300 ~ 600 ºC, respectively [5-13]. Further annealing to 800 ~ 900 ºC would cause the surface to disorder. The room temperature cleavage of Ge(111) results in a (2 × 1) structure, and the c(2 × 8) reconstructed structure is very well-known when annealing the substrate up to 300 ~ 500 ºC [5, 6, 14-20]. Like Si(111), Ge(111) also goes to disorder when the heat reaches up to 800 ºC, and the crystal melts at around 1000 ºC. GaAs(100) substrate has several reconstructions, depending on annealing temperatures and surface stoichiometry. When annealed to 300 ~ 600 ºC, in order of decreasing As/Ga ratio, a series of structures is formed in the order c(4 × 4), c(2 × 8), (1 × 6), (4 × 6), and c(8 × 2) [5, 21-27]. c(2 × 8) (or c(8 × 2)) structures are built out of (2 × 4) (or (4 × 2)) units, and it is reported that there are at least four serious candidates for the structure of the As dimmer (2 × 4) units [5, 28, 29]. Chadi et. al. suggested that GaAs(100) surface would be reconstructed to (2 × 2) vacancy model with Ga dimmer by calculations when half Ga covered the surface [30, 31].

Another issue regarding to semiconductor substrates has been the electrochemistry in aqueous solutions with different pH in order to study their stabilities in the solutions [32-34]. The stability of semiconductor substrates, especially anodic etching reactions of Ge or GaAs substrates, has been studied in acidic solutions, such as HCl [35-38], H_2SO_4 [39-45], $HClO_4$ [46], HIO_3 [47], or NH_4BF_4 [48], or in basic solutions, such as NaOH [49, 50], NH_4OH [36, 51], NH_4Br in liquid NH_3 [52, 53]. Prior to the electrochemistry in aqueous solutions, good ohmic contacts to the substrates [54, 55] and cleaning the substrates [32-34] are required. Semiconductor substrate cleaning is more challengeable than cleaning noble metal substrates, because the semiconductor substrates are more reactive to carbon and oxygen in the air [45, 56]. Cleaning the semiconductor substrates usually involves cleaning with organic solvent, such as

methyl chloride, acetone, methanol, ethanol, or trichloroethane, followed by etching off the substrate with impurities, using mixture of HF-HNO_3-CH_3COOH (CP4) [12, 40, 44, 46, 49, 51, 57-62], mixture of HCl-HNO_3 [37], mixture of H_2SO_4-H_2O_2-H_2O [22, 36, 42, 45, 48, 63], mixture of NH_4OH-H_2O_2-H_2O [63, 64], or Br_2/CH_3OH [36, 48, 53, 63, 65]. Ne^+, Ar^+, or Xe^+ ion sputtering or bombardment appears to be the most effective method, up to date, to remove the residual impurities on the semiconductor surface, after wet etching [1, 6, 7, 14, 15, 18-20, 43, 45, 57, 61, 66-72]. However, the ion sputtering or bombardment would result to possible rough surfaces. Therefore, the subsequent annealing is required to smooth the roughen surface. Ion sputtering or bombardment, followed by post-annealing, is then repeated until a desirable clean and reconstructed surface is obtained. That surface should be confirmed by surface analysis, such as AES, X-ray photoelectron spectroscopy (XPS), LEED, or STM. Thermal desorption of oxide [11, 73] or water [58] on the semiconductor substrate surfaces can be occurred by simple annealing the substrates.

In this article, the surface structures of n-type Ge(111) and n-type GaAs(100) semiconductor substrates were studied by ultrahigh vacuum-electrochemical (UHV-EC) surface analysis and in-situ electrochemical-scanning tunneling microscopy (EC-STM). n-type semiconductors were used in this study in order to minimize the photoeffect at negative potentials in an aqueous solution, where the substrates is expected to be in accumulation mode [32-34, 74]. The substrate cleaning procedures will be introduced in this article. Cyclic voltammograms (CV) in aqueous solutions, AES, LEED patterns, and STM images of the clean substrates were also obtained from this study.

Experimental

The n-type, Sb-doped (~ 10^{18} cm^{-3}), Ge(111)(IBM) was used as a substrate in this study. It was cut from the Ge(111) wafer into 1.0 × 2.3 cm^2. The ohmic contact was made by wrapping Au foil on top of the substrate between the molybdenum bars. Figure 5.1 shows the schematic diagram of Ge(111) substrate holder. The as-received substrate was transferred into ultrahigh vacuum (UHV) chamber, and the surface was characterized by AES (Perkin-Elmer) and LEED (Princeton Research Instruments, Inc.). The substrate was then transferred to the sealed ante-chamber for electrochemistry in an aqueous solution under room light. The ante-chamber was back-filled with ultrahigh pure (UHP) Ar gas (National Welder, 99.998 %), which would prevent contacting air when emersed (withdrawn from the solution). The solution was also deaerated with UHP Ar gas for at least 30 minutes prior to the electrochemistry, so the solution was free of possible oxygen. In electrochemical cell in this study, a gold wire was used as an auxiliary electrode, and a Ag/AgCl electrode (3 M NaCl, Bioanalytical System, Inc.) was used as a reference electrode. All potentials shown in this article are reported with respect to the reference electrode. After obtaining cyclic voltammograms from μAutolab Type III Potentiostat (Eco Chemie B.V.) in 0.1 M $HClO_4$ (Sigma-Aldrich Co.) solution and the substrate was emersed, the ante-chamber was evacuated back to UHV. The substrate was then transferred back to the main analysis chamber, without exposing to air, and AES and LEED patterns were obtained. The substrate was taken out from the UHV chamber, and some excess carbon on the substrate could be removed by ultraviolet (UV) ozone cleaning (Jelight Company, Inc.) for 5 minutes on each front and back side of the substrate. However, UV ozone cleaning usually produces a heavily oxidized surface. In that case, immersing in a diluted acid solution, such as 10 mM H_2SO_4 (Sigma-Aldrich Co.) solution, tends to dissolve much of the oxide, while scanning the potential

negatively to −1.5 V or below to reduce the remaining oxide from the surface. Any residual contamination was removed by Ar^+ ion bombardment (IBB) at room temperature, using 1 keV ions, at a current density of about 2.5 μA/cm^2. The subsequent annealing was done by flowing current through the tungsten wire which was connected to the substrate. LEED and AES were obtained to confirm that the substrate was clean and reconstructed. Ar^+ IBB with simultaneous annealing, hot IBB, and the subsequent annealing, were also done to give more distinctive LEED patterns.

The n-type GaAs(100) substrate, used in this study, was doped with Si of carrier density of about 2×10^{18} cm^{-3}. The substrate holder is described elsewhere [75]. The as-received n-GaAs(100) substrate was treated with 10 % HF acid for 5 minutes and UV ozone cleaning for 5 minutes each side. The substrate was then transferred to the ante-chamber, and the resulting oxide from UV ozone cleaning was reduced in 10 mM H_2SO_4 solution by scanning negatively to −1.5 V and below. After the oxide was reduced, the substrate was then transferred to main analysis chamber, and the surface was characterized by AES. The residual contamination was removed by Ar^+ IBB at room temperature, and the subsequent annealing served to obtain some LEED patterns with different beam energies. Hot IBB and the subsequent annealing were also tried in this case, and AES and LEED patterns were obtained.

The stability of n-GaAs(100) substrate was studied in aqueous solutions with different pH, 2, 5, and 11. 10 mM H_2SO_4 solution, 5 mM CH_3COONa/CH_3COOH (J.T. Baker) buffer solution, and 1 mM KOH (J.T. Baker) solution were used in this study as pH 2, 5, and 11 aqueous solutions, respectively. Again, CVs were obtained from the μAutolab Type III Potentiostat. Auger spectra were then obtained when emersed at the surface oxidation potentials.

In-situ STM images of a substrate were obtained with a Nanoscope III (Digital Instruments) while the substrate was in an aqueous solution. The tungsten tip was electrochemically etched in 1 M KOH (15 VAC) from a 0.25 mm wire, and the tip was coated with transparent nail polish to minimize Faradaic currents. The EC-STM flow cell used in this study was designed to allow flow and exchange of solutions over the working electrode with flow rate of 0.9 mL/min, so the solutions were exchanged without losing the potential control. The reference/auxiliary compartment was downstream, to avoid contamination.

Results and Discussion

Prior to the cleaning, the as-received n-Ge(111) substrate was put into the main analysis UHV chamber, and the surface was characterized by AES. Figures 5.2a and 5.3a show that the as-received substrate had some carbon (C/Ge ≈ 4) and oxygen (O/Ge ≈ 1.7) on the surface. The carbon on the surface could be any form of impurities, such as carbohydrate, adsorbed on the surface. The oxygen on the surface is suggested to be oxide forms of Ge adsorbed on the surface, rather than oxygen molecules adsorbed on the surface, since Ge is reactive with oxygen to form Ge oxide. The substrate was then transferred to the ante-chamber, followed by back-filling it with UHP Ar gas. The substrate was immersed in 0.1 M $HClO_4$ solution (pH 1), and the open circuit potential (OCP) showed −0.3 V. Figure 5.2b shows the cyclic voltammogram of the as-received substrate in 0.1 M $HClO_4$ solution. The potential was scanned from −0.75 V positively first, and the slightly negative current (~ −10 μA) suggests that the oxide on the surface was slightly reduced. The substrate started to be oxidized at about −0.3 V, and a shoulder oxidation feature was shown between −0.3 V and −0.1 V. This feature is suggested to be Ge oxidation to GeO, according to the Pourbaix diagram of Ge in pH 1 solution [76], and about a monolayer

(ML) of oxide formed at this potential range (−0.3 V ~ −0.1 V). A ML can be defined as the electrodeposition of one oxygen atom for each Ge surface atom (7.22×10^{14} atoms/cm^2). The Pourbaix diagram of Ge usually tells us what kind of Ge species are present in different pH solutions, depending on the applied potentials; however, the Pourbaix diagram of Ge can also be applicable to this study when Ge is studied as a substrate in different pH solutions. At −0.1 V and above is suggested to be Ge oxidized off the surface as GeO_2 form, according to the Pourbaix diagram. On negative-going scan from 0 V, a broad reduction peak, about a ML, was shown between −0.4 V and −0.8 V.

The Pourbaix diagram of Ge clearly shows that Ge oxide forms as GeO between −0.4 V and −0.1 V, and GeO_2 at −0.1 V and above, in pH 1 solution [43, 76]. However, some researchers suggested that hydroxylated surface would form on the surface as Ge-OH at −0.3 V and above in acidic solution, since Ge on the surface only has one dangling bond [40, 41, 44, 46, 77, 78]. They also suggested that hydrided surface would form as Ge-H between −0.3 V and −0.8 V. At −0.8 V and below, hydrogen evolution reaction (HER: $2H^+ + 2e^- \rightarrow H_2$ (g)) occurred. On second positive-going scan from −1.2 V, about half less oxidation occurred at −0.1 V, suggesting that H-terminated surface could be protected from the oxidation.

The substrate was emersed at −1.2 V from the second negative-going scan from 0.1 V (Figure 5.2b), and it was transferred back to main analysis chamber. The surface was characterized by AES. The Auger spectrum (Figure 5.3b) shows O/Ge Auger ratio was reduced to about 1, while C/Ge ratio increased, more contamination being caught from UHP back-filled ante-chamber. Even the ante-chamber was back-filled with UHP Ar gas, about a few mTorr of impurities may have existed, and the impurities may have been adsorbed on the surface, contaminating the substrate. The substrate was then cleaned by Ar^+ IBB at room temperature

(cold IBB) for 30 minutes, and all the oxygen was completely removed, but a trace of carbon was still on the surface (C/Ge ≈ 1, Figure 3c). UV ozone cleaning was then tried for 5 minutes, each side of the substrate. After the ozone cleaning, due to heavily oxidized surface, O/Ge Auger ratio did not change much before and after 30 minute cold IBB (Figure 5.3d and 5.3e), while a trace of carbon was completely removed after 30 minute cold IBB. To get rid of the heavily oxide on the surface, the substrate was transferred to the ante-chamber again, and the oxide on the surface was reduced in 10 mM H_2SO_4 solution (pH 2), followed by 30 minute cold IBB. The clean Ge(111) substrate was then obtained (Figure 5.3f).

When the substrate was cleaned by cold IBB only (Figure 5.3f), no LEED pattern was observed. However, after 30 minute resistive annealing, the substrate was cooled down to room temperature, and (1 × 1) LEED patterns were observed, as in Figure 5.4. Sharper pattern was obtained with higher beam energy (Figure 5.4b). Note that, in Figure 5.4b, (1, 0), (0, 1), and (−1, −1) integral beams are brighter than other integral beams. This is probably because six-fold axis of symmetry, C_6, is predominated by three-fold axis of symmetry, C_3.

30 minute IBB with annealing at the same time, hot IBB, and the subsequent 30 minute annealing were tried, the substrate was cooled down to room temperature, and LEED patterns were obtained (Figure 5.5). As in Figure 5.5, more fractional beams appear. In Figure 5.5a, with 30 eV beam energy, fractional beams appear to be splitted, and they were shown between integral beams. The splitted fractional beams suggest that there are some steps formed on the surface. Three splitted fractional beams are observed at (1/2, 0), (0, 1/2), and (−1/2, −1/2), which suggests that 30 minute hot IBB and annealing lead the substrate surface to (2 × 1) reconstructed structure [19], while only (1 × 1) surface structure was observed after 30 minute cold IBB and annealing. When increasing the beam energy to 50 eV, some more fractional beams were

observed (Figure 5.5b). The proposed top-viewed surface model of the (2 × 1) reconstructed Ge substrate after 30 minute hot IBB and annealing is shown in Figure 5.5c.

In-situ STM image of the Ge substrate was obtained in 50 mM H_2SO_4 solution at about −0.5 V (Figure 5.6). No (2 × 1) was observed in this image. However, (1 × 1) was clearly observed inside the white dashed circle in Figure 5.6, which is suggested to be the hydrated surface at this potential. The distance between the dots, hydride on each Ge atom, appears to be about 2.7 Å. Gewirth et. al. once studied the hydride growth on Ge(110) and Ge(111) by STM and atomic force microscopy (AFM) [41], and they observed rather uniform hydride growth on the substrates. Some steps are also observed in Figure 5.6, which is somehow consistent with the splitted spots in the LEED pattern, Figure 5.5a.

Spontaneous chemisorption of I^- ions on Ge substrate was studied by immersing the substrate in both 0.1 mM KI (J. T. Baker) + 0.1 M $HClO_4$ solution and 1 mM KI + 0.1 M $HClO_4$ solution at open circuit for 2 minutes. The OCP was about −0.5 V in both solutions. I^- ions are well-known for the spontaneous adsorption on some noble metal surfaces, such as Au [79-83], Pt [84-88], Cu [79, 80, 83, 89-91], and Pd [92, 93]. No iodine was observed from the AES after the substrate was emersed from 0.1 mM KI + 0.1 M $HClO_4$ solution (Figure 5.7a). Instead, much carbon (C/Ge ≈ 2.5) and oxygen (O/Ge ≈ 2) were observed in Figure 7a. These contaminations may have come from the trace of impurities in the UHP Ar gas back-filled ante-chamber. Even when the substrate was immersed in 1 mM KI + 0.1 M $HClO_4$ solution, ten times higher concentration of KI, for 2 minutes at open circuit and emersed, no iodine was observed from the AES (Figure 5.7b). However, some potassium (K) was clearly observed on the surface, instead. One possible explanation for the adsorbed K on the surface is that K^+ ions may have been exchanged with hydride on the surface in the solution at open circuit. It is promising that the

adsorbed K could protect the surface from contaminating because C/Ge and O/Ge were reduced to 1 and 0.5, respectively.

As-received n-type GaAs(100), used as a substrate in this study, was put into the main analysis UHV chamber, and AES was performed. Carbon and oxygen are observed in Figure 5.8a, and the expected Ga (1060 eV) and As (1220 eV) Auger peaks were not evident in the as-received substrate. The substrate was then taken out from the chamber, immersed in 10 % HF acid solution for 5 minutes, rinsed with Milli-Q distilled water (10^{18} MΩ-cm), and dried with nitrogen gas. The front and back side of the substrate were cleaned by UV ozone for 5 minutes each. The resulting oxide on the surface was then reduced by scanning the potential negative to −1.5 V. The emersed substrate was transferred back to main analysis chamber, and cold IBB was performed for 30 minutes. The clean n-GaAs(100) substrate, with traces of carbon and oxygen, was then obtained, confirmed by AES (Figure 5.8b). The As/Ga Auger ratio of clean substrate was appreciably observed to be 0.575 ± 0.025. Auger signals are a function of the Auger yields, and to compare coverages of two elements, the yield factors, or sensitivity factors, must be taken into account [94]. Therefore, the actual elemental As/Ga Auger ratio is: (Observed Auger ratio) ÷ (Auger sensitivity factor ratio) = $(0.575) \div (0.08/0.14) \approx 1$. This calculation, therefore, suggests that the stoichiometry of the GaAs substrate in this study is: Ga : As ≈ 1 : 1.

After 30 minute cold IBB and 30 minute subsequent annealing, the (1×1) diffused LEED patterns were observed, while 30 minute hot IBB and 30 minute subsequent annealing resulted to more distinctive $c(2 \times 2)$ LEED patterns [28-31]. Figure 5.9 shows the resulting LEED patterns with different beam energies after 30 minute hot IBB and 30 minute subsequent annealing. Note that the (1, 1), (−1, 1), (1, −1), and (−1, −1) spots appear brighter than the others in the LEED patterns with beam energies of 40 eV (Figure 5.9a) and 45 eV (Figure 5.9b), while

the other spots, (1, 0), (−1, 0), (0, 1), and (0, −1) spots, are brighter in the patterns with beam energies of 50 eV (Figure 5.9c) and 55 eV (Figure 5.9d). These LEED patterns indicate that brighter spots, (1, 1), (−1, 1), (1, −1), and (−1, −1) positions, in the patterns with 40 eV and 45 eV were diffracted from the first layer atoms, while brighter spots in the patterns with 50 eV and 55 eV were diffracted from the second layer atoms. The n-GaAs(100) top-viewed surface structure is proposed as Figure 5.9e. Identifying whether Ga or As is the first layer atom is not possible simply with AES and LEED patterns. Ion scattering spectroscopy (ISS) would elucidate what is the first substrate atom.

LEED patterns showed the distinctive (2 × 4) reconstructed surface structure when n-type InP(100) substrate was cleaned and annealed [56]. However, after metallic indium (In) was reduced in 10 mM HCl solution (pH 2), the reconstructed (2 × 4) surface was changed to a (1 × 1) unreconstructed surface. This phenomenon has not been observed with the GaAs substrate in this study. This discrepancy between InP and GaAs substrate reconstruction can be explained by the fact that GaAs substrate is more stable than InP substrate, so it is harder to be reconstructed.

The stability of n-GaAs(100) substrate in aqueous solutions with different pHs, 2, 5, and 11, was studied. The clean and annealed substrate, c(2 × 2), was immersed in pH 2 solution (10 mM H_2SO_4 solution). The OCP showed −0.5 V, and the potential was scanned negatively first from the OCP to −1 V. Figure 5.10a shows the cyclic voltammogram in pH 2 solution. No specific feature besides HER was observed in the first negative-going scan. When the potential was subsequently scanned from −1 V to 0 V, the oxidation of the substrate occurred at −0.5 V. Some photocurrent may have been involved in the oxidation feature because the CV was performed under the room light. When the substrate was emersed at 0 V, some oxide formed on the surface, observed from AES (Figure 5.11a). The subsequent negative-going scan shows no

reduction feature besides HER in Figure 5.10a, indicating that the oxide on the surface was not reduced on the negative-going scan, but only hydrogen was evoluted. Also, AES, after emersed at −1 V on the second negative-going scan from 0 V, showed some oxide still remained on the surface. Therefore, on the subsequent positive-going scan from −1 V, less oxidation shows at 0 V in Figure 10a because the remained oxide covered the surface would have prevented the surface from further surface oxidation. In pH 5 solution (5 mM CH_3COONa/CH_3COOH buffer solution) and pH 11 solution (1 mM KOH solution), the OCP showed −0.6 V and −0.9 V, respectively. The similar features as in Figure 5.10a are shown in Figure 5.10b and 5.10c. No specific features besides HER were shown on the first and the second negative-going scan from the OCP in pH 5 and pH 11 solutions, and the substrate oxidations occurred at −0.6 V and −0.9 V in pH 5 and pH 11 solutions, respectively. Less oxidation occurred on the second positive-going scans in both pH 5 and 11 solutions.

Figure 5.11 shows AES after the n-GaAs(100) substrate was emersed at the oxidation potentials in (a) pH 2 solution, (b) pH 5 solution, and (c) pH 11 solution. The clean and annealed GaAs substrate was immersed in pH 2 solution, the potential was scanned from the OCP to −1 V, and the substrate was held at 0 V for about a minute on the subsequent positive-going scan from −1 V. AES, Figure 5.11a, was then obtained. As/Ga Auger ratio increased to about 1, compared to the ratio of the clean substrate (As/Ga ≈ 0.575, Figure 5.8b), due to the Ga oxidation ($Ga^0 \rightarrow Ga^{3+} + 3e^-$) according to the Pourbaix diagram of Ga in pH 2 solution [76, 95-97]. The oxygen shown in Figure 5.11a (O/Ga ≈ 2) is suggested to be As oxide, As_2O_3, from the Pourbaix diagram of As in pH 2 solution [76, 95-97]. After the substrate was held at 0 V for a minute and emersed in pH 5 solution, Figure 5.11b was obtained. In the AES, however, a larger oxygen was observed (O/Ga ≈ 5) than in Figure 5.11a, while the As/Ga Auger ratio (~ 0.5) remained almost

the same as the clean substrate. The Pourbaix diagrams of Ga and As clearly show that both Ga_2O_3 and As_2O_3 form at 0 V in pH 5 solution, so the larger oxygen was due to the Ga and As oxide, which is consistent with the XPS studies in literatures [36, 48], with no Ga and As lost. In pH 11 solution, the potential was scanned from the OCP to −1.8 V, was held at −0.25 V for about a minute on the subsequent positive-going scan, the substrate was emersed, and AES (Figure 5.11c) was then obtained. In this case, a large K was observed (K/Ga ≈ 7). It can be suggested that Ga atoms were spontaneously replaced by K^+ ions ($Ga^0 + 3K^+ \rightarrow Ga^{3+} + 3K^0$), since As/Ga Auger ratio was increased to 1, indicating some Ga was lost. However, it is promising that less oxygen (O/Ga ≈ 1.5) was observed than expected in pH 11 solution (Figure 5.11c), suggesting that K adsorbed on the surface would have somehow protected the surface from oxidation. The fact that no LEED patterns were shown at the emersed potentials described above in each solution suggests that the oxides on the surfaces made the surfaces disordered at those potentials.

Conclusions

The surface structures and stabilities in aqueous solutions of n-Ge(111) and n-GaAs(100) substrates were studied. n-Ge(111) substrate started to be oxidized from −0.3 V and the hydroxylated Ge, Ge-OH, formed between −0.3 V and −0.1 V. At −0.1 V and above, the substrate is suggested to be dissolved as GeO_2 form. On the subsequent negative-going scan from 0 V, hydrided Ge, Ge-H, formed between −0.3 V and −0.8 V, and below −0.8 V, hydrogen was evoluted. n-Ge(111) substrate was then cleaned by UV ozone cleaning. The reduction, in 10 mM H_2SO_4 solution, of the resulting oxide formed on the surface and the following Ar^+ IBB resulted in the clean substrate. The 30 minute hot IBB and the 30 minute subsequent annealing

resulted in the surface structure with the splitted (2 × 1) LEED pattern. The desirable c(2 × 8) LEED pattern was not observed in this study. That is probably because the substrate has not been reached the reconstructed temperature when annealing. The efficiency of heat transferring from the tungsten wire to the substrate should be improved. In-situ STM image of the substrate in 50 mM H_2SO_4 showed (111) surface and the distance between the surface atoms was measured about 2.7 Å. Iodine atoms did not appear to be adsorbed on the substrate, instead, potassium was observed on the surface.

n-GaAs(100) substrate was cleaned by 10 % HF treatment, UV ozone cleaning, reduction in 10 mM H_2SO_4 solution, and the following IBB. The hot IBB and the subsequent annealing resulted in the c(2 × 2) substrate. The substrate started to be oxidized at −0.5 V, −0.6 V, and −0.9 V in pH 2, 5, and 11 solutions, respectively. From the Auger spectra, some oxides formed at near 0 V in three solutions, but no oxide reduction evidence was shown on the subsequent negative-going scans. The oxide formed on the surface was not totally reduced on the subsequent negative-going scan from the Auger spectra. When emersed at 0 V in pH 2 solution, Ga was oxidized to Ga^{3+} ions, and As oxide formed. When emersed at 0 V in pH 5 solution, both Ga oxide and As oxide are suggested to form. When emersed at −0.25 V in pH 11 solution, large potassium and less oxide formed on the surface. This potassium is suggested to be exchanged with Ga atoms, since As/Ga Auger ratio increased. No LEED patterns were observed after emersed at those potentials in three solutions.

Acknowledgements

The financial support from National Science Foundation, Divisions of Materials and Chemistry, and the Department of Energy, is gratefully acknowledged.

References

1. R.E. Schlier and H.E. Farnsworth, *J. Chem. Phys.*, **30**, 917 (1959).
2. J.A. Venables, *Introduction to Surface and Thin Film Processes*, Cambridge University Press, Cambridge, 2000.
3. J.P. LaFemina, *Surf. Sci. Rep.*, **16**, 133 (1992).
4. C.B. Duke, *Appl. Surf. Sci.*, **65**, 543 (1993).
5. C.B. Duke, *Chem. Rev.*, **96**, 1237 (1996).
6. R.S. Becker, B.S. Swartzentruber, J.S. Vickers, and T. Klitsner, *Phys. Rev. B*, **39**, 1633 (1989).
7. W. Bock, H. Gnaser, and H. Oechsner, *Surf. Sci.*, **282**, 333 (1993).
8. S. Yoshida, M. Itoh, N. Yamamoto, T. Nagamura, M. Oyama, and S. Okazaki, *Langmuir*, **15**, 6813 (1999).
9. H.-C. Jeong and E.D. Williams, *Surf. Sci. Rep.*, **34**, 171 (1999).
10. P. Sobotik, I. Ost'adal, J. Myslivecek, and T. Jarolimek, *Surf. Sci.*, **454**, 847 (2000).
11. S.E. Sysoev, D.V. Potapenko, A.V. Ermakov, B.J. Hinch, D.R. Strongin, A.P. Wright, and C. Kuivila, *J. Phys. Chem. B*, **106**, 2018 (2002).
12. J.S. Pan, R.S. Liu, Z. Zhang, S.W. Poon, W.J. Ong, and E.S. Tok, *Surf. Sci.*, **600**, 1308 (2006).
13. S. Stepanovsky, M. Yakes, V. Yeh, M. Hupalo, and M.C. Tringides, *Surf. Sci.*, **600**, 1417 (2006).
14. P.W. Palmberg and W.T. Peria, *Surf. Sci.*, **6**, 57 (1967).
15. B.Z. Olshanetsky, S.M. Repinsky, and A.A. Shklyaev, *Surf. Sci.*, **69**, 205 (1977).
16. B.Z. Olshanetsky, V.I. Mashanov, and A.I. Nikiforov, *Surf. Sci.*, **111**, 429 (1981).

17. J.J. Metois and G. LeLay, *Surf. Sci.*, **133**, 422 (1983).

18. R.S. Becker, J.A. Golovchenko, and B.S. Swartzentruber, *Phys. Rev. Lett.*, **54**, 2678 (1985).

19. R.J. Phaneuf and M.B. Webb, *Surf. Sci.*, **164**, 167 (1985).

20. T. Klitsner and J.S. Nelson, *Phys. Rev. Lett.*, **67**, 3800 (1991).

21. M.D. Pashley, K.W. Haberern, W. Friday, J.M. Woodall, and P.D. Kirchner, *Phys. Rev. Lett.*, **60**, 2176 (1988).

22. D.K. Biegelsen, R.D. Bringans, J.E. Northrup, and L.E. Swartz, *Phys. Rev. B*, **41**, 5701 (1990).

23. T. Hashizume, Q.K. Xue, J. Zhou, A. Ichimiya, and T. Sakurai, *Phys. Rev. Lett.*, **73**, 2208 (1994).

24. J.M. Heitzinger, J.M. White, and J.G. Ekerdt, *Surf. Sci.*, **300**, 892 (1994).

25. Q.K. Xue, T. Hashizume, J.M. Zhou, T. Sakata, T. Ohno, and T. Sakurai, *Phys. Rev. Lett.*, **74**, 3177 (1995).

26. I. Chizhov, G. Lee, R.F. Willis, D. Lubyshev, and D.L. Miller, *Surf. Sci.*, **419**, 1 (1998).

27. J.J. Kolodziej, B. Such, M. Goryl, F. Krok, P. Piatkowski, and M. Szymonski, *Appl. Surf. Sci.*, **252**, 7614 (2006).

28. J.E. Northrup and S. Froyen, *Phys. Rev. Lett.*, **71**, 2276 (1993).

29. J.E. Northrup and S. Froyen, *Phys. Rev. B*, **50**, 2015 (1994).

30. G.-X. Qian, R.M. Martin, and D.J. Chadi, *J. Vac. Sci. Tech. B*, **5**, 933 (1987).

31. G.-X. Qian, R.M. Martin, and D.J. Chadi, *Phys. Rev. B*, **38**, 7649 (1988).

32. N.S. Lewis and A.B. Bocarsly, in *Semiconductor Electrodes*, H.O. Finklea (Ed.), Elsevier Science Publishers B.V., Amsterdam, 1988.

33. K.W. Frese Jr., in *Semiconductor Electrodes*, H.O. Finklea (Ed.), Elsevier, New York, 1988.

34. R. Memming, *Semiconductor Electrochemistry*, Wiley-VCH, Weinheim, 2001.

35. M. Green, *J. Phys. Chem. Solids*, **14**, 77 (1960).

36. T. Solomun, R. McIntyre, W. Richtering, and H. Gerischer, *Surf. Sci.*, **169**, 414 (1986).

37. M. Koinuma and K. Uosaki, *J. Vac. Sci. Technol. B*, **12**, 1543 (1994).

38. A. Nemcsics, M. Schuszter, L. Dobos, and G. Ballai, *Mater. Sci. Eng. B*, **90**, 67 (2002).

39. W.W. Harvey, *J. Phys. Chem. Solids*, **14**, 82 (1960).

40. R. Memming and G. Neumann, *J. Electroanal. Chem.*, **21**, 295 (1969).

41. K.D. Kepler and A.A. Gewirth, *Surf. Sci.*, **303**, 101 (1994).

42. H. Yao, S.-L. Yau, and K. Itaya, *Appl. Phys. Lett.*, **68**, 1473 (1996).

43. B.W. Gregory, S. Thomas, S.M. Stephens, R.A. Dluhy, and L.A. Bottomley, *Langmuir*, **13**, 6146 (1997).

44. C. Ehlers, U. Konig, and J.W. Schultze, *Electrochimica Acta*, **49**, 129 (2003).

45. L.C. Ward, M. Muthuvel, and J.L. Stickney, *Proc. Electrochem. Soc.*, **2003-11**, 152 (2003).

46. C. Ehlers, U. Konig, G. Staikov, and J.W. Schultze, *Electrochim. Acta*, **47**, 379 (2001).

47. P.J. Verpoort, I.E. Vermeir, and W.P. Gomes, *J. Electroanal. Chem.*, **411**, 67 (1996).

48. T. Solomun, W. Richtering, and H. Gerischer, *Phys. Chem. Chem. Phys.*, **91**, 412 (1987).

49. T. Thundat, L.A. Nagahara, and S.M. Lindsay, *J. Vac. Sci. Technol. A*, **8**, 539 (1990).

50. S. Eriksson, P. Carlsson, B. Holmstrom, and K. Uosaki, *J. Electroanal. Chem.*, **313**, 121 (1991).

51. W.H. Brattain and P.J. Boddy, *Surf. Sci.*, **4**, 18 (1966).

52. A.M. Goncalves, C. Mathieu, M. Herlem, and A. Etcheberry, *J. Electroanal. Chem.*, **420**, 25 (1997).

53. O. Seitz, C. Mathieu, A.M. Goncalves, M. Herlem, and A. Etcheberry, *J. Electrochem. Soc.*, **150**, E461 (2003).

54. V.L. Rideout, *Solid-State Electron.*, **18**, 541 (1975).

55. A.G. Baca, F. Ren, J.C. Zolper, R.D. Briggs, and S.J. Pearton, *Thin Solid Films*, **308**, 599 (1997).

56. M. Muthuvel and J.L. Stickney, *J. Electrochem. Soc.*, **153**, C67 (2006).

57. M.T. Thomas, S. Shimaoka, and J.A. Dillon, *Surf. Sci.*, **6**, 261 (1967).

58. J. Sochanski and H.C. Gatos, *Surf. Sci.*, **13**, 393 (1969).

59. H.F. Winters and J.W. Coburn, *Surf. Sci. Rep.*, **14**, 161 (1992).

60. Z.H. Lu, B. Bryskiewicz, J. McCaffrey, Z. Wasilewski, and M.J. Graham, *J. Vac. Sci. Technol. B*, **11**, 2033 (1993).

61. M. Tanaka, M. Takeguchi, H. Yasuda, and K. Furuya, *Thin Solid Films*, **398**, 374 (2001).

62. W. Shao, G. Pattanaik, and G. Zangari, *J. Electrochem. Soc*, **154**, D339 (2007).

63. M. Beerbom, O. Henrion, A. Klein, T. Mayer, and W. Jaegermann, *Electrochim. Acta*, **45**, 4663 (2000).

64. R.F. Kopf, A.P. Kinsella, and C.W. Ebert, *J. Vac. Sci. Technol. B*, **9**, 132 (1991).

65. M. Beerbom, T. Mayer, and W. Jaegermann, *J. Phys. Chem. B*, **104**, 8503 (2000).

66. L. Seehofer, G. Falkenberg, and R.L. Johnson, *Surf. Sci.*, **290**, 15 (1993).

67. F.L. Metcalfe and J.A. Venables, *Surf. Sci.*, **369**, 99 (1996).

68. M. Gothelid, G. LeLay, C. Wigren, M. Bjorkqvist, and U.O. Karlsson, *Surf. Sci.*, **371**, 264 (1997).

69. V.S. Smentkowski, *Prog. Surf. Sci.*, **64**, 1 (2000).

70. L. Floreano, D. Cvetko, F. Bruno, G. Bavdek, A. Cossaro, R. Gotter, A. Verdini, and A. Morgante, *Prog. Surf. Sci.*, **72**, 135 (2003).

71. H.M. Zhang and R.I.G. Uhrberg, *Surf. Sci.*, **546**, L789 (2003).

72. M. Zier, S. Oswald, R. Reiche, M. Kozlowska, and K. Wetzig, *J. Electron Spec. Related Phenomena*, **137**, 229 (2004).

73. A. Guillen-Cervantes, Z. Rivera-Alvarez, M. Lopez-Lopez, E. Lopez-Luna, and I. Hernandez-Calderon, *Thin Solid Films*, **373**, 159 (2000).

74. J.J. Kelly and D. Vanmaekelbergh, in *Electrochemistry of Nanomaterials*, G. Hodes (Ed.), Wiley-VCH, Weinheim, 2001.

75. J.Y. Kim and J.L. Stickney, *Electrochem. Soc. Trans.*, **11**, 145 (2007).

76. M.J.N. Pourbaix, *Atlas of Electrochemical Equilibria in Aqueous Solutions*, Pergamon Press, Oxford, 1949.

77. H. Gerischer, A. Mauerer, and W. Mindt, *Surf. Sci.*, **4**, 431 (1966).

78. H. Gerischer and W. Mindt, *Surf. Sci.*, **4**, 440 (1966).

79. A. Martinez-Ruiz, J. Valenzuela-Benavides, L.M. de la Garza, and N. Batina, *Surf. Sci.*, **476**, 139 (2001).

80. A. Martinez-Ruiz, M. Palomar-Pardave, J. Valenzuela-Benavides, M.H. Farias, and N. Batina, *J. Phys. Chem. B*, **107**, 11660 (2003).

81. Y.-G. Kim, J.Y. Kim, D. Vairavapandian, and J.L. Stickney, *J. Phys. Chem. B*, **110**, 17998 (2006).

82. Y.-G. Kim, J.Y. Kim, C. Thambidurai, and J.L. Stickney, *Langmuir*, **23**, 2539 (2007).

83. J.Y. Kim, Y.-G. Kim, and J.L. Stickney, *J. Electrochem. Soc.*, **154**, D260 (2007).

84. A.T. Hubbard, J.L. Stickney, S.D. Rosasco, M.P. Soriaga, and D. Song, *J. Electroanal. Chem.*, **150**, 165 (1983).

85. J.L. Stickney, S.D. Rosasco, D. Song, M.P. Soriaga, and A.T. Hubbard, *Surf. Sci.*, **130**, 326 (1983).

86. J.L. Stickney, S.D. Rosasco, and A.T. Hubbard, *J. Electrochem. Soc.*, **131**, 260 (1984).

87. A. Wieckowski, B.C. Schardt, S.D. Rosasco, J.L. Stickney, and A.T. Hubbard, *Surf. Sci.*, **146**, 115 (1984).

88. J.L. Stickney, D.A. Stern, B.C. Schardt, D.C. Zapien, A. Wieckowski, and A.T. Hubbard, *J. Electroanal. Chem.*, **213**, 293 (1986).

89. H. Matsumoto, J. Inukai, and M. Ito, *J. Electroanal. Chem.*, **379**, 223 (1994).

90. J. Inukai, Y. Osawa, and K. Itaya, *J. Phys. Chem. B*, **102**, 10034 (1998).

91. S. Huemann, N.T.M. Hai, P. Broekmann, K. Wandelt, H. Zajonz, H. Dosch, and F. Renner, *J. Phys. Chem. B*, **110**, 24955 (2006).

92. Y.-G. Kim and M.P. Soriaga, *J. Phys. Chem. B*, **102**, 6188 (1998).

93. Y.G. Kim, J.H. Baricuatro, M.P. Soriaga, and D.W. Suggs, *J. Electroanal. Chem.*, **509**, 170 (2001).

94. L.E. Davis, N.C. MacDonald, P.W. Palmberg, G.E. Riach, and R.E. Weber, *Handbook of Auger Electron Spectroscopy*, Physical Electronics Industries, Inc., Eden Prairie, 1976.

95. G.G. Perrault, *J. Electrochem. Soc*, **136**, 2845 (1989).

96. I. Villegas and J.L. Stickney, *J. Electrochem. Soc.*, **139**, 686 (1992).

97. I. Villegas and J.L. Stickney, *J. Vac. Sci. Technol. A*, **10**, 3032 (1992).

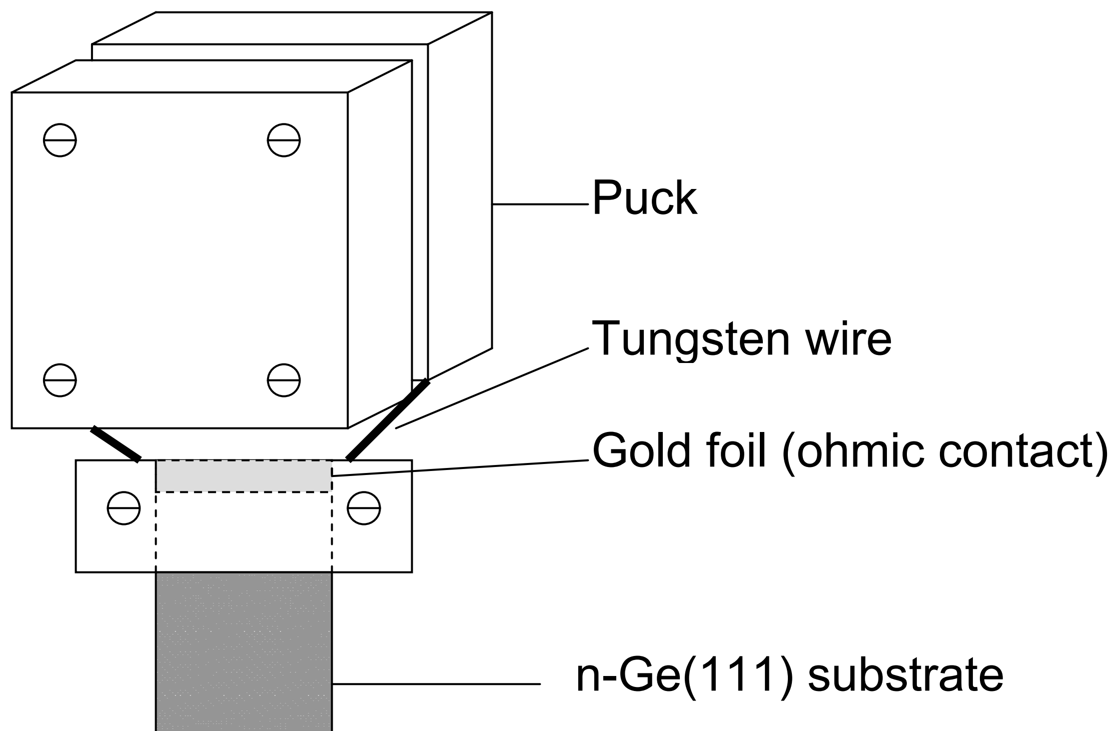

Figure 5.1 Schematic diagram of the n-Ge(111) substrate holder.

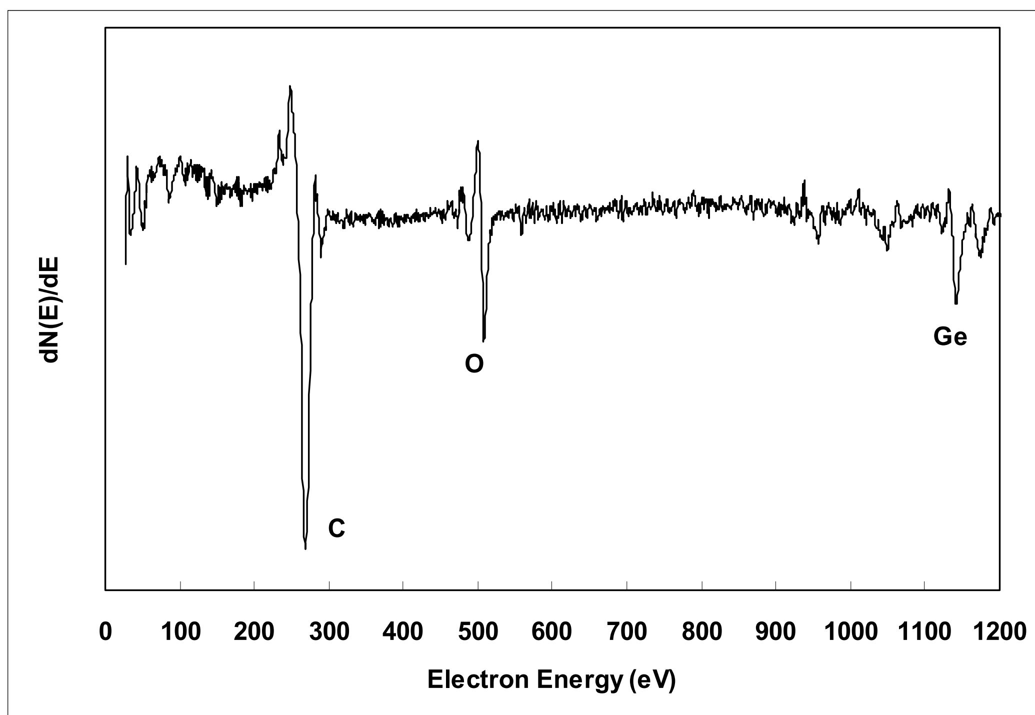

(a)

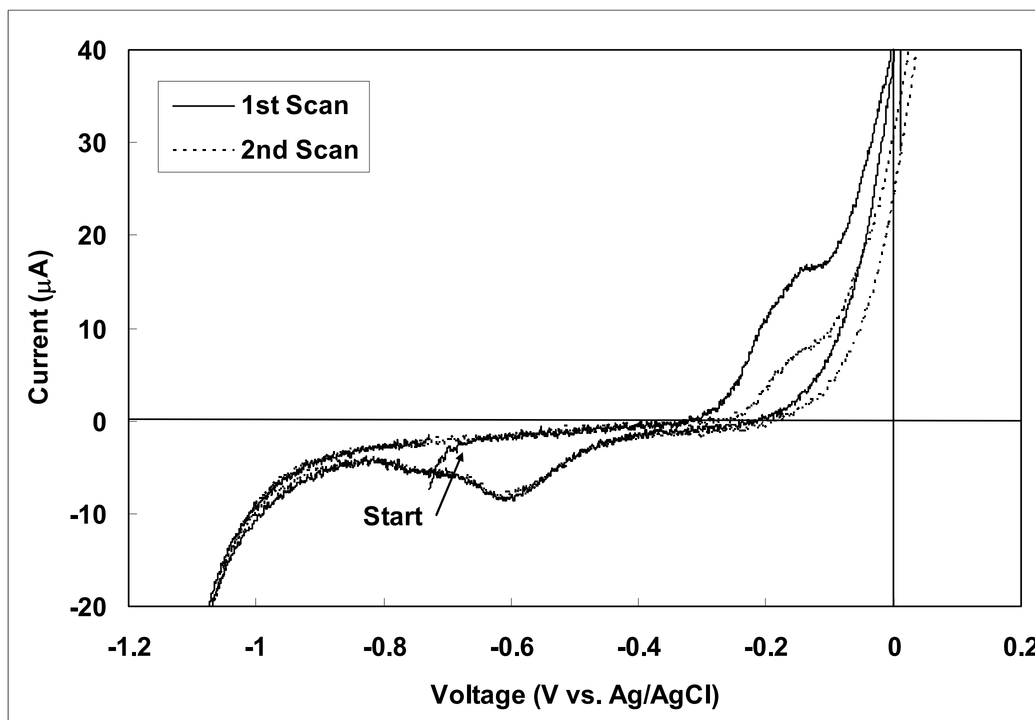

(b)

Figure 5.2 (a) Auger electron spectrum of the as-received n-Ge(111) substrate and (b) cyclic voltammogram of the as-received n-Ge(111) substrate in 0.1 M $HClO_4$ solution (pH 1).

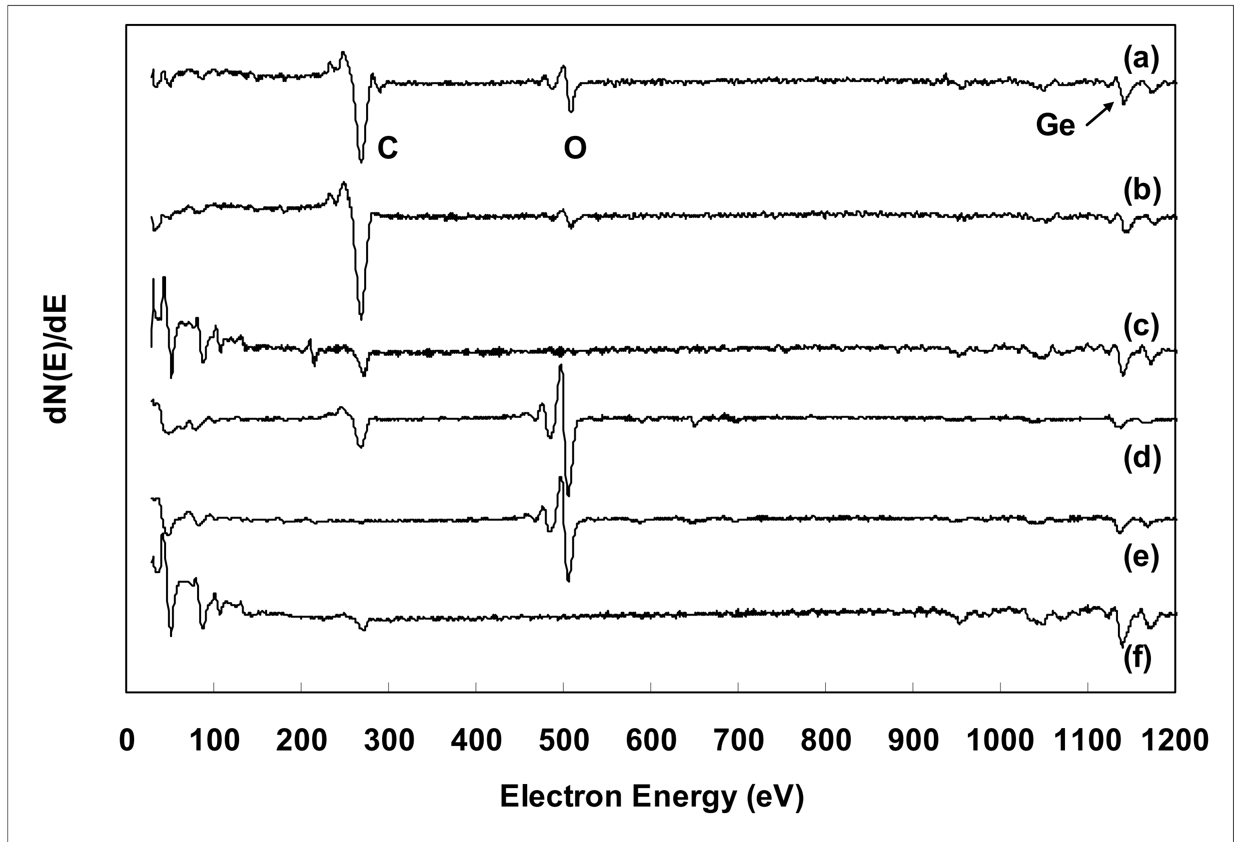

Figure 5.3 Auger electron spectra of (a) the as-received n-Ge(111) substrate, (b) after reducing the oxide on the surface in 0.1 M $HClO_4$ solution, (c) after the subsequent 30 min cold ion bombardment (IBB), (d) after 5 minute UV ozone cleaning both sides, (e) after the subsequent 30 min cold IBB, and (f) after reducing the oxide on the surface in 10 mM H_2SO_4 solution and the subsequent 30 min cold IBB.

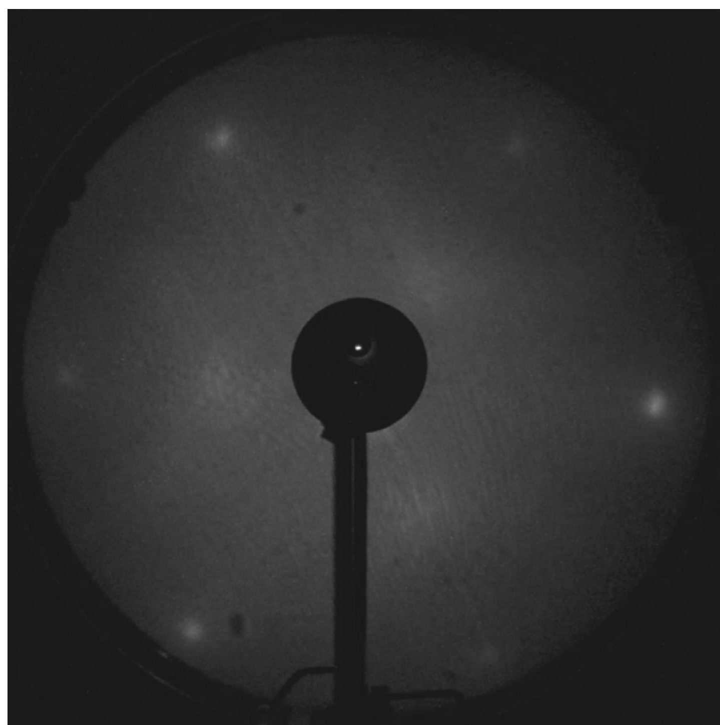

(a)

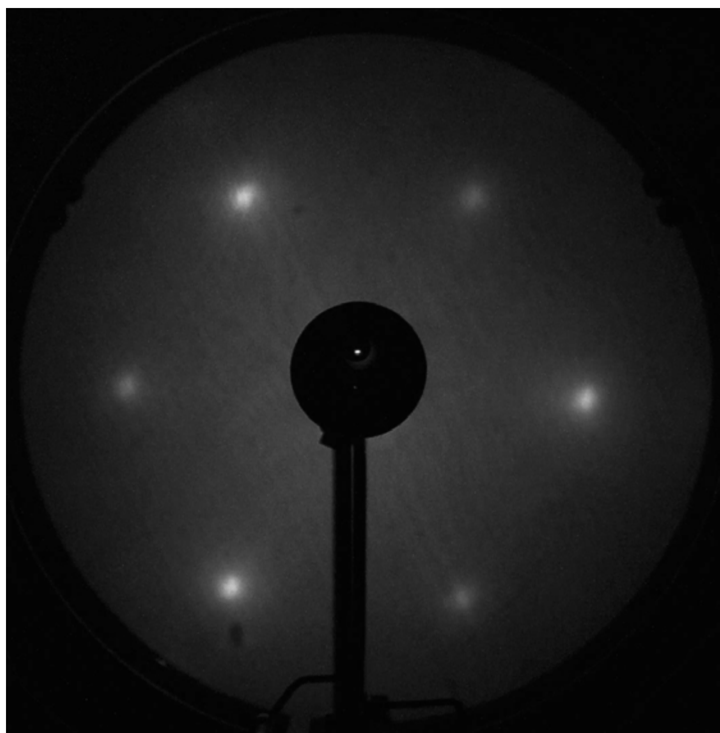

(b)

Figure 5.4 Low energy electron diffraction patterns after 30 minute cold IBB and the subsequent 30 minute annealing with the beam energies of (a) 30 eV and (b) 50 eV.

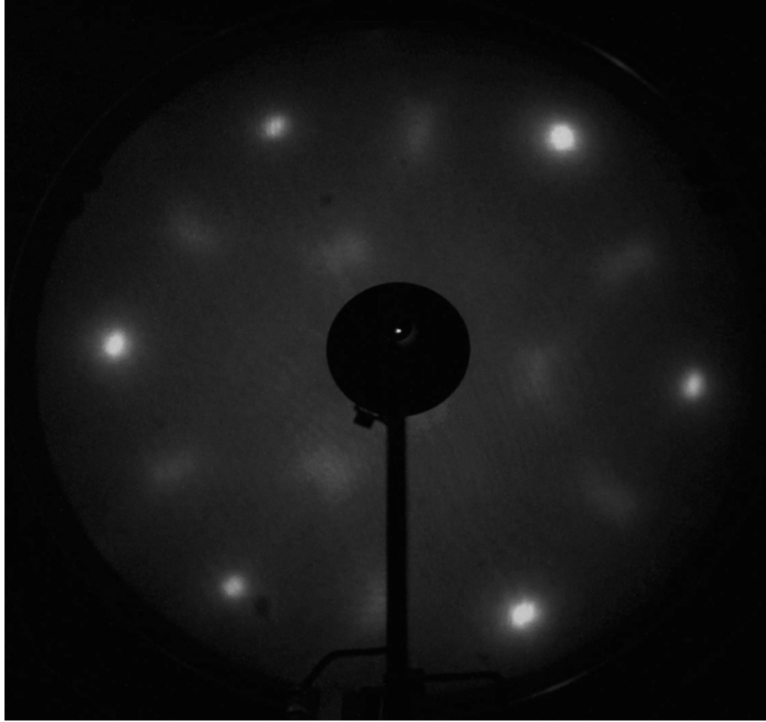

(a)

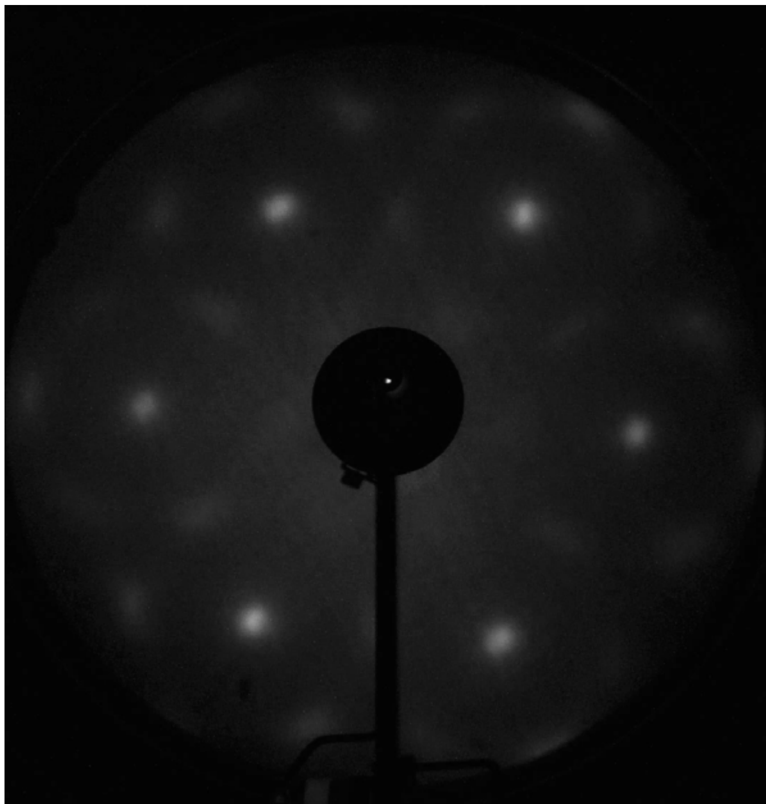

(b)

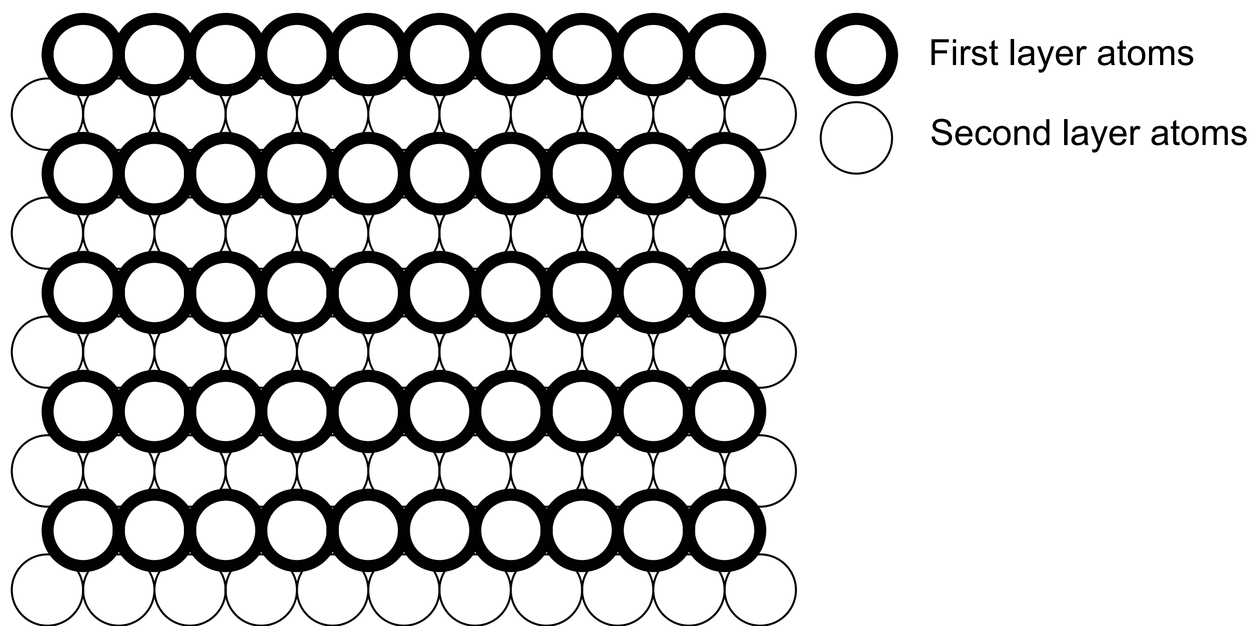

(c)

Figure 5.5 Low energy electron diffraction patterns after 30 minute hot IBB and the subsequent 30 minute annealing with the beam energies of (a) 30 eV and (b) 50 eV, and (c) the proposed top-viewed n-Ge(111) substrate surface model after the hot IBB and annealing.

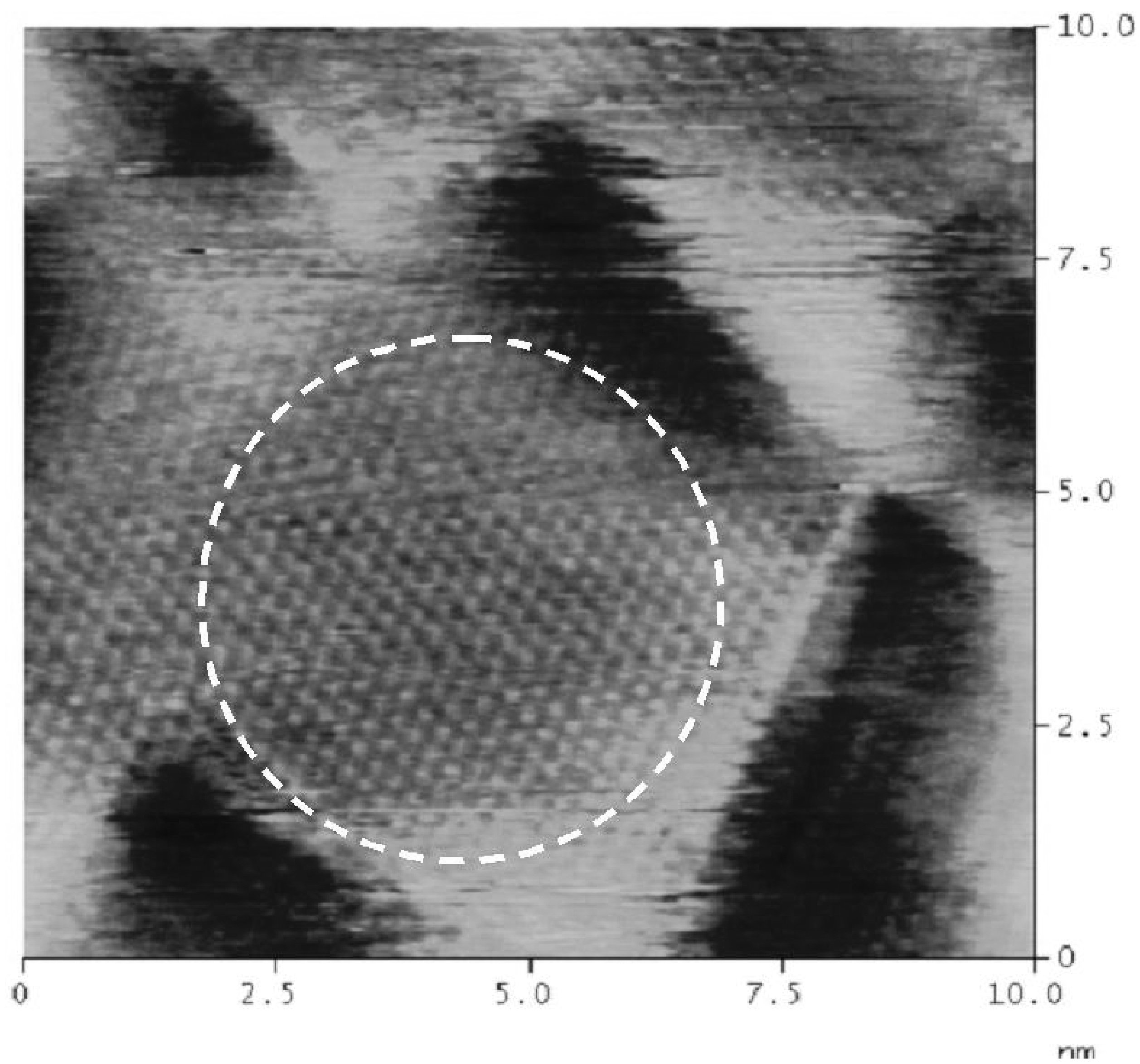

Figure 5.6 In-situ scanning tunneling microscopy image of clean n-Ge(111) substrate in 50 mM H_2SO_4 at about −0.5 V.

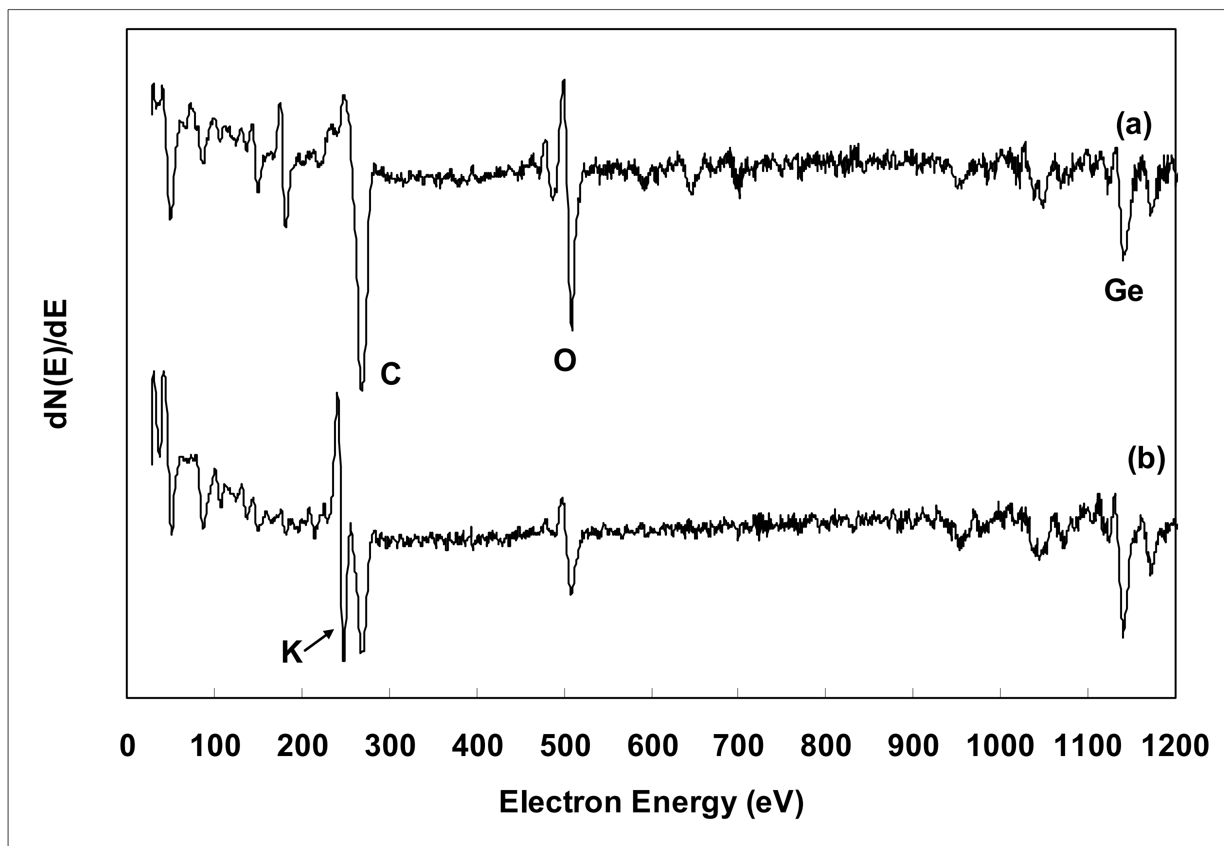

Figure 5.7 Auger electron spectra after immersing in (a) 0.1 mM KI + 0.1 M $HClO_4$ solution for 2 minutes and (b) 1 mM KI + 0.1 M $HClO_4$ solution for 2 minutes.

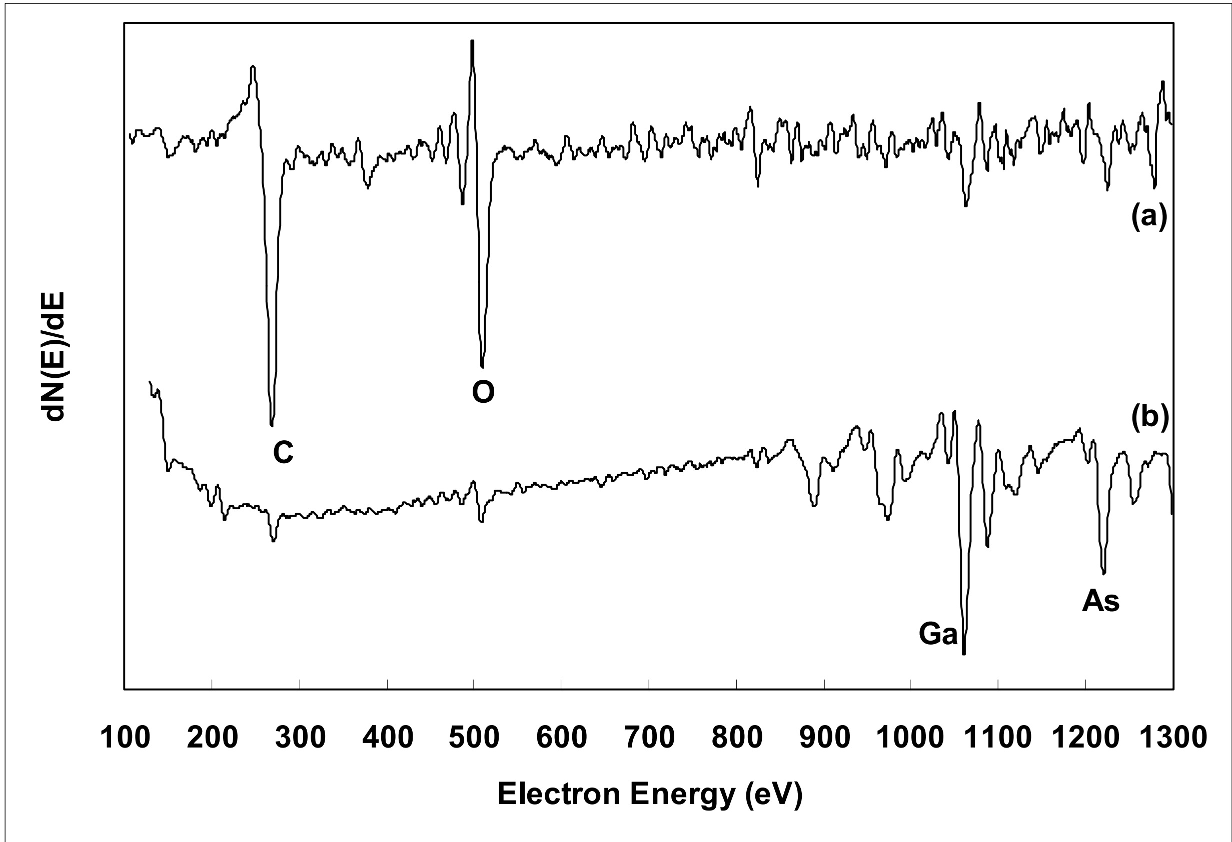

Figure 5.8 Auger electron spectra of (a) the as-received n-GaAs(100) substrate and (b) the clean substrate.

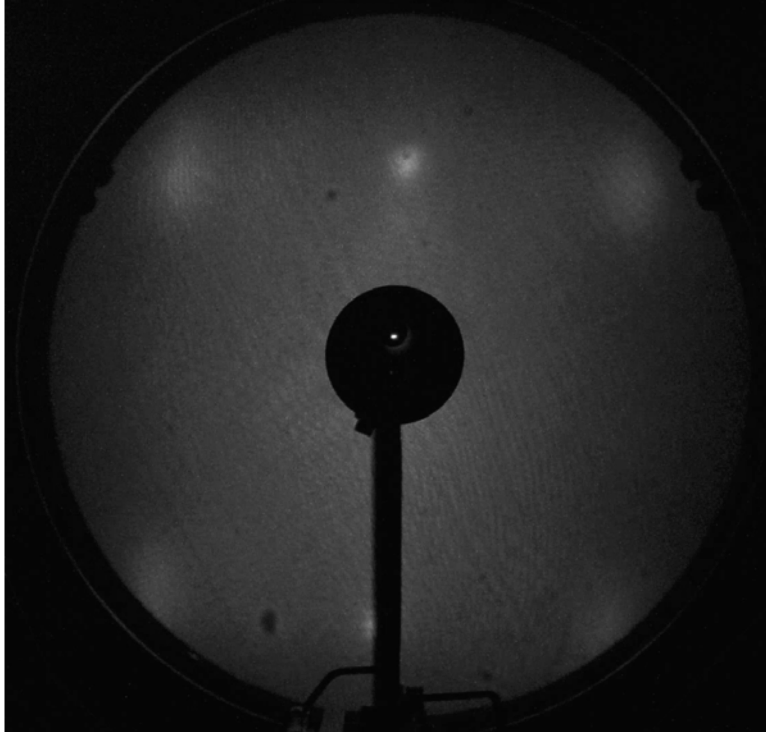

(a)

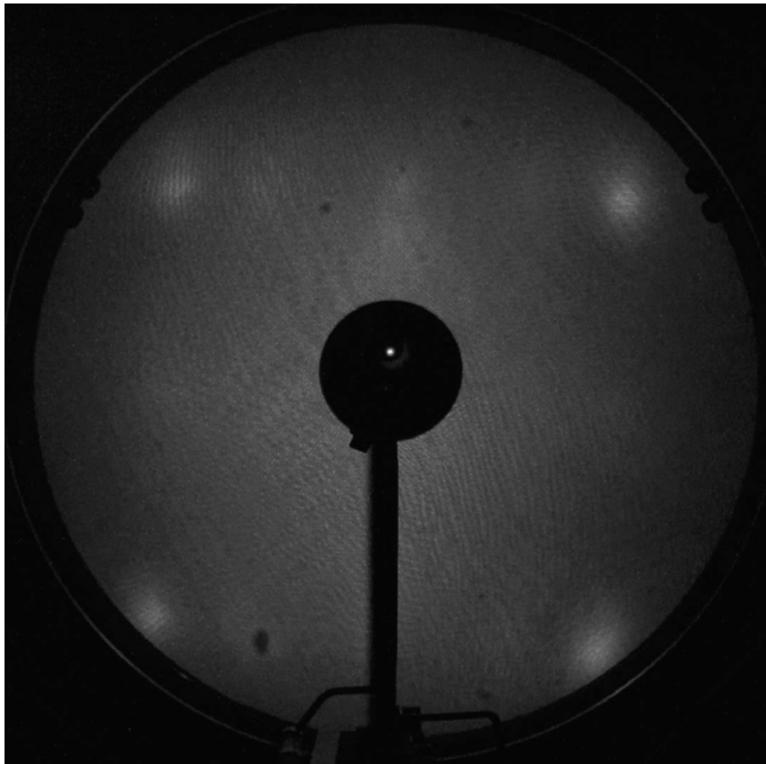

(b)

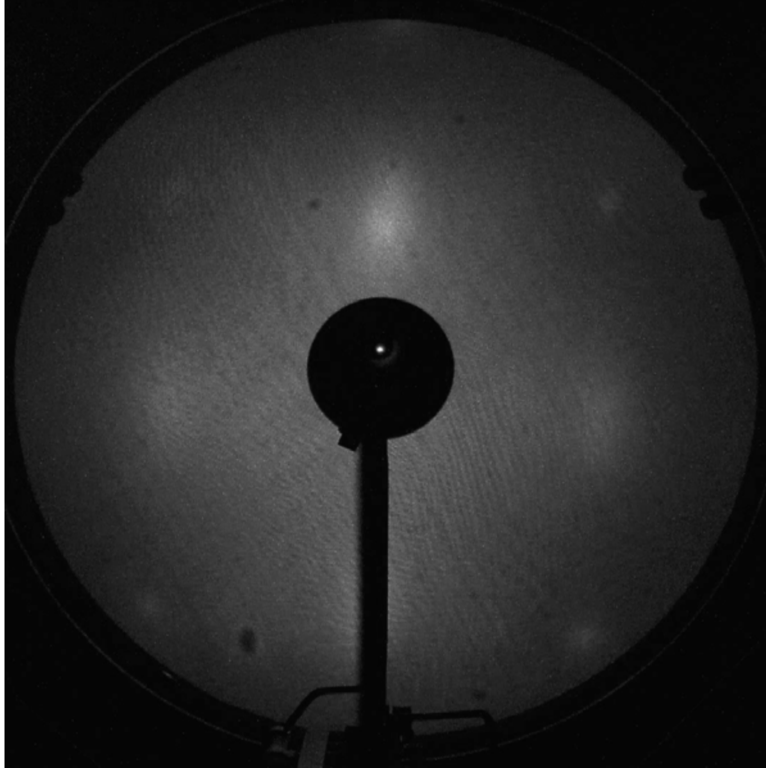

(c)

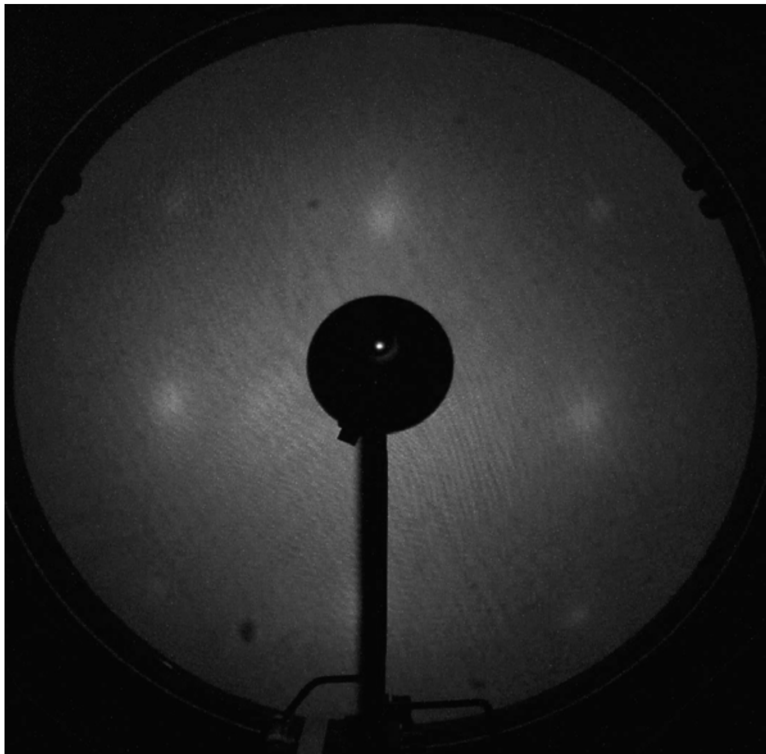

(d)

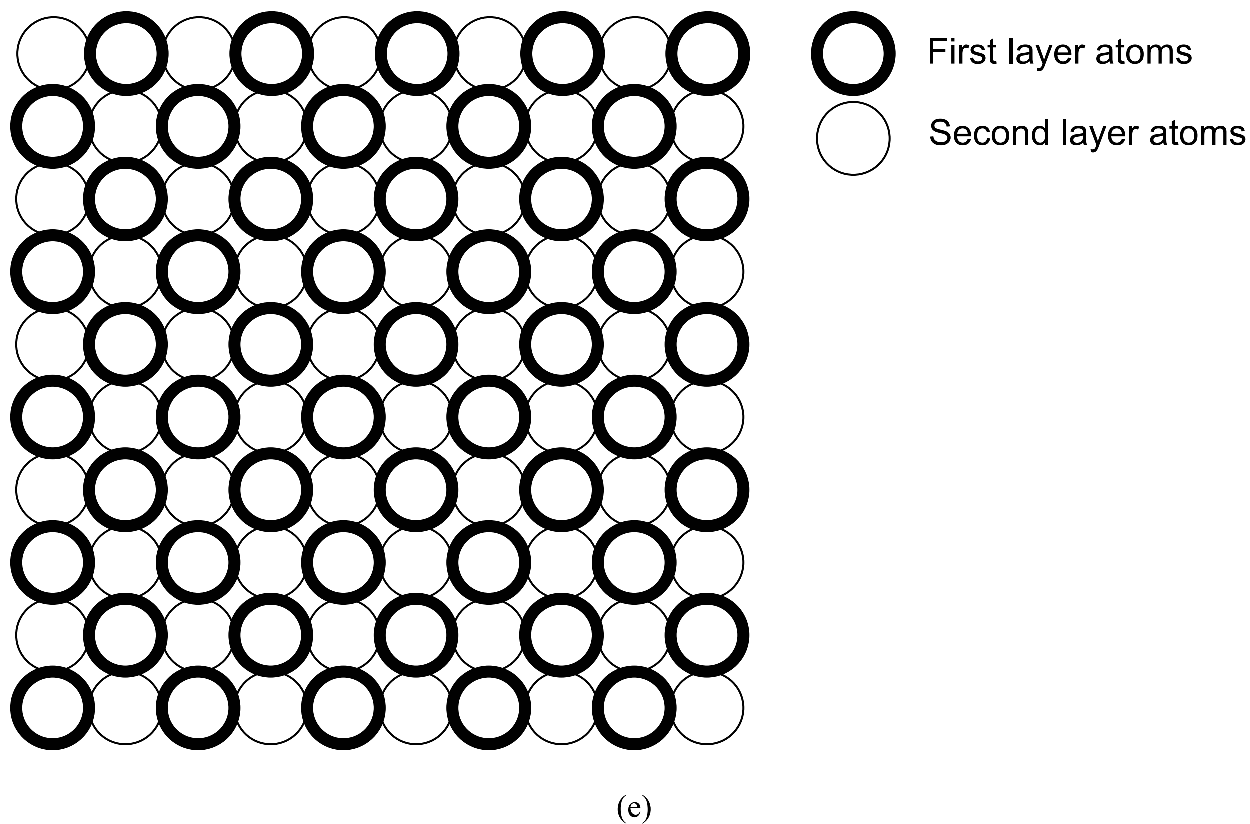

(e)

Figure 5.9 Low energy electron diffraction patterns after 30 minute hot IBB and the subsequent 30 minute annealing with the beam energies of (a) 40 eV, (b) 45 eV, (c) 50 eV, and (d) 55 eV, and (e) the proposed top-viewed n-GaAs(100) substrate surface model after the hot IBB and annealing.

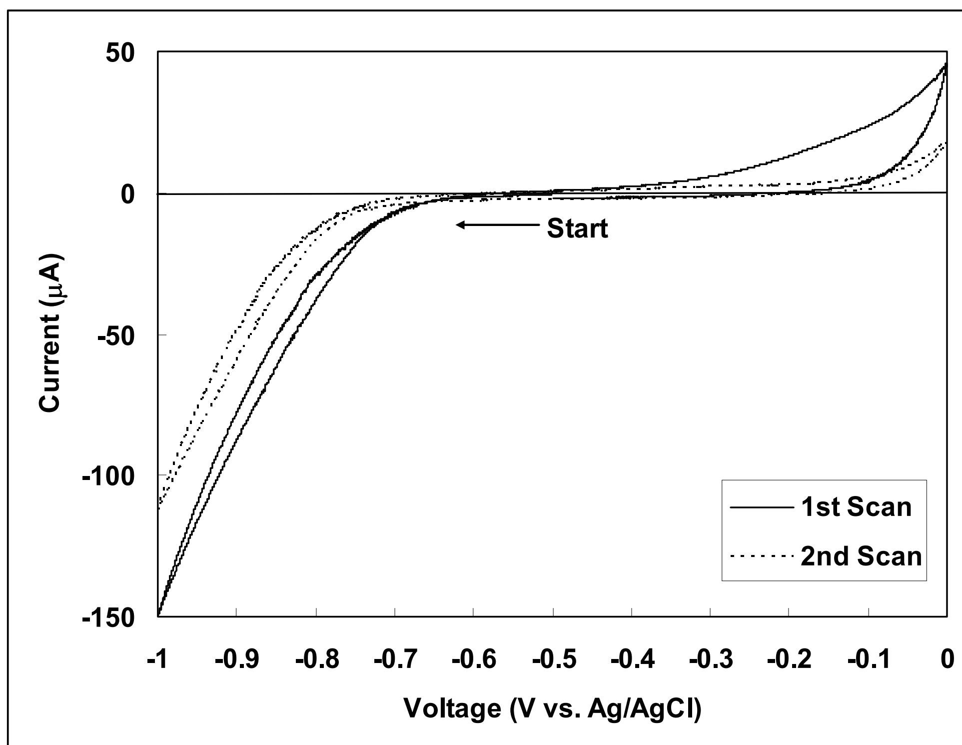

(a)

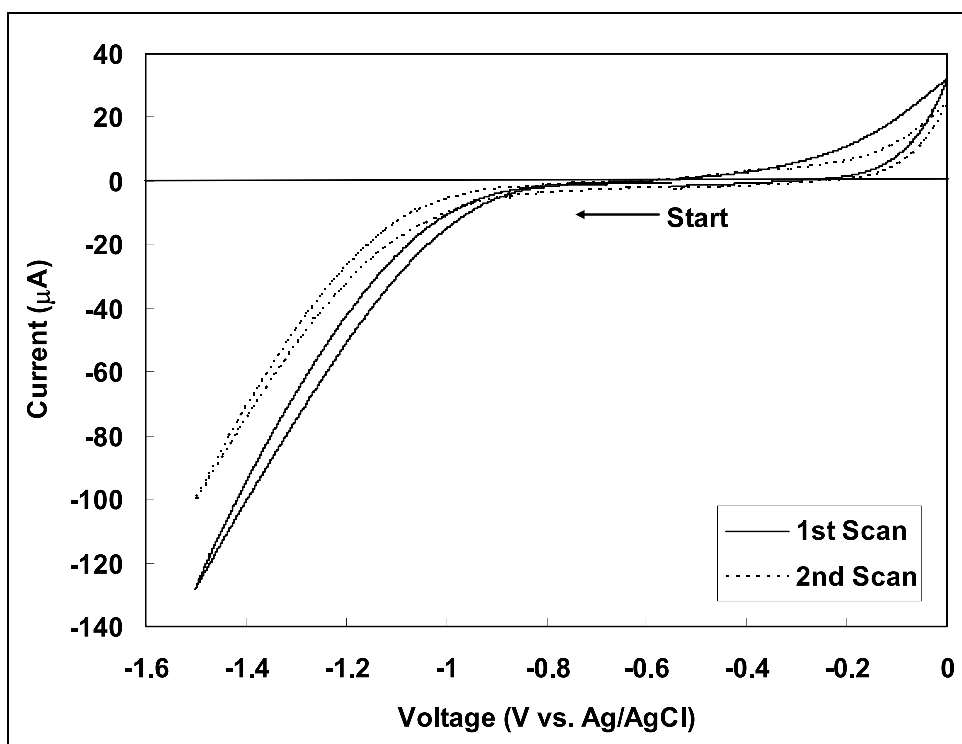

(b)

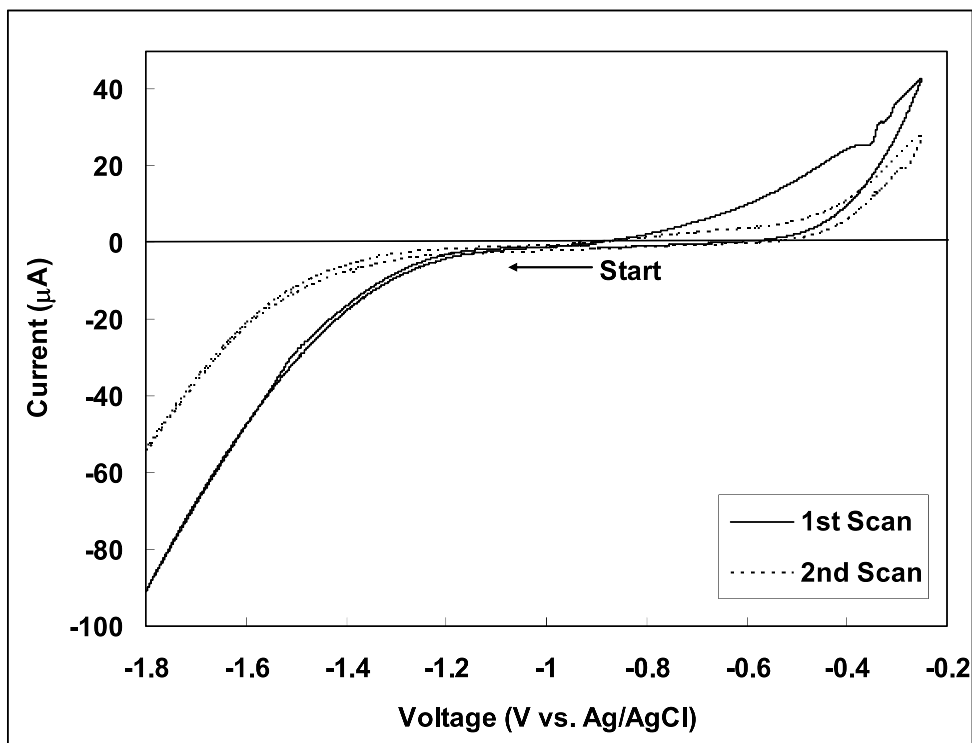

(c)

Figure 5.10 Cyclic voltammograms of the clean and annealed n-GaAs(100) substrate in (a) pH 2 solution, (b) pH 5 solution, and (c) pH 11 solution.

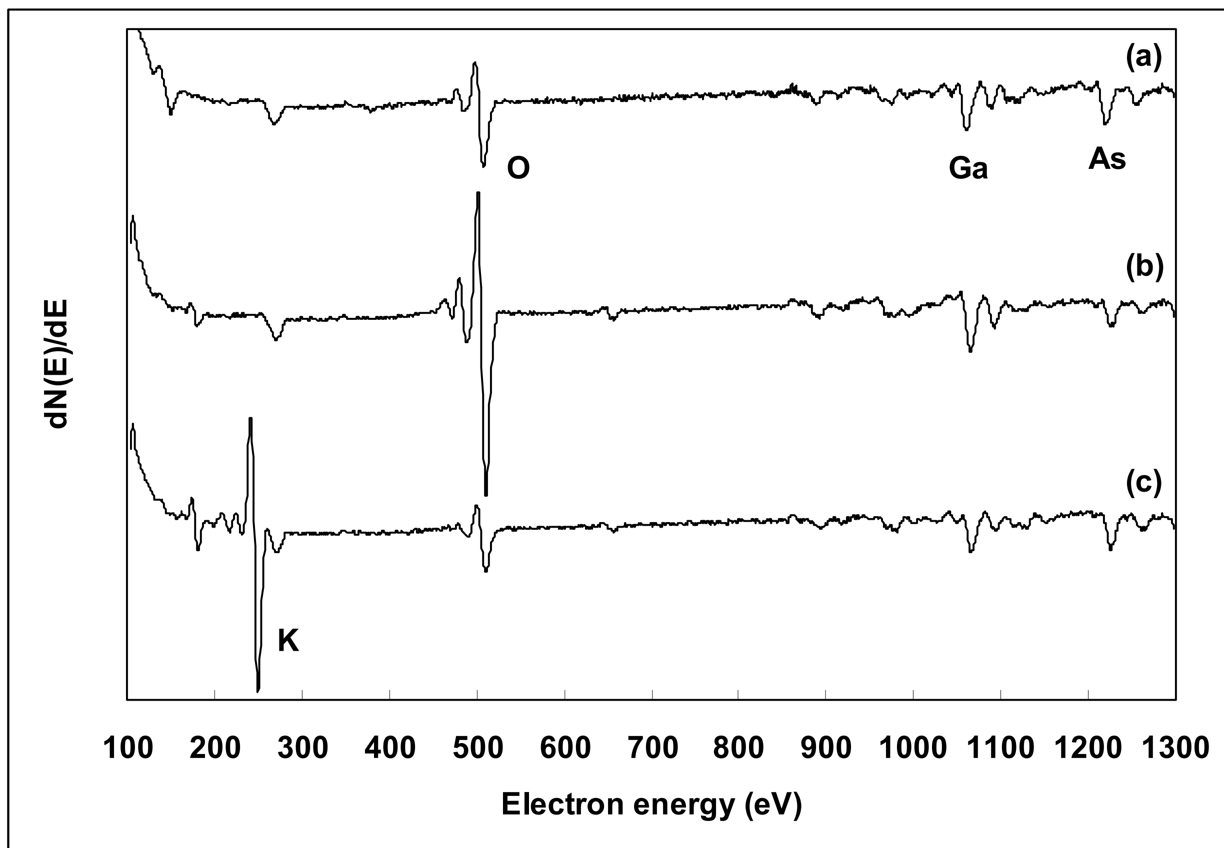

Figure 5.11 Auger electron spectra after emersed at (a) 0 V in pH 2 solution, (b) 0 V in pH 5 solution, and (c) −0.25 V in pH 11 solution.

CHAPTER 6

ULTRAHIGH VACUUM SURFACE STUDIES OF THE ELECTROCHEMICAL ATOMIC LAYER DEPOSITION OF INDIUM TELLURIDE ON N-TYPE GAAS(100)[5]

[5] J.Y. Kim and J.L. Stickney, *J. Phys. Chem. C*, **112**, 5966-5971 (2008). Reprinted here with permission of publisher.

Abstract

The electrodeposition of tellurium (Te) and indium (In) atomic layers on n-type GaAs(100) substrates is described. As-received n-GaAs(100) substrates were treated in 10 % HF and ultraviolet (UV) ozone cleaned. The substrates were then transferred to an ultrahigh vacuum (UHV) chamber and cleaned by Ar^+ ion bombardment. The clean substrate was then transferred into an attached electrochemistry ante-chamber, and immersed in a telluride solution, where a number of deposition potentials were investigated. The resulting Auger peak height ratios, Te/Ga, were plotted versus the Te deposition potential. From the Auger ratios it was evident that bulk Te was formed between −0.4 V and −0.8 V, while below −0.8 V a reduction feature was observed corresponding to the reduction of Te to telluride ion ($Te^0 + 2e^- \rightarrow Te^{2-}$). Below −0.9 V only a surface-limited atomic layer of Te was left on the GaAs surface. Indium deposition on this Te coated GaAs surface was also performed, and electrodeposited adlayer thicknesses were calculated from the Auger data. Indium electrodeposited directly on the GaAs surface resulted in 3D nucleation and growth of widely spaced In clusters. Electrodeposition of In on an atomic layer of Te on the GaAs surface resulted in layer by layer growth. Alternation of atomic layers of Te and In resulted in formation of indium telluride nanofilms, probably In_2Te_3, by electrochemical atomic layer deposition (ALD). Deposits with up to three cycles were performed.

Keywords: Electrodeposition, compound semiconductor, surface-limited, cyclic voltammograms, Auger electron spectroscopy

Introduction

Gallium arsenide (GaAs) is a very important III-V compound semiconductor, and substrate. The present article describes studies of the formation of In and Te atomic layers on GaAs surfaces in aqueous solutions, and the formation of a compound nanofilm by electrochemical ALD. There have been a number of electrodeposition studies where GaAs was used as a substrate [1-9]. However, atomic level studies of GaAs surfaces in electrochemical environments have been few [10, 11]. Previous studies concerning the preparation of GaAs surfaces for use as a substrate for electrodeposition suggested that GaAs was very hard to clean, as it reacted facilely with both oxygen and carbon [11, 12]. Oxygen is easily removed by electrochemical reduction, but carbon is considerably more stable than GaAs to oxidation, making it hard to remove.

It has been reported that GaAs substrates can be passivated using chalcogenides, such as S, Se or Te, which serve to protect it from contaminants and improve its electronic properties [13-19]. Unlike the formation of insulating SiO_2 layers on a Si substrates, the oxide formed on a GaAs substrate is not an effective passivating layer, obstructing the performance and reliability of GaAs-based devices [13].

Electrochemical atomic layer deposition (ALD), or electrochemical atomic layer epitaxy (EC-ALE), is a method designed to form materials layer-by-layer using surface-limited reactions. It is presently being developed by a number of groups as a method for the bottom up growth of smooth and homogeneous nanofilms [20-29]. The work presented here is intended to show that electrochemical ALD is a viable methodology for the formation of nanofilms on semiconductor surfaces [30]. It is felt by these authors that electrochemical ALD can produce deposits comparable with gas phase deposition techniques such as chemical vapor deposition (CVD) or

molecular beam epitaxy (MBE), but with the advantages of conformal deposition and inexpensive hardware [31]. In electrodeposition, surface-limited reactions are frequently referred to as underpotential deposition (UPD), a phenomenon where an atomic layer of one element is deposited on a second at a potential prior to (under) that needed to deposit the element on itself [32]. This process is the result of the thermodynamics (free energy) of surface compound formation. ALD describes a process where nanofilms of material are deposited an atomic layer at a time using surface limited reactions in a cycle. Electrochemical ALD is then the use of UPD in an ALD cycle.

Chalcogenide layers can act as passivation layers, as well as precursors to the formation of other compounds on GaAs substrates [33-35]. Tu et al. studied the (110) and (100) interfaces between GaAs and ZnSe or Se deposited in ultrahigh vacuum (UHV) on sputter-annealed substrates, via low-energy electron diffraction (LEED), Auger electron spectra (AES), and electron energy loss spectra (EELS) [36]. They grew ZnSe thin films by evaporating ZnSe powder, followed by post-deposition annealing, to a variety of temperatures. Norton et al. attempted to grow Fe epitaxially on S-passivated GaAs(100) by MBE [37]. They suggested that the S passivation layer could inhibit over-layer interdiffusion, for growth at 25 °C. LEED and reflection high-energy electron diffraction (RHEED) patterns, suggested high quality Fe epitaxial film was formed on an S layer. Kampen et al. studied indium [38] and antimony [39] adsorption on S-passivated GaAs(100). Both In and Sb were deposited using MBE on S passivation layers and studied using X-ray photoelectron spectroscopy (XPS), which suggested that both In and Sb reacted with the S layer, but did not disturb the interface.

Etcheberry et al. electrodeposited CdSe on InP (100), GaAs(100), and GaAs(111) [5-8]. They co-deposited Cd and Se from a single solution, at a couple of different potentials on the

substrates, and analyzed the surface with X-ray diffraction (XRD), XPS, LEED, and RHEED. Allongue et al. electrodeposited metals such as Pt, Pd, Ni, Co, Cu, and Ag, on n-GaAs(100), from separate solutions, without the use of any passivation layer [1-4].

Stickney et al. formed 100 nm In_2Se_3 thin films on Au substrates by electrochemical ALD, using UPD to form the individual atomic layers [40]. The room temperature phase, β-In_2Se_3, was formed up to 350 cycles, as confirmed with XRD. Epitaxial growth of the compound semiconductor CdTe has been performed on the compound semiconductor substrate InP(100) using electrochemical ALD, where the results were confirmed using Auger electron spectroscopy (AES) [30]. The Cd and Te were electrodeposited from separate $HTeO_2^+$ and Cd^{2+} solutions. Te atomic layers were formed on n-type InP(100), by initially depositing several layers of bulk Te, followed by reductive dissolution in a blank electrolyte solution. This converted the excess bulk Te into telluride ion which then diffused away to leave a surface-limited Te atomic layer. Cd UPD was then formed on the Te atomic layer. Cd deposition directly on the clean n-type InP(100) surface resulted in nucleation and growth, with no atomic layer. A series of three CdTe ALD cycles were performed, starting with a Te atomic layer. Those results suggested n-GaAs(100) might also be used as a substrate, and that a Te atomic layer might limit contamination by oxygen or carbon. In addition, Te coated GaAs might allow deposition of compound nanofilms using electrochemical ALD. That is, the Te atomic layer on the substrate might promote the subsequent formation of metallic atomic layers, such as Cd or In, allowing the electrochemical formation of a compound by ALD.

This article concerns the electrodeposition of Te and In atomic layers on clean n-type GaAs(100) substrates, and on each other. Cyclic voltammetry (CV) was used with an n-type GaAs(100) substrate in Te and In solutions to investigate their electrochemical reactivity, while

Auger electron spectroscopy was used to follow the resulting coverages and surface composition. The alternated deposition of In and Te were performed with the intention of growing indium telluride nanofilms.

Experimental

An n-type, Si-doped, GaAs(100) (IBM), carrier density of 2×10^{18} cm^{-3}, was used as the substrate in these studies. The substrate was cut into rectangular pieces, 1.0×2.3 cm^2, and the ohmic contact was made by soldering Au foil on top of the substrate with metallic indium (Figure 6.1). The as-received n-GaAs(100) substrate was then treated by 10 % HF acid. The HF was used to remove any SiO_2 polishing compound which might have been present. UV ozone cleaning was then used to oxidatively remove any carbon contamination, and resulted in an oxidized surface. Immersion in 10 mM H_2SO_4 (Aldrich Chemical Co.) tended to dissolve any oxide material, while scanning negatively to −1.5 V or below served to reduce any remaining surface oxide. The substrate was then transferred to the ultrahigh vacuum (UHV) chamber, where it was characterized using Auger electron spectroscopy and cleaned by Ar^+ ion bombardment (1 keV ions, at a current density of ~2.5 $\mu A/cm^2$). It should be noted that the commercial GaAs(100) wafer was cut 2° from the (100), resulting in a highly stepped surface, with terrace widths of about 5 nm at best.

The cleaned substrate was then transferred to an electrochemistry ante-chamber of the UHV system, where an electrochemical cell was held, and placed into a Te solution (0.2 mM TeO_2 (Aldrich Chemical Co., 99.995 %) + 50 mM H_2SO_4 (pH 1.5)). A series of experiments were then performed where $HTeO_2^+$ ions were reduced ($HTeO_2^+ + 4e^- + 3H^+ \rightarrow Te^0 + 2H_2O$) at a range of potentials. All potentials in this article are reported with respect to a Ag/AgCl reference

electrode (3 M KCl, BAS Inc.). The scan rate was 5 mV/sec for each experiment, and all CVs were performed under room light conditions. Photo-effects were expected to be minimal due to the use of n-type GaAs at negative potentials, where the substrate would be expected to be in accumulation mode. All solutions were deaerated with ultrahigh purity (UHP) (99.998 %) Ar gas for at least 30 minutes prior to each experiment. Electrochemistry experiments were performed using a μAutolab Type III Potentiostat (Eco Chemie B.V.).

The crystal was rinsed once with 10 mM H_2SO_4 after each Te deposition experiment, and then transferred to the analysis chamber. The electrochemical UHV ante-chamber was interfaced directly to the analysis chamber with a 6 inch gate-valve, so substrates were not exposed to ambient air during transfer, but kept under UHP Ar. Samples were characterized using Auger Electron Spectroscopy, with a simple CMA (Perkin-Elmer) [41]. Auger ratios for Te/Ga, O/Ga, and As/Ga were plotted versus the deposition potentials: where the potential scan was ended and the electrode was emersed (withdrawn from solution).

CVs and Auger spectra were also obtained after Indium (In) electrodeposition on the GaAs substrate. Indium was electrodeposited from 0.2 mM $In_2(SO_4)_3$ (Johnson Matthey Co., 99.999 %) + 50 mM H_2SO_4 (pH 1.5) at various potentials, with and without a Te atomic layer (formed at −1 V) on the substrate. Auger ratios of In/Ga and O/Ga were then compared.

Results and Discussion

Figure 6.2a shows a CV of a clean n-GaAs(100) substrate in the Te solution, starting negatively from the open circuit potential (OCP), −0.1 V. Two reduction features are apparent, at −0.3 V and −0.9 V, besides the hydrogen evolution feature below −0.8 V. In addition, the whole CV sits on a reduction wave of nearly −40 μA. $HTeO_2^+$ ions began to reduce near −0.1 V

($HTeO_2^+ + 4e^- + 3H^+ \rightarrow Te^0 + 2H_2O$), resulting in the first reduction feature (−0.3 V) which is associated with the diffusion-limited formation of bulk Te^0. Te/Ga Auger ratios are shown in Figure 6.2b, for a series of studies done by scanning potential to a series of deposition potentials on a clean substrate. At each of these potentials (Figure 6.2b) the electrode was emersed, transferred to the UHV analysis chamber, and an Auger spectrum was taken. From −0.1 V to −0.6 V, the Te/Ga ratio was very large, 5 ~ 20, suggesting a high Te coverage.

The second reduction feature, a shoulder on hydrogen evolution ($2H^+ + 2e^- \rightarrow H_2$ (gas)) peaked at −0.9 V, resulted in a sharp decrease in the Te/Ga Auger ratio, beginning near −0.8 V (Figure 6.2b). This feature appears to correspond to reduction of excess Te^0 to telluride ions ($Te^0 + 2e^- \rightarrow Te^{2-}$), as well as conversion of tellurite species to telluride ions, which are soluble and diffused away from the surface. The Te/Ga Auger ratios in Figure 6.2b at −1 V and below were essentially constant at 1.8, a value of the Te/Ga ratio so low that it suggests the presence of only an atomic layer of Te, at −1 V and below. This last atomic layer shows greatly increased stability, compared with bulk Te^0, due to its bonding with the GaAs substrate. It is not reduced from the surface, even at potentials as low −1.4 V. The reduction wave, beginning near −0.8 V (Figure 6.2a), was mostly hydrogen evolution and a small amount of $HTeO_2^+$ conversion to some telluride species such as HTe^-. The Auger ratios for O/Ga and As/Ga are essentially constant, below 1, with no particular trend. It does not appear that the resulting surfaces are oxidized appreciably during the transfer from the cell to the analysis chamber, indicating that Te is acting as a passivation agent, at least under the present conditions.

Reversing the scan direction at −1 V and scanning to −0.1 V (Figure 6.2a) revealed no oxidative features, only the continuous −40 μA current due to $HTeO_2^+$ reduction, which began to

decrease at −0.3 V and above. Large Te/Ga Auger ratios were again recorded for the substrate emersed between −0.8 and −0.1 V, during the positive going scan (Te/Ga ≈ 15).

For Te to be an optimal passivating agent, it should be removable prior to deposition. To investigate the possibility of complete removal of Te, the CV shown in Figure 6.3a was performed in 10 mM H_2SO_4, after formation of a high Te coverage n-GaAs(100) at −0.6 V in the tellurite solution (Te/Ga = 20). Starting from the OCP in the 10 mM H_2SO_4, −0.3 V (I), the potential was scanned negatively to −1.0 V (II) and emersed (withdrawn from the solution), and transferred to the analysis chamber, where the Auger spectrum shown in Figure 6.3b(II) was obtained. As expected, the Te/Ga ratio dropped to about 2, as all the excess Te was reduced to telluride. In separate attempts to remove all the Te by reduction, similar reductive scans were performed in a pH 11 solution, 1 mM KOH solution, to decrease the hydrogen evolution current, and the potential was scanned all the way to −2.4 V. The Te/Ga ratio was dropped to 0.9, but it was not possible, even under those conditions of pH and potential, to remove the last traces of Te by reduction.

To examine the possibility of oxidative removal of Te, the same procedure was repeated (Figure 6.3a): cleaning by ion bombardment, deposition of Te, and immersion in the 10 mM H_2SO_4 at OCP. The potential was then scanned to −1 V, where the scan was reversed and the substrate was emersed at −0.25 V (III), and an Auger spectrum was run. The Te/Ga ratio at (III) was 4, compared with 2 at (II), a little higher than initially expected. However, from Figure 6.3a, it is clear that some of the telluride ions formed at more negative potentials were re-deposited in a small oxidation feature at −0.7 V (Figure 6.3a), accounting for the Te/Ga ratio of 4. Finally, the procedure was performed again, the Te-coated substrate was scanned to −1 V, reversed and scanned to 0.1 V, Figure 6.3b(IV). The Te/Ga was again back down to 2, suggesting only the

presences of an atomic layer. Also present was a small amount of oxygen. It is known from studies of Te deposition on Au surfaces, that Te does not oxidized till 0.1 V or positive, suggesting that a majority of the oxidation current was for GaAs oxidation, and not all the Te was removed from the surface [22, 42-48]. The dotted curve in Figure 6.3a, the equivalent CV for GaAs with no Te, shows considerably more oxidation than the Te-coated surface, above −0.2 V, suggesting the passivating nature of the Te atomic layer. It is probable that the small amount of oxygen evident in Figure 6.3b(IV) is due to the presences of some gallium or arsenic oxide on sites not protected by Te.

Figure 6.4 shows GaAs CVs in the In solution, both with (dotted line) and without (solid line) a Te atomic layer. The OCP in the In solution was −0.4 V with a Te atomic layer present, and −0.45 V without. No specific features are evident during the negative potential scan, from the OCP (besides hydrogen evolution), except for a slight excess of reductive current between the OCP and −0.8 V for the GaAs substrate coated with a Te atomic layer. In the subsequent positive going scans, In oxidation was evident starting at −0.75 V. The resulting oxidative charge was equivalent to 3 ~ 4 ML of In (where a monolayer (ML) is defined as the deposition of one In atom for each surface atom (6.265×10^{14} atoms/cm^2)). The oxidative charge was calculated by integrating the In oxidation peak from −0.75 V to −0.6 V. Note that in the blank CV (Figure 6.3a, the dotted line), in 10 mM H_2SO_4, no oxidation feature was evident until −0.4 V. That is, the oxidation feature at −0.7 V in Figure 6.4 was due to In oxidation. Also note that the features at −0.7 V (Figure 6.4) were essentially equivalent, whether the Te atomic layer was present on the substrate or not. In addition, a nearly constant current of 20 ~ 30 μA was present from the end of the bulk In oxidation peak (−0.65 V) to about −0.2 V, suggesting some In continued to be oxidized.

Figure 6.5 shows Auger ratios for (a) In/Ga and (b) O/Ga, with and without a Te atomic layer on the substrate, as a function of the potential at which the substrate was emersed from the In solution. Each point was the result of In deposition to −1.2 V and then scanning positively to the noted potentials and emersion of the GaAs substrate. Figure 6.5a shows a large In/Ga ratio at −1 V for the GaAs substrate with the Te atomic layer, and a rather low In/Ga ratio without Te. As the potential was scanned positively, the ratio dropped dramatically, starting at −0.8 V, for GaAs with the Te, while the low ratio slowly decreased for the GaAs without the Te atomic layer. The dramatic drop in the In/Ga ratio is consistent with the In oxidation evident in Figure 6.4. There appears to be a kind of plateau near an In/Ga ratio of 2.5, for potentials between −0.6 V and −0.4 V, and then a steady drop, for the GaAs substrate with the Te atomic layer (Figure 6.5a).

The disparity in the In/Ga ratios with and without a Te atomic layer is very striking and important. It suggests that In was not deposited homogeneously on the GaAs surface without the Te layer, though the voltammetry contradicts such a statement. It is clear that the amounts of oxidatively stripped In were similar with and without the Te atomic layer (Figure 6.4). It is thus suggested here that the disparity comes from the nature of the In deposition. Apparently, the In deposited on bare GaAs forms by nucleation and growth, with relatively few nucleation sites, separated on the surface. Indium is deposited, but it forms three dimensional (3D) features with taking up only a small fraction of the substrate surface area, and thus results in a low In/Ga ratio. On the other hand, deposition of In on GaAs covered by a Te atomic layer resulted in a homogenous deposit, covering the whole surface, and resulting in an In/Ga ratio proportional to the deposit thickness.

Figure 6.5b shows the O/Ga Auger ratios for the In deposits as a function of the emersion potential. With no Te layer present (open squares), the O/Ga Auger ratio remained nearly

constant at about 2.5, consistent with the In depositing in a small number of widely spaced 3D In islands, covering only a small % of the surface, and thus the surface resembled at slightly oxidized GaAs surface at all the emersion potentials. With the Te atomic layer present, however, a very large O/Ga ratio (between 6 and 7) was evident at the lowest potentials, below −0.6 V. While at potentials above −0.6 V, only a small O/Ga ratio was observed (0.5 to 1.5). This data suggests that the surface was homogeneously covered with bulk In below −0.6 V, and upon emersion for analysis, some form of In oxide or hydroxide was spontaneously formed in the UHP Ar make up gas, due to the metallic In reacting with traces of O_2 and water. The same In oxidation reaction occurred with the sample with no Te present, but as the In did not cover much of the surface, this In oxidation had little overall influence on the O/Ga ratio. At −0.6 V and positive, all the bulk In was oxidized away, leaving only an atomic layer of In bound to the Te atomic layer, and the resulting stability provided by the indium binding to the tellurium species was sufficient to prevent oxidation upon emersion for analysis. The data in Figure 6.5b clearly supports the discussion above, concerning formation of 3D islands without the Te present, and the layer-by-layer growth with the single atomic layer of Te present. Oxidation of the GaAs surface was less extensive with the Te atomic layer present, as well, again showing the passivating nature of the Te atomic layer.

The above experiments were performed by depositing, or not, a Te atomic layer followed by bulk In, and then scanning positive to strip In as a function of the emersion potential. The following experiments (Figure 6.6) were performed by, again, depositing an initial Te atomic layer, and then depositing In by scanning to a series of deposition potentials and emersing. Figure 6.6 shows Auger ratios for In/Te (open square) and Ga/Te (filled square), versus the In deposition potentials. The Ga/Te Auger ratio was constant, as expected, as the coverage of both

did not change in the In solution. Increases in the In coverage resulted in scattering of both Te and Ga Auger electrons, so that both signals were decreased, but the ratio remained constant at about 0.5. At 0 V, no In was present on the surface: none had been deposited. Negative of 0 V, the In/Te Auger ratio began to increase slowly, and a plateau is suggested between −0.4 V and −0.6 V, corresponding to formation of an In atomic layer on the Te atomic layer. Auger signals are a function of the Auger yields, and to compare coverages of two elements, the yield factors, or sensitivity factors, must be taken into account. An estimate of the actual elemental ratio should thus be calculated, depending on the structure of the deposit, using Eq. (6.1):

$$\text{(Actual Elemental Ratio)} = \text{(Observed Auger Ratio)} \div \text{(Auger Sensitivity Factor Ratio)} \quad (6.1)$$

The actual In/Te elemental ratio in the plateau would then be: $(\sim 1.4) \div (0.9/0.45) = \sim 0.7 \approx 2/3$; suggesting the formation of a surface compound with In_2Te_3 as the stoichiometry, for In deposits formed between −0.4 V and −0.6 V, in the presence of a Te atomic layer. In_2Te_3 is a known compound [49-51], and the related compound In_2Se_3 has previously been formed using electrochemical ALD by this group [40]; therefore, a 2/3 stoichiometry might be expected.

One, two, and three In-Te ALD cycles were then performed, each after cleaning the substrate. Figure 6.7 shows the Auger ratios for In/Ga, Te/Ga, O/Ga, and As/Ga versus the number of In-Te ALD cycles. The 0.5, 1.5, and 2.5 designations on the X-axis of Figure 6.7 signify Te on top and bottom: Te, Te-In-Te, and Te-In-Te-In-Te on the substrate, respectively. In Figure 6.7, the In/Ga and Te/Ga Auger ratios consistently increased, and clearly displayed steps, indicating no change in the Te/Ga ratio during In deposition, and no change in the In/Ga ratio during Te deposition. The O/Ga Auger ratio displayed a modulation in the points consistent with less oxidation when the surface was Te-terminated, and a slight increase when In was terminating. This is consistent with the much greater reactivity of In to traces of oxygen during

transfer, than Te. It appears that the oxygen signal increased steadily, but that is mostly a result of using Ga as the internal standard. The fact is, normalizing by Ga only works well for a monolayer or so. The size of the Ga peaks decreased as the layers were formed, thus normalization by Ga resulted in division by a smaller and smaller number. The As/Ga Auger ratio displayed a constant value of 0.6 ~ 0.7, indicating the ability of the In-Te deposit to passivate the substrate, under these conditions.

The electrodeposited layer thickness (x) can be calculated in Å from the Auger spectra using Eq. (6.2) [52]:

$$x = -\lambda_{Ga} \times \ln(I/I_0) \qquad (6.2)$$

where λ_{Ga} is the inelastic mean free path of Ga Auger electron in Å [52], I is the Ga Auger peak-to-peak height after deposition, and I_0 is the Ga Auger peak-to-peak height for the clean substrate. Figure 6.8 displays the deposit thickness, determined by using Eq. (6.2), as a function of the number of In-Te ALD cycles. The total adlayer thickness clearly increases linearly, as expected for an ALD process. From the slope of the best-fit line (Figure 6.8), the In-Te layer thickness increased by about 4.8 Å per cycle. This is somewhat larger than expected for a single compound monolayer (between 3 and 4 Å). Possible explanations include the simplistic nature of Eq. (6.2), which does not even take into account the electronic structure of the material scattering the Ga Auger electrons. The structure of the In-Te layer is not clear, though the atomic ratio calculated above suggests a stoichiometry of In_2Te_3. In addition, it may be that more than a compound monolayer was deposited each cycle. Overall, the suggestion that 4.8 Å are deposited each cycle is encouraging, as it indicates that a layer-by-layer process was present, since 3D growth of the deposit would have resulted in a lower value of the thickness/cycle, not excess.

Conclusions

An n-type GaAs(100) was studied as a substrate for the electrodeposition of compound semiconductors using ALD, and specifically the formation of In_2Te_3. The intent was to better understand the surface chemistry of GaAs in aqueous solutions, and how best to form electrodeposits. It was shown that an atomic layer of Te could be formed by deposition at potentials below −1 V. An atomic layer of In was then formed on the Te. Without the Te atomic layer, the In was deposited as 3D nucleation and growth, which did not cover the GaAs surface under the conditions used. That is, a surface compound was formed between the GaAs surface and the Te atomic layer, and also between the Te atomic layer and an In atomic layer. This compound formation provided increased stability, resulting in surface-limited reactions. No such reaction was evident between the GaAs and In. From studies of the In/Te atomic ratio from Auger, the deposit stoichiometry appeared to be In_2Te_3. Three ALD cycles were performed, alternating the deposition of Te and In, and the Auger data confirmed the layer by layer growth. That is, a linear plot of the deposit coverage vs. cycle number was obtained, using the Ga escape depth and Ga Auger peak to peak heights following deposition of each atomic layer. The slope suggested 4.8 Å/cycle, which was a little higher than expected, but clearly showed that the GaAs surface was steadily covered as the deposition proceeded, suggesting a homogeneous deposition process.

Acknowledgement

The financial support from National Science Foundation, Divisions of Materials and Chemistry, the Department of Energy, is gratefully acknowledged.

References

1. P. Allongue and E. Souteyrand, *J. Vac. Sci. Tech. B*, **5**, 1644 (1987).
2. P. Allongue and E. Souteyrand, *J. Electroanal. Chem.*, **286**, 217 (1990).
3. P. Allongue and E. Souteyrand, *J. Electroanal. Chem.*, **362**, 79 (1993).
4. P. Allongue, E. Souteyrand, and L. Allemand, *J. Electroanal. Chem.*, **362**, 89 (1993).
5. L. Beaunier, H. Cachet, M. Froment, and G. Maurin, *J. Electrochem. Soc.*, **147**, 1835 (2000).
6. H. Cachet, R. Cortes, M. Froment, and A. Etcheberry, *Thin Solid Films*, **361-362**, 84 (2000).
7. L. Beaunier, H. Cachet, R. Cortes, M. Froment, and A. Etcheberry, *Thin Solid Films*, **387**, 108 (2001).
8. A. Etcheberry, H. Cachet, R. Cortes, and M. Froment, *Surf. Sci.*, **482**, 954 (2001).
9. J. Zegenhagen, F.U. Renner, A. Reitzle, T.L. Lee, S. Warren, A. Stierle, H. Dosch, G. Scherb, B.O. Fimland, and D.M. Kolb, *Surf. Sci.*, **573**, 67 (2004).
10. I. Villegas and J.L. Stickney, *J. Electrochem. Soc.*, **139**, 686 (1992).
11. L.C. Ward, M. Muthuvel, and J.L. Stickney, *Proc. Electrochem. Soc.*, **2003-11**, 152 (2003).
12. M. Muthuvel and J.L. Stickney, *J. Electrochem. Soc.*, **153**, C67 (2006).
13. T. Ohno, *Surf. Sci.*, **255**, 229 (1991).
14. P. Moriarty, B. Murphy, and G. Hughes, *J. Vac. Sci. Technol. A*, **11**, 1099 (1993).
15. P. Moriarty, B. Murphy, L. Roberts, A.A. Cafolla, G. Hughes, L. Koenders, and P. Bailey, *Phys. Rev. B*, **50**, 14237 (1994).
16. M.D. Pashley and D. Li, *J. Vac. Sci. Technol. A*, **12**, 1848 (1994).

17. H. Xia, W.N. Lennard, G.R. Massoumi, J.J.J. van Eck, L.J. Huang, W.M. Lau, and D. Landheer, *Surf. Sci.*, **324**, 159 (1995).

18. Y. Ke, S. Milano, X.W. Wang, N. Tao, and Y. Darici, *Surf. Sci.*, **415**, 29 (1998).

19. D.R.T. Zahn, T.U. Kampen, S. Hohenecker, and W. Braun, *Vacuum*, **57**, 139 (2000).

20. B.W. Gregory and J.L. Stickney, *J. Electroanal. Chem.*, **300**, 543 (1991).

21. U. Demir and C. Shannon, *Langmuir*, **10**, 2794 (1994).

22. L.B. Goetting, B.M. Huang, T.E. Lister, and J.L. Stickney, *Electrochim. Acta*, **40**, 143 (1995).

23. G.D. Aloisi, M. Cavallini, M. Innocenti, M.L. Foresti, G. Pezzatini, and R. Guidelli, *J. Phys. Chem. B*, **101**, 4774 (1997).

24. B.E. Hayden and I.S. Nandhakumar, *J. Phys. Chem. B*, **102**, 4897 (1998).

25. T. Torimoto, S. Nagakubo, M. Nishizawa, and H. Yoneyama, *Langmuir*, **14**, 7077 (1998).

26. S. Zou and M.J. Weaver, *Chem. Phys. Lett.*, **312**, 101 (1999).

27. T. Oznuluer and U. Demir, *J. Electroanal. Chem.*, **529**, 34 (2002).

28. J. Yang, W. Zhu, X. Gao, S. Bao, and X. Fan, *J. Electroanal. Chem.*, **577**, 117 (2005).

29. L.T. Viyannalage, R. Vasilic, and N. Dimitrov, *J. Phys. Chem. C*, **111**, 4036 (2007).

30. M. Muthuvel and J.L. Stickney, *Langmuir* **22**, 5504 (2006).

31. J.L. Stickney, in *Advances in Electrochemical Science and Engineering*, R.C. Alkire and D.M. Kolb (Eds.), Wiley-VCH, Weinheim, 2002.

32. D.M. Kolb, M. Przasnyski, and H. Gerischer, *J. Electroanal. Chem.*, **54**, 25 (1974).

33. Y. Gobil, J. Cibert, K. Saminadayar, and S. Tatarenko, *Surf. Sci.*, **211**, 969 (1989).

34. V.H. Etgens, R. Pinchaux, M. Sauvage-Simkin, J. Massies, N. Jedrecy, N. Greiser, and S. Tatarenko, *Surf. Sci.*, **251**, 478 (1991).

35. A.C. Ferraz and R.C. da Silva, *Surf. Sci.*, **352**, 379 (1996).

36. D.W. Tu and A. Kahn, *J. Vac. Sci. Technol. A*, **3**, 922 (1985).

37. G.W. Anderson, M.C. Hanf, X.R. Qin, P.R. Norton, K. Myrtle, and B. Heinrich, *Surf. Sci.*, **346**, 145 (1996).

38. S. Hohenecker, T.U. Kampen, T. Werninghaus, D.R.T. Zahn, and W. Braun, *Appl. Surf. Sci.*, **142**, 28 (1999).

39. S. Hohenecker, T.U. Kampen, W. Braun, and D.R.T. Zahn, *Surf. Sci.*, **435**, 347 (1999).

40. R. Vaidyanathan, J.L. Stickney, S.M. Cox, S.P. Compton, and U. Happek, *J. Electroanal. Chem.*, **559**, 55 (2003).

41. M.P. Soriaga and J.L. Stickney, in *Modern Techniques in Electroanalysis*, P. Vanysek (Eds.), Chemical Analysis Series, 1996.

42. D.W. Suggs and J.L. Stickney, *Surf. Sci.*, **290**, 362 (1993).

43. D.W. Suggs and J.L. Stickney, *Surf. Sci.*, **290**, 375 (1993).

44. T.A. Sorenson, D.W. Suggs, I. Nandhakumar, and J.L. Stickney, *J. Electroanal. Chem.*, **467**, 270 (1999).

45. T.A. Sorenson, K. Varazo, D.W. Suggs, and J.L. Stickney, *Surf. Sci.*, **470**, 197 (2001).

46. K. Varazo, M.D. Lay, T.A. Sorenson, and J.L. Stickney, *J. Electroanal. Chem.*, **522**, 104 (2002).

47. B.H. Flowers Jr., T.L. Wade, J.W. Garvey, M. Lay, U. Happek, and J.L. Stickney, *J. Electroanal. Chem.*, **524-525**, 273 (2002).

48. M.D. Lay and J.L. Stickney, *J. Electrochem. Soc.*, **151**, C431 (2004).

49. N.A. Hegab, M.A. Afifi, A.E. El-Shazly, and A.E. Bekheet, *J. Mater. Sci.*, **33**, 2441 (1998).

50. O. Madelung, *Semiconductors: Data Handbook*, Springer, Berlin, 2004.

51. R.R. Desai, D. Lakshminarayana, P.B. Patel, P.K. Patel, and C.J. Panchal, *Mater. Chem. Phys.*, **94**, 308 (2005).

52. L.C. Feldman and J.W. Mayer, *Fundamentals of Surface and Thin Film Analysis*, Prentice-Hall Inc., New Jersey, 1986.

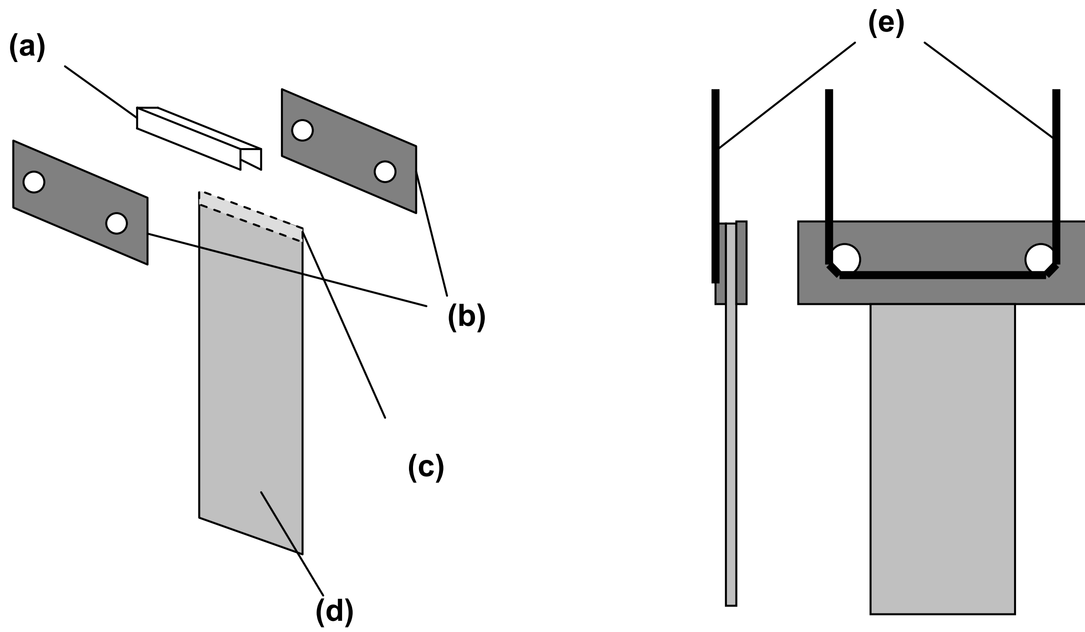

Figure 6.1 Schematic diagram of GaAs(100) sample arrangement in the sample holder. (a) Gold foil, (b) molybdenum bars, (c) indium contact, (d) n-GaAs(100) substrate, and (e) tungsten wire.

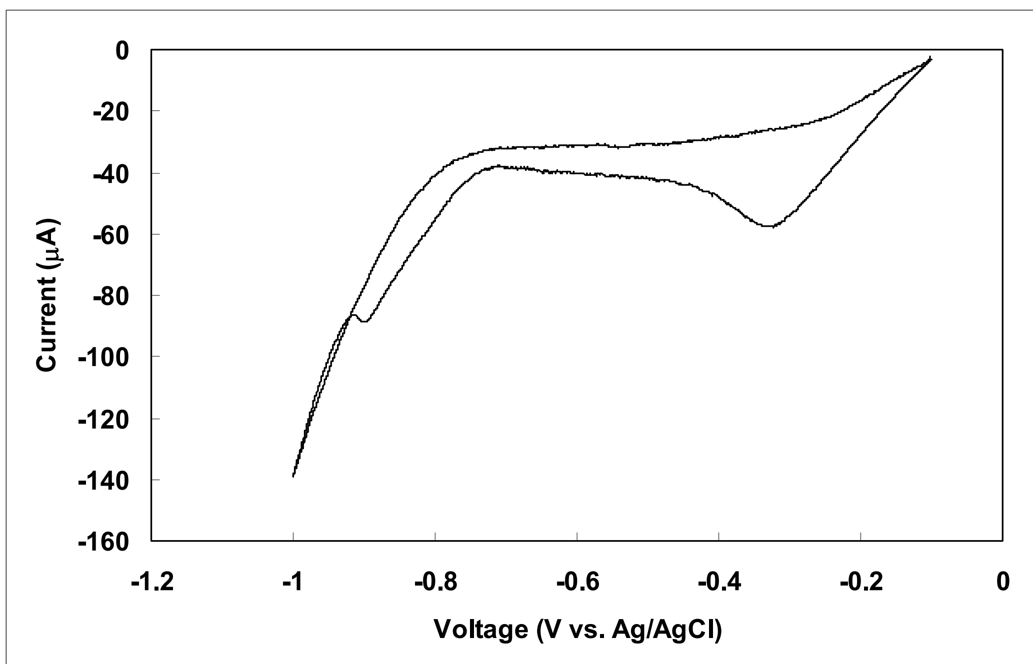

(a)

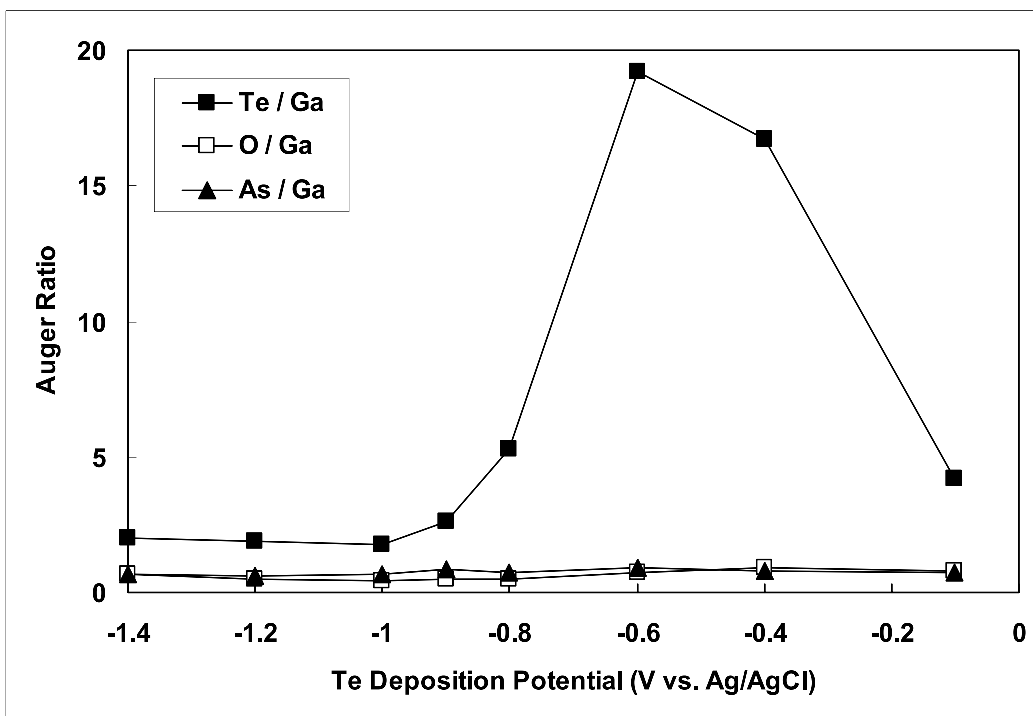

(b)

Figure 6.2 (a) Cyclic voltammogram in Te solution after cleaning n-GaAs(100) and (b) Auger ratios versus Te deposition potentials.

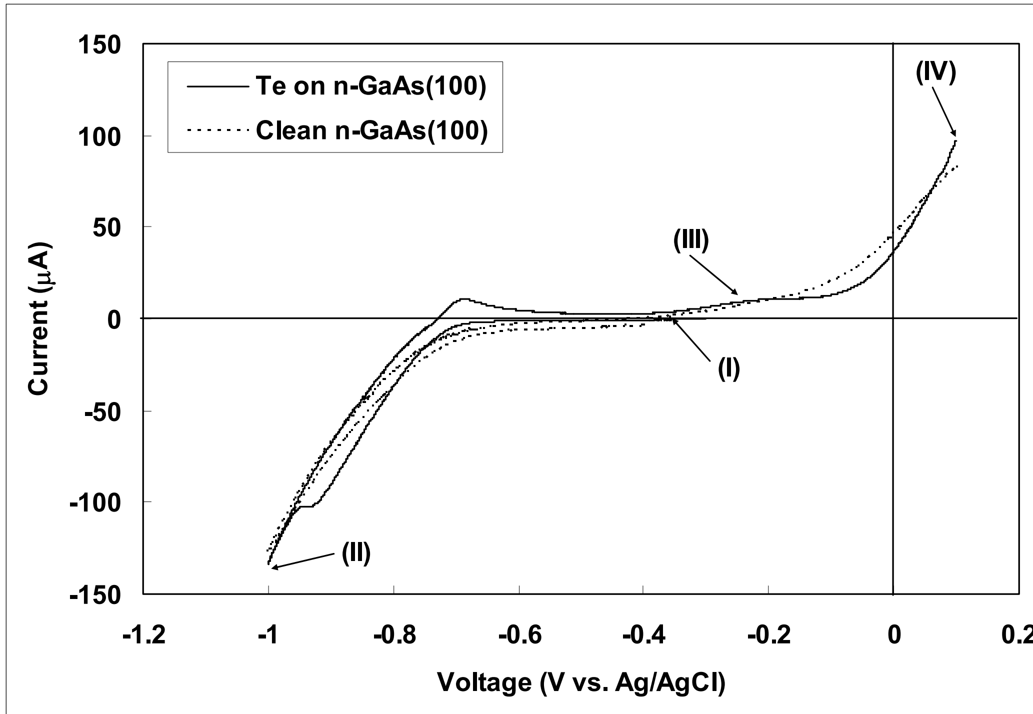

(a)

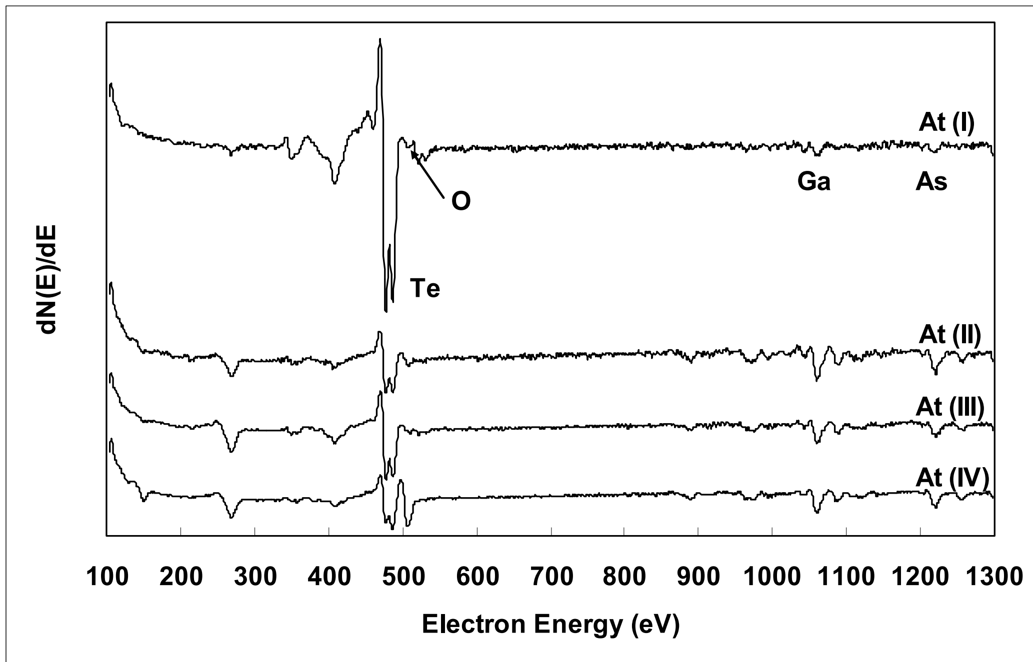

(b)

Figure 6.3 (a) Cyclic voltammograms in 10 mM H_2SO_4 solution after cleaning n-GaAs(100) (dotted line) and after Te deposition on n-GaAs(100) at −0.6 V (high coverage of Te) (solid line) and (b) Auger spectra comparison at each point.

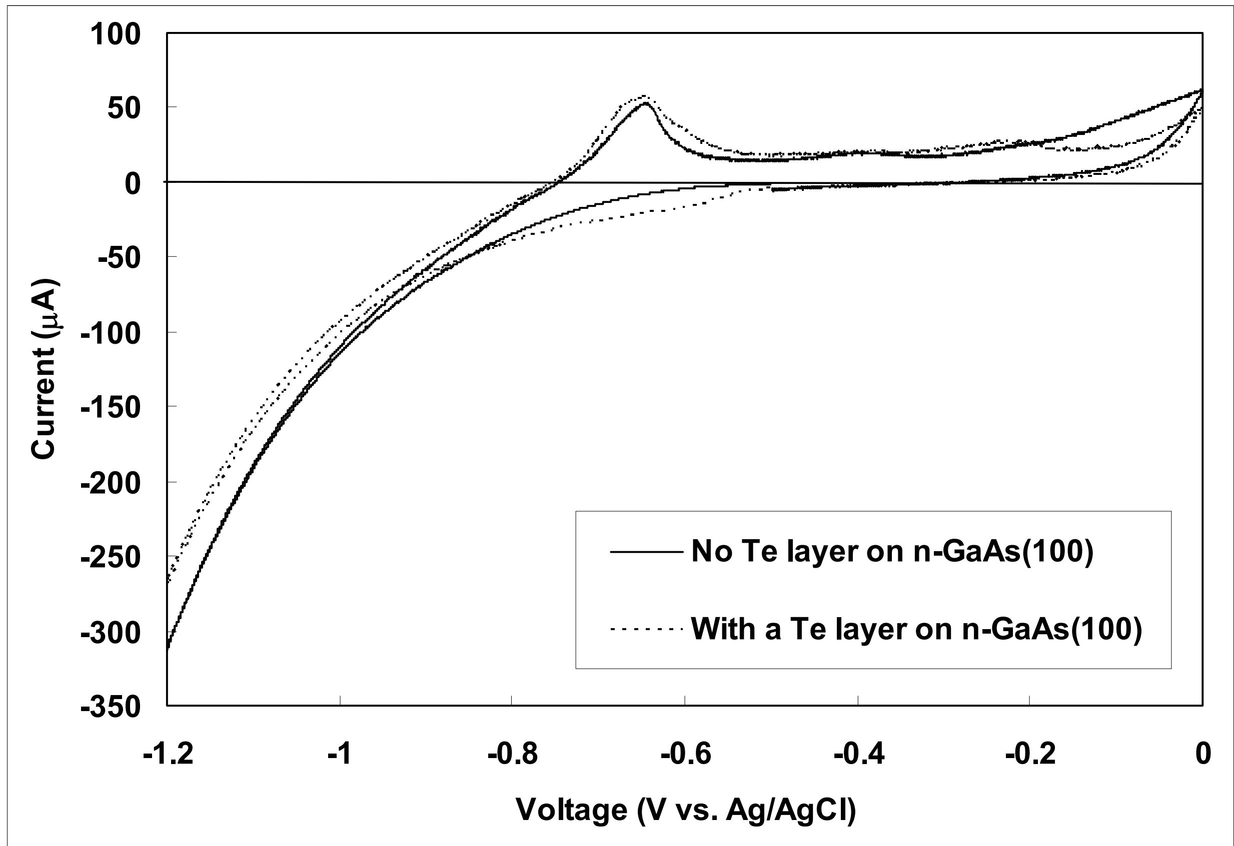

Figure 6.4 Cyclic voltammograms in In solution with and without a Te atomic layer on the substrate.

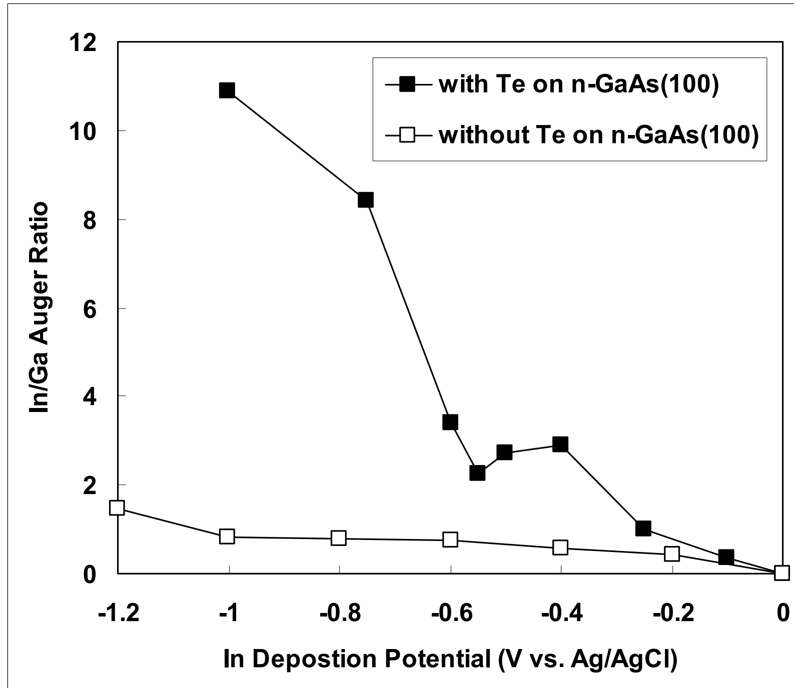

(a)

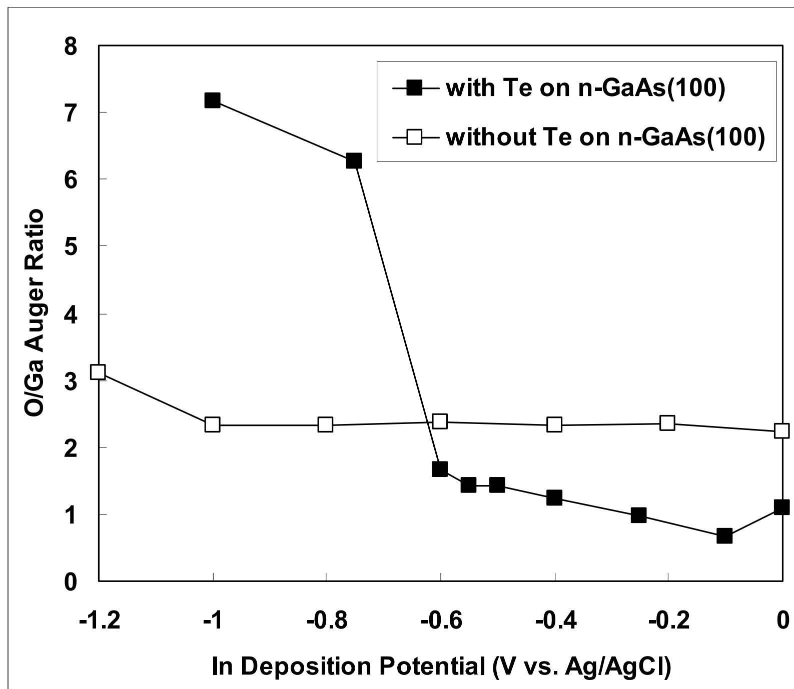

(b)

Figure 6.5 Auger ratios versus In deposition potentials with and without a Te atomic layer on n-GaAs(100): (a) In/Ga, (b) O/Ga.

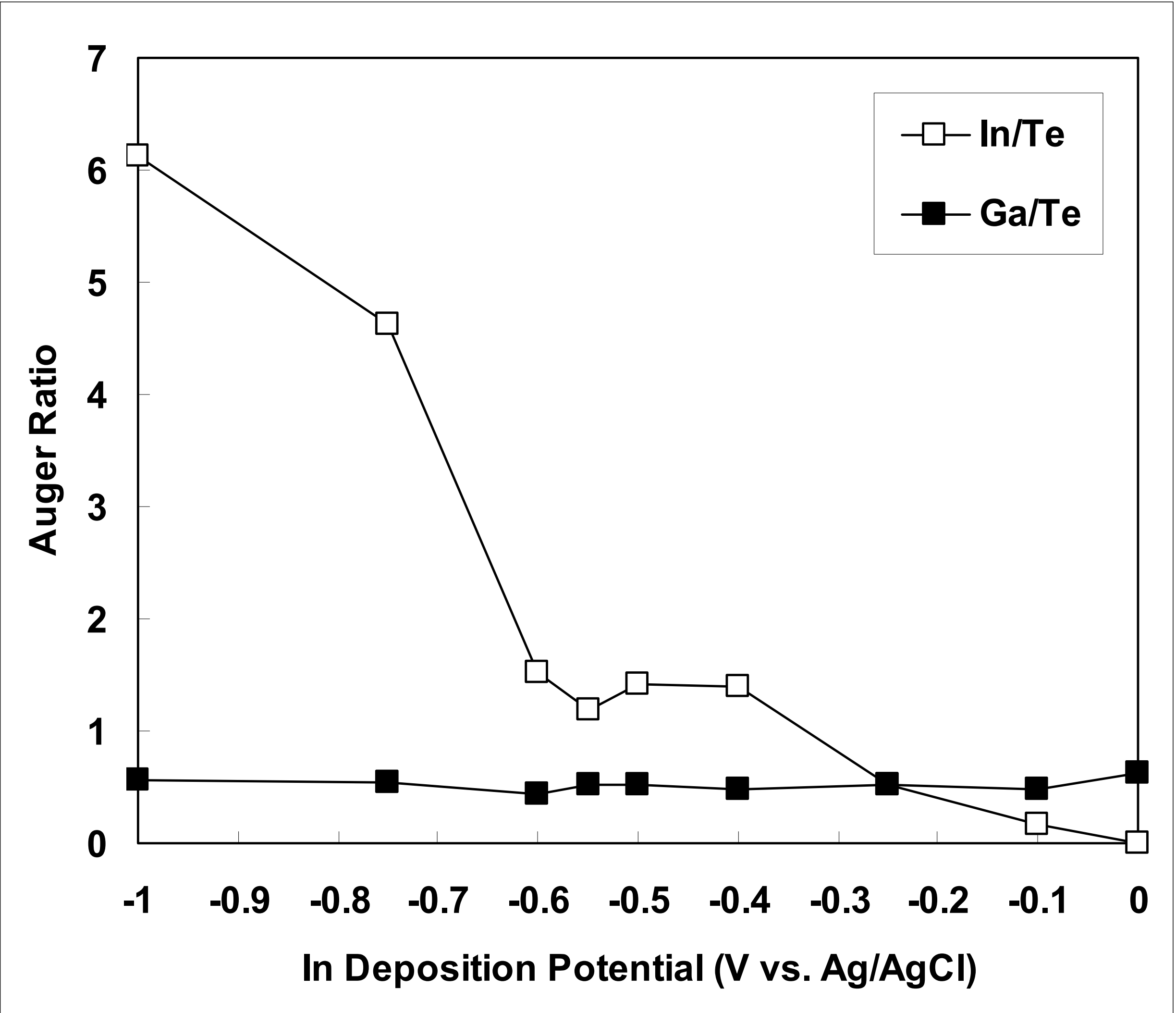

Figure 6.6 Auger ratios versus In deposition potentials with a Te atomic layer on n-GaAs(100).

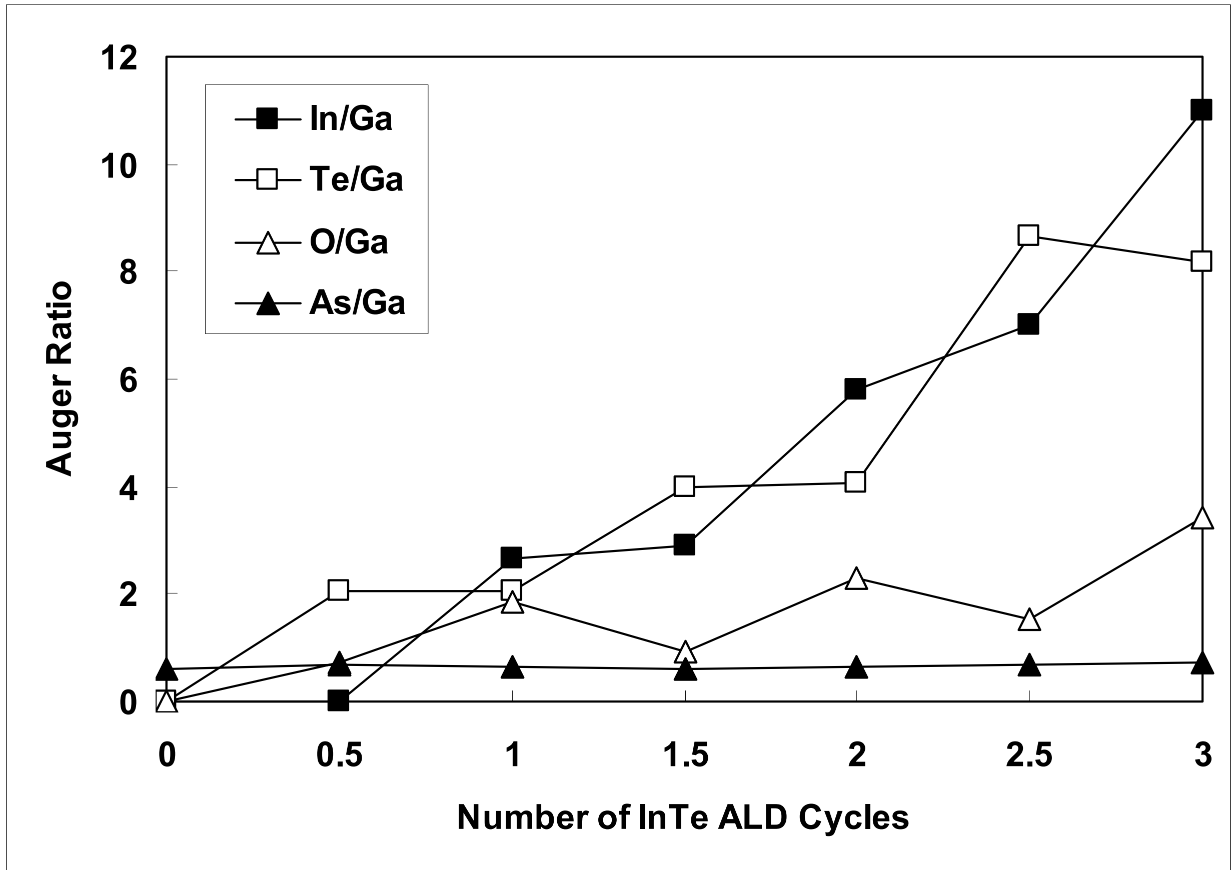

Figure 6.7 Auger ratios versus the number of In-Te ALD cycles on n-GaAs(100).

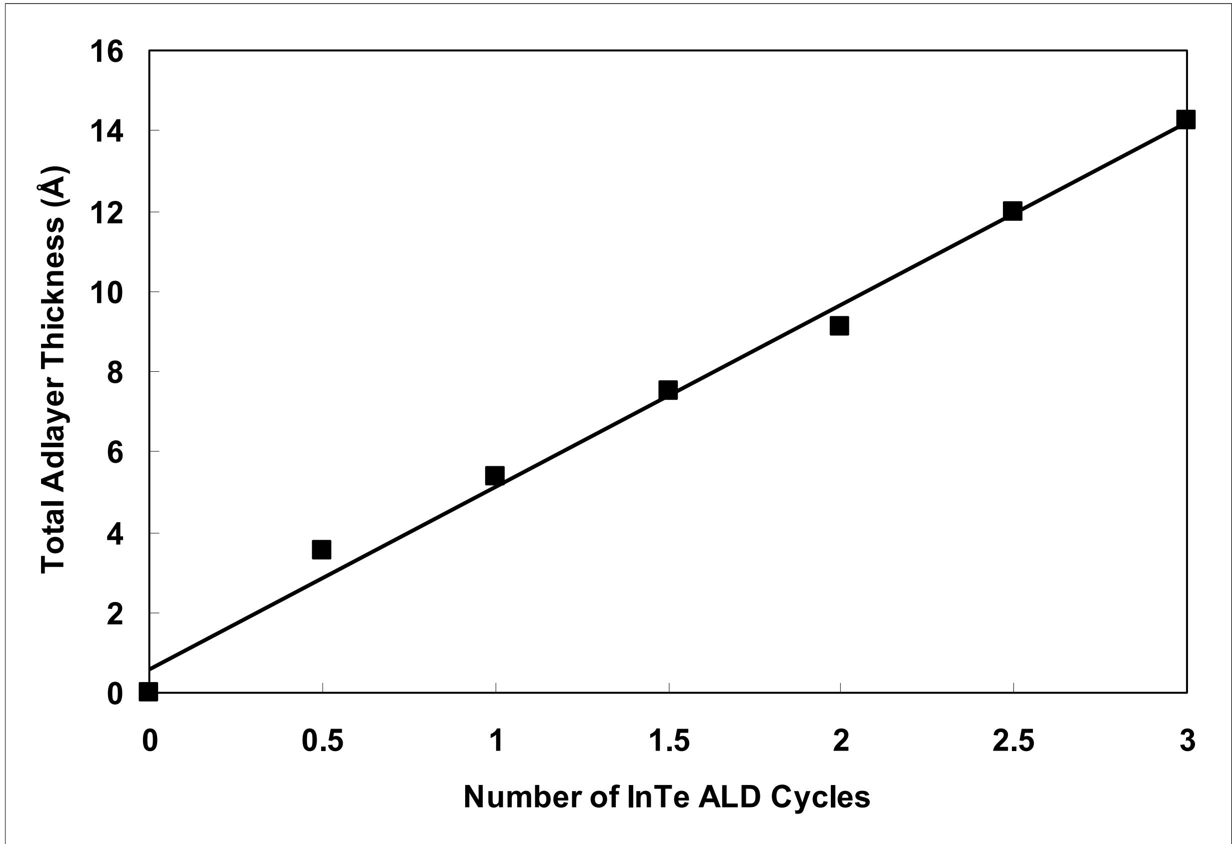

Figure 6.8 The electrodeposited atomic layer thickness in Å versus the number of In-Te ALD cycles (solid line: the best-fit line).

CHAPTER 7

ELECTROCHEMICAL ATOMIC LAYER DEPOSITION (ALD) OF INDIUM ANTIMONIDE ON N-TYPE GAAS(100)[6]

[6] J.Y. Kim and J.L. Stickney, To be submitted to *Electrochem. Solid-State Lett.* (2008).

Abstract

In this paper, it was attempted to electrodeposit indium antimonide (InSb) on n-type GaAs(100) substrate, using atomic layer deposition (ALD). Electrochemical ALD is the electrochemical version of ALD, and is a way to grow compounds, one atomic layer at a time, to achieve layer-by-layer growth. The first Sb atomic layer was deposited at −0.1 V on the clean GaAs substrate. After Sb deposition, indium was deposited at various potentials on the Sb atomic layer. Auger electron spectroscopy was used to monitor deposit composition for the deposition of each indium atomic layer. In/Ga, Sb/Ga, O/Ga, and As/Ga Auger ratios were plotted as a function of the potential used for indium deposition. The atomic In/Sb Auger ratio was calculated and plotted at each indium deposition potential. Another Sb atomic layer was then attempted to be formed on an InSb layer.

Keywords: Electrochemical ALD, UPD, UHV, Auger, GaAs, InSb

Introduction

Electrodeposition has been a thin film growth technique for many years, with the advantages of ease of control and operation at low temperature, relative to molecular beam epitaxy (MBE) or vapor phase epitaxy (VPE) [1]. Several electrochemical methods and variations have been developed to deposit non-oxide compounds, such as the II-VI and III-Vs. The most prominent compound electrodeposition methods include co-deposition, precipitation, and two-stage techniques. Co-deposition is a methodology where both elements are deposited at the same time from the same solution [1]. Stoichiometry is generally maintained by having the more noble element as the limiting reagent, and poising the potential where the less noble

element is deposited at an underpotential only on the more noble element. However, in most cases, the deposits are improved greatly by annealing. The precipitation method involves electrochemical generation of a precursor for one of the constituent elements, in a solution containing precursors to the other elements [1]. The reaction is essentially homogeneous, but as one reactant is formed at the electrode surface, most of the product precipitates on the surface. The quality of the resulting deposit is questionable, and the process is difficult to control. Two-stage methods are where thin-films of the component elements or an alloy are first deposited, at least one by electrodeposition. A second stage, annealing, then results in interdiffusion and reaction of the elements to form the compound [1]. The deposits are annealed in air, inert gas, or a gaseous precursor to one of the compound's component elements. Given the need for annealing, this method has limitations for the formation of more involved device structures.

In this article, studies of the electrochemical ALD of indium antimonide (InSb) on n-type GaAs(100) substrates are reported. The principle of electrochemical ALD is to use surface-limited reactions to form each atomic layer of a deposit [1]. Surface-limited reactions are well-known in electrochemistry, and are generally referred to as underpotential deposition (UPD) [1-4]. UPD is a phenomenon that the first element forms an atomic layer at a potential prior to (under) that needed to deposit the element on itself. A surface compound, or alloy, is formed, and the shift in potential results from the free energy of formation of the surface compound [1]. Electrochemical ALD is the combination of UPD and ALD. Atomic layers of a compound's component elements are deposited at underpotentials in a cycle, to directly form a compound.

Several compound growths have been attempted on III-V semiconductor, GaAs. GaAs is an important and promising compound as a substrate, because of its larger mobility and higher crystallinity than Si [5]. Thin films of chalcogenide atoms (S, Se, and Te) were grown on GaAs

substrate, by mostly MBE, and the surfaces were characterized [6-8]. They act not only as substrate-passivating layers but also precursors for metal (such as Cd, Fe, or Zn) depositions [9-14]. However, there are few attempts of growing compounds on GaAs by electrodeposition. A II-VI compound, CdSe, was co-deposited on GaAs and InP substrates [15-18].

Another III-V compounds, such as InP, InAs, and InSb, can be grown on GaAs substrate, and is expected to have more lattice-matched than II-VI compounds. There have been some studies of Sb and InSb growths by MBE on GaAs(100), GaAs(110), and GaAs(111) substrates, and their surfaces were characterized [19-27]. In these studies, Sb overlayer was deposited on the substrates, and then an indium layer was grown on the Sb layer. The Sb overlayer acted as a surfactant for an indium layer. However, attempts to electrodeposit InSb compound on the substrate are very few.

Experimental

An n-type, Si-doped, GaAs(100) (IBM), carrier density of 2×10^{18} cm^{-3}, was used as the substrate in these studies. The ohmic contact and sample holder are described elsewhere [28, 29]. Photoeffect is expected to be minimized with n-type GaAs(100) substrate under the room light, where the substrate is in the accumulation mode. The as-received n-GaAs(100) substrate was then treated by 10 % HF acid. The HF was used to remove any SiO_2 polishing compound which might have been present. UV ozone cleaning was then used to oxidatively remove any carbon contamination, and resulted in an oxidized surface. Immersion in 10 mM H_2SO_4 (Aldrich Chemical Co.) tended to dissolve any oxide material, while scanning negatively to −1.5 V or below served to reduce any remaining surface oxide. The substrate was then transferred to the ultrahigh vacuum (UHV) chamber, where it was characterized using Auger electron

spectroscopy and cleaned by Ar^+ ion bombardment (1 keV ions, at a current density of ~2.5 $\mu A/cm^2$). It should be noted that the commercial GaAs(100) wafer was cut 2° from the (100), resulting in a highly stepped surface, with terrace widths of about 5 nm at best.

The cleaned substrate was then transferred to an electrochemistry ante-chamber of the UHV system, where an electrochemical cell was held, and placed into a 0.2 mM Sb_2O_3 (Strem Chemicals Inc., 99+%) + 50 mM H_2SO_4 (pH 1.5) solution (Sb solution). From the previous studies, In was deposited as a nucleation and growth on n-GaAs(100) [29], so a Sb atomic layer was attempted to be deposited first on the substrate in this study. Cyclic voltammograms (CV) were obtained by using μAutolab Potentiostat Type III (Eco Chemie B.V.). All potentials in this article are reported with respect to a Ag/AgCl reference electrode (3 M KCl, BAS Inc.). The scan rate was 5 mV/sec for each experiment, and all CVs were performed under room light conditions. All solutions were deaerated with ultrahigh purity (UHP) (99.998 %) Ar gas for at least 30 minutes prior to each experiment. Auger electron spectra (AES), with a simple CMA (Perkin-Elmer), were also obtained separately after immersing the clean n-GaAs(100) substrate at −1.25 V, −1 V, −0.75 V, −0.5 V, −0.25 V, −0.1 V, and 0 V for 30 seconds in Sb solution. After each Sb deposition, the deposit was once rinsed with 10 mM H_2SO_4 solution, prior to AES.

Deposition of a Sb atomic layer was made by immersing the clean substrate at −0.1 V for 30 seconds, and the subsequent immersion at −1 V for 1 minute in 10 mM H_2SO_4 solution. Immersion at −1 V for 1 minute in 10 mM H_2SO_4 solution is for reducing Sb oxide. After depositing a Sb atomic layer on GaAs(100) substrate, In^{3+} ions were reduced from 0.2 mM $In_2(SO_4)_3$ (Johnson Matthey Co., 99.999 %) + 50 mM H_2SO_4 (pH 1.5) solution (In solution). The crystal with a Sb atomic layer on the surface was immersed in indium solution at −1.4 V, −1.2 V, −1 V, −0.8 V, −0.6 V, −0.5 V, −0.4 V, and −0.2 V, for 30 seconds, and the crystal was emersed.

Again, after the indium deposition, the crystal was immersed in 10 mM H_2SO_4 solution at −1 V for about a minute. Then, the crystal was transferred to the main analysis chamber. The electrochemical UHV ante-chamber was interfaced directly to the analysis chamber with a 6 inch gate-valve, so substrates were not exposed to ambient air during transfer, but kept under UHP Ar. Samples were characterized using AES, then.

Results and Discussion

Figure 7.1 shows CV of clean n-GaAs(100) substrate in Sb solution. The potential scan was started negatively from the open circuit potential (OCP), −0.25 V. The potential was then scanned positively from −0.5 V to 0 V. An oxidation peak, about 1.5 monolayer (ML) versus substrate, was shown from the OCP. A ML is defined as the deposition of one Sb atom for each surface atom (6.265×10^{14} atoms/cm^2). The potential was then scanned negatively from 0 V to the OCP, and this was the first scan. The potential was then scanned negatively to −0.75 V, and this time a broad reduction peak, ~ 2 ML, was shown. From Figure 7.2, a large Sb/Ga Auger ratio of ~ 12.5 at −0.75 V, this broad reduction peak is suggested to be Sb bulk reduction (Sb^{3+} + $3e^- \rightarrow Sb^0$ (bulk)). Figure 7.2 was obtained from AES after depositing Sb on the clean substrate at different potentials. Each Sb deposition was done by immersing the substrate in Sb solution at each potential for 30 seconds, and rinsed once in 10 mM H_2SO_4 solution. On positive-going scan from −0.75 V to 0 V, a larger oxidation peak, ~ 2.5 ML, was shown from the OCP, and this oxidation peak is suggested to be mainly bulk Sb stripping peak. The potential was then scanned from 0 V to the OCP (second scan). The third and the fourth scans were then made by scanning potential from OCP → −1 V → 0 V → OCP and from OCP → −1.25 V → 0 V → OCP, respectively. The third and the fourth scan show a similar amount of reduction, as well as the

second one, and no specific feature besides hydrogen evolution peaks ($2H^+ + 2e^- \rightarrow H_2$ (g)) were shown at −0.75 V and below. The oxidation peaks from the OCP in the third and the fourth scan show almost similar amounts, 4.0 and 4.3 ML, respectively. The same Sb/Ga Auger ratio of ~ 20 is shown in Figure 7.2 both at −1 V and −1.25 V.

Figure 7.2 clearly shows that Sb was still left on the surface at −0.1 V and 0 V after the oxidation peak in Figure 7.1. Sb/Ga Auger ratio was ~ 1.8 at −0.1 V. However, a significant amount of oxygen was also shown in AES at −0.1 V and above in Figure 7.2. This oxygen is suggested to have come from Sb oxide [30]. The most effective way to remove the oxide appears to reduce the oxide in a diluted acidic solution. AES showed the oxygen amount decreased significantly after reducing the oxide in 10 mM H_2SO_4 solution. A good way to reduce the oxide is suggested to be immersion in 10 mM H_2SO_4 at −1 V for 1 minute.

An indium atomic layer was tried to be formed on a Sb atomic layer. A Sb atomic layer was deposited by immersing the clean n-GaAs(100) substrate in Sb solution at −0.1 V for 30 seconds, and it was then immersed in 10 mM H_2SO_4 solution at −1 V for 1 minute to reduce the Sb oxide. The crystal was then immersed in indium solution, and the OCP showed −0.27 V. Figure 7.3 shows the CV in indium solution after depositing a Sb atomic layer on the substrate. The potential was scanned negatively from −0.4 V to −1.2 V. At −1.2 V, the potential was held for about 1 minute to allow enough time for indium deposition on the Sb atomic layer. The potential was then scanned positively from −1.2 V to −0.4 V. A broad oxidation peak, ~ 1.5 ML, is shown from −0.8 V to −0.5 V, and almost 0 μA current is shown from −0.5 V to −0.4 V, in Figure 7.3.

Figure 7.4 shows In/Ga, Sb/Ga, O/Ga, and As/Ga Auger ratios at various indium deposition potentials. AES were obtained after depositing indium on a Sb atomic layer on the

substrate at −1.4 V, −1.2 V, −1 V, −0.8 V, −0.6 V, −0.5 V, −0.4 V, and −0.2 V. The deposition time was 30 seconds at each potential. The crystal was then immersed in 10 mM H_2SO_4 at −1 V for 1 minute after each indium deposition. In/Ga Auger ratio of decreases from about 6 at −1.4 to about 1.5 at −0.6 V, and a distinctive plateau between −0.6 V and −0.4 V is clearly shown in Figure 7.4. This plateau suggests that indium was still left at −0.6 V and above, right after the oxidation peak on positive-going scan in Figure 7.3. This left indium strongly suggests that it is strongly bonded to the Sb atomic layer; therefore, it is an indium atomic layer on a Sb atomic layer. However, some indium was oxidized at −0.2 V, shown in Figure 7.4. It is promising that Sb/Ga Auger ratio shows constant value, ~ 1.8, over all indium deposition potential, strongly suggesting that Sb was not oxidized at all indium deposition potentials. It is also noteworthy that the constant trend of As/Ga Auger ratio suggest the substrate itself was not affected by forming InSb compound on the substrate. However, there was still oxygen observed on the surface from AES, the O/Ga Auger ratio trend appears to be similar as the In/Ga trend in Figure 7.4, though the oxide reduction in 10 mM H_2SO_4 solution involved after each indium deposition. Indium is well-known for reacting with oxygen a trace of which may exist in UHP Ar gas back-filled ante-chamber. Indium oxide may have formed on the surface when the crystal was emersed from the indium solution.

The atomic In/Sb Auger ratio is plotted according to indium deposition potential in Figure 7.5. Since each element has different Auger sensitivity factor, the atomic In/Sb Auger ratio can be calculated by Eq. (7.1) [29]:

(Atomic In/Sb Auger ratio) = (Observed In/Sb Auger ratio) / (In/Sb sensitivity factor ratio) (7.1)

The atomic In/Sb Auger ratio is 1 when indium deposition potential is about −1.05 V, from Figure 7.5. Therefore, InSb compound with appropriate stoichiometry (In:Sb = 1:1) is formed

when indium deposition potentials of −1.05 V are used to deposit an indium atomic layer on a Sb atomic layer. More negative indium deposition potentials than −1.05 V would result in indium rich InSb compounds, and more positive potentials than −1.05 V would result in Sb rich InSb compounds.

After having formed InSb on n-GaAs(100) substrate, another Sb atomic layer was attempted to be formed. Figure 7.6a shows AES of an InSb layer formed on the substrate. A Sb atomic layer was first formed at −0.1 V on the clean substrate, and the oxide was reduced at −1 V for 1 minute in 10 mM H_2SO_4 solution, as described above. An indium atomic layer was then formed at −0.6 V on a Sb atomic layer, the oxide was reduced with the same method. On an InSb layer (Figure 7.6a), Sb was reduced at −0.5 V in Sb solution for about 30 seconds, and the oxide was reduced at −1 V for 1 min in 10 mM H_2SO_4 solution. Figure 7.6b, the resulting AES, shows that bulk Sb (Sb/Ga ≈ 10) was formed on an InSb layer, and In/Ga Auger ratio (≈1.4) suggests that Indium was not oxidized. However, when the substrate with an InSb layer was immersed in Sb solution at open circuit, OCP was shifted from −0.36 V to −0.32 V, and a significant amount of In was oxidized, in Figure 7.6c. The In/Ga Auger ratio is shown about 2/3 in Figure 7.6c. When Sb was deposited at −0.15 V on an InSb layer, Figure 7.6d suggests that indium was almost completely oxidized. However, the Sb/Ga Auger ratio is doubled in Figure 7.6d (Sb/Ga ≈ 3.6), compared to Figure 7.6a (Sb/Ga ≈ 1.8), suggesting that another Sb atomic layer was formed on the first Sb atomic layer.

Conclusion

III-V compound semiconductor, InSb, has been attempted to be formed on n-type GaAs(100) substrate by electrochemical ALD. Electrochemical ALD involves a series of

surface-limited reactions. The substrate was cleaned by Ar^+ ion bombardment. Since indium was grown as a nucleation and growth, a Sb atomic layer was first tried to be deposited. A Sb atomic layer appeared to be deposited at −0.1 V on the substrate. However, there was a significant amount of oxygen, which is suggested to be Sb oxide, so the oxide was reduced in 10 mM H_2SO_4 solution after the Sb deposition. Auger ratios of In/Ga, Sb/Ga, O/Ga, and As/Ga were obtained from AES after depositing indium on a Sb atomic layer at various potentials in indium solution. Sb/Ga and As/Ga Auger ratio showed almost constant. In/Ga Auger ratio trend had a plateau between −0.6 V and −0.4 V, which suggests that an indium atomic layer was left after the bulk indium was stripped. The atomic In/Sb Auger ratios were calculated from the observed In/Sb Auger ratio and Auger sensitivity factors of indium and Sb. Again, the atomic In/Sb Auger ratio of 1 at the indium deposition potential of −1.05 V suggests that an InSb compound with In:Sb = 1:1 stoichiometry is formed at that potential.

Acknowledgement

The financial supports from National Science Foundation and Department of Energy are gratefully acknowledged.

References

1. J.L. Stickney, in *Advances in Electrochemical Science and Engineering*, R.C. Alkire and D.M. Kolb (Eds.), Wiley-VCH, Weinheim, 2002.
2. M.H. Holzle and D.M. Kolb, *Phys. Chem. Chem. Phys.*, **98**, 330 (1994).

3. M.P. Soriaga, D.A. Harrington, J.L. Stickney, and A. Wieckowski, in *Modern aspects of electrochemistry*, B. Conway, J.O.M. Bockris and R. White (Eds.), Plenum Press, New York, 1996.

4. J.L. Stickney, in *Electroanalytical Chemistry*, A.J. Bard and I. Rubinstein (Eds.), Marcel Dekker, New York, 1999.

5. P.D. Angnello, *IBM J. Res. Dev.*, **46**, 317 (2002).

6. P. Moriarty, B. Murphy, and G. Hughes, *J. Vac. Sci. Technol. A*, **11**, 1099 (1993).

7. M.D. Pashley and D. Li, *J. Vac. Sci. Technol. A*, **12**, 1848 (1994).

8. P. Moriarty, B. Murphy, L. Roberts, A.A. Cafolla, G. Hughes, L. Koenders, and P. Bailey, *Phys. Rev. B*, **50**, 14237 (1994).

9. D.W. Tu and A. Kahn, *J. Vac. Sci. Tech. A*, **2**, 511 (1984).

10. D.W. Tu and A. Kahn, *J. Vac. Sci. Technol. A*, **3**, 922 (1985).

11. Y. Gobil, J. Cibert, K. Saminadayar, and S. Tatarenko, *Surf. Sci.*, **211**, 969 (1989).

12. G.W. Anderson, M.C. Hanf, X.R. Qin, P.R. Norton, K. Myrtle, and B. Heinrich, *Surf. Sci.*, **346**, 145 (1996).

13. S. Hohenecker, T.U. Kampen, W. Braun, and D.R.T. Zahn, *Surf. Sci.*, **435**, 347 (1999).

14. S. Hohenecker, T.U. Kampen, T. Werninghaus, D.R.T. Zahn, and W. Braun, *Appl. Surf. Sci.*, **142**, 28 (1999).

15. L. Beaunier, H. Cachet, M. Froment, and G. Maurin, *J. Electrochem. Soc.*, **147**, 1835 (2000).

16. H. Cachet, R. Cortes, M. Froment, and A. Etcheberry, *Thin Solid Films*, **361-362**, 84 (2000).

17. L. Beaunier, H. Cachet, R. Cortes, M. Froment, and A. Etcheberry, *Thin Solid Films*, **387**, 108 (2001).

18. A. Etcheberry, H. Cachet, R. Cortes, and M. Froment, *Surf. Sci.*, **482**, 954 (2001).

19. P. Skeath, C.Y. Su, W.A. Harrison, I. Lindau, and W.E. Spicer, *Phys. Rev. B*, **27**, 6246 (1983).

20. G.P. Srivastava, *Phys. Rev. B*, **47**, 16616 (1993).

21. W.G. Schmidt, B. Wenzien, and F. Bechstedt, *Phys. Rev. B*, **49**, 4731 (1994).

22. W.G. Schmidt, B. Wenzien, and F. Bechstedt, *Surf. Sci.*, **307-309**, 235 (1994).

23. P.V. Santos, N. Esser, J. Groenen, M. Cardona, W.G. Schmidt, and F. Bechstedt, *Phys. Rev. B*, **52**, 17379 (1995).

24. C. Nowak, J. Krujatz, A. Markl, C. Meyne, A. Chasse, W. Braun, W. Richter, and D.R.T. Zahn, *Surface Science*, **331-333**, 619 (1995).

25. A.A. Cafolla, C. McGinley, E. McLoughlin, G. Hughes, P. Moriarty, A.W. Dunn, Y.R. Ma, D. Teehan, B. Murphy, S. Downes, and D.A. Woolf, *Surf. Sci.*, **377-379**, 130 (1997).

26. S. Schintke, U. Resch-Esser, N. Esser, A. Krost, W. Richter, and B.O. Fimland, *Surf. Sci.*, **377-379**, 953 (1997).

27. H. Ascolani, J. Avila, N. Franco, and M.C. Asensio, *Phys. Rev. B*, **58**, 13811 (1998).

28. M. Muthuvel and J.L. Stickney, *J. Electrochem. Soc.*, **153**, C67 (2006).

29. J.Y. Kim and J.L. Stickney, *J. Phys. Chem. C*, **112**, 5966 (2008).

30. M.J.N. Pourbaix, *Atlas of Electrochemical Equilibria in Aqueous Solutions*, Pergamon Press, Oxford, 1949.

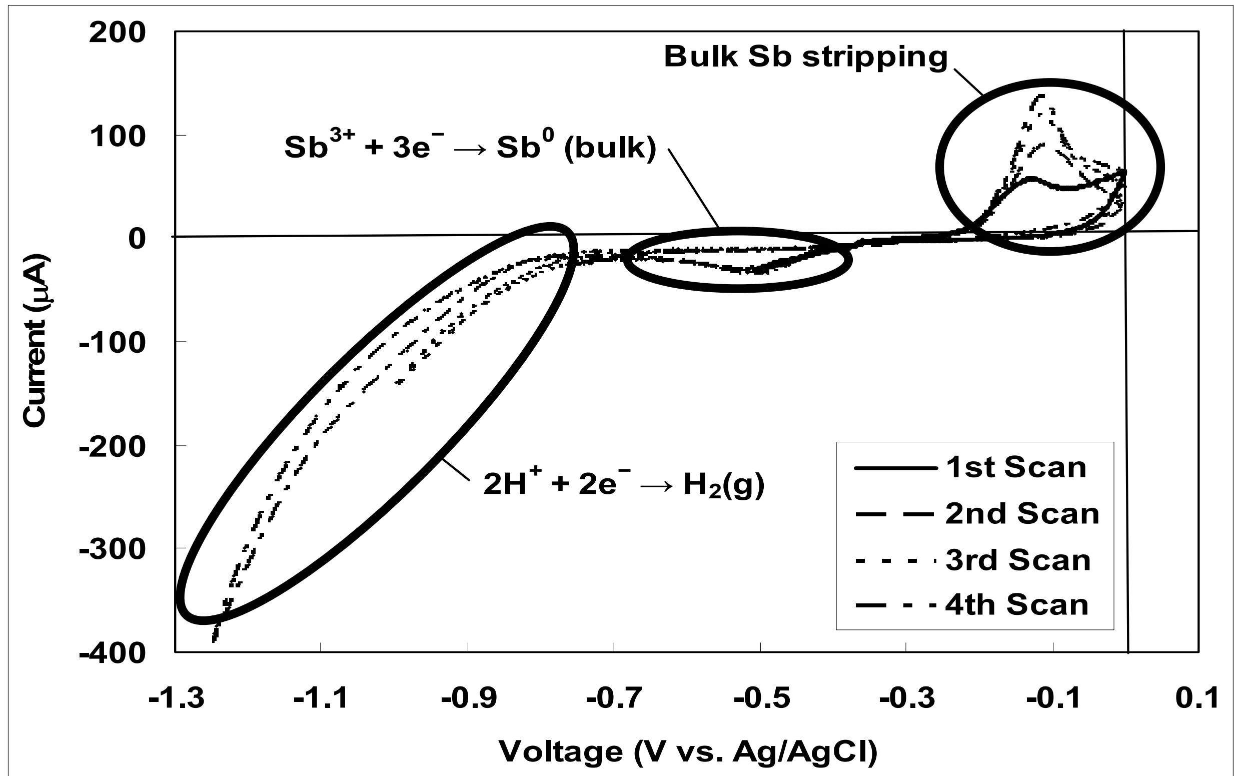

Figure 7.1 Cyclic voltammogram of clean n-GaAs(100) substrate in Sb solution.

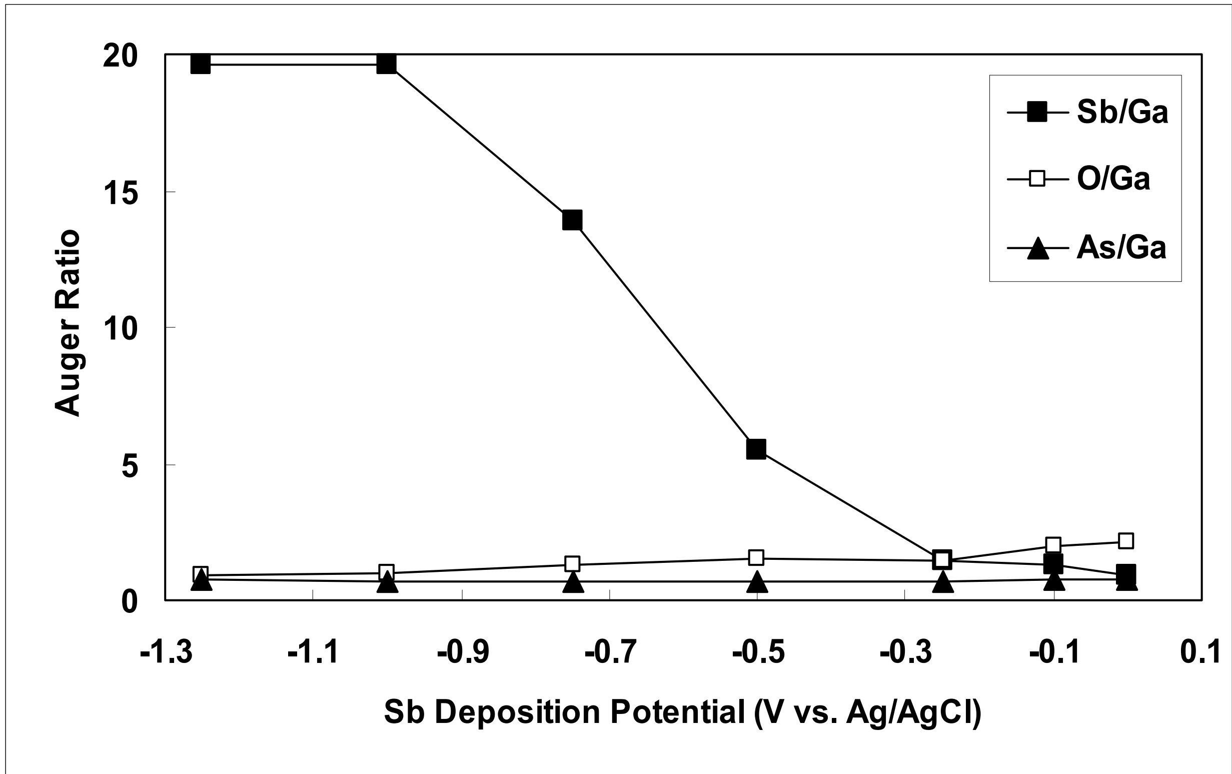

Figure 7.2 Auger ratio versus Sb deposition potential.

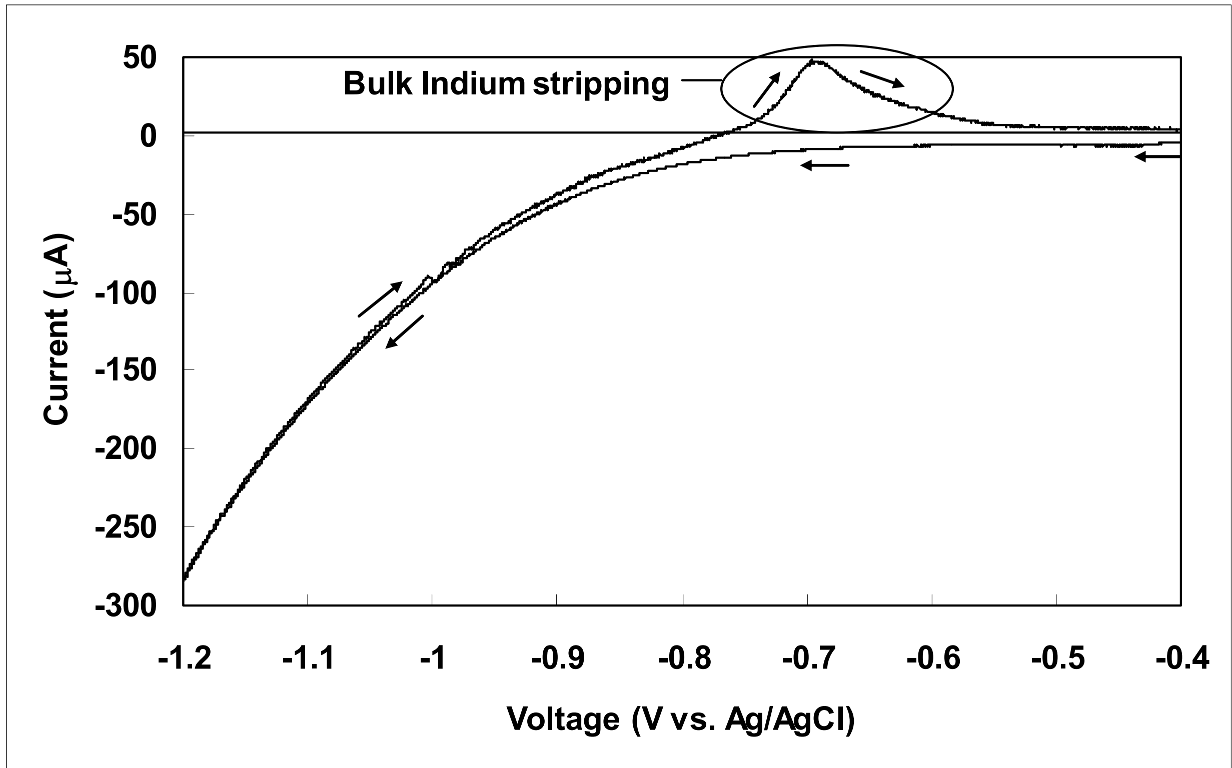

Figure 7.3 Cyclic voltammogram in indium solution on a Sb atomic layer on n-GaAs(100).

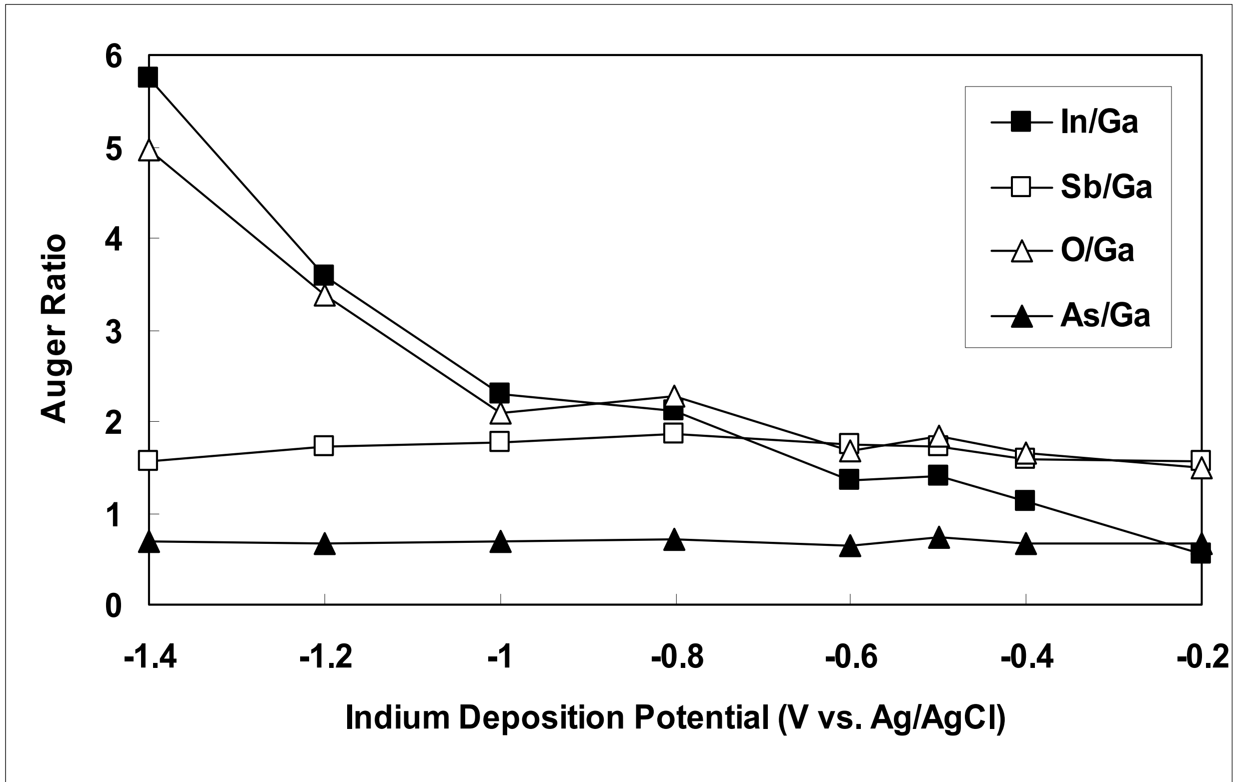

Figure 7.4 Auger ratio versus indium deposition potential on a Sb atomic layer on n-GaAs(100).

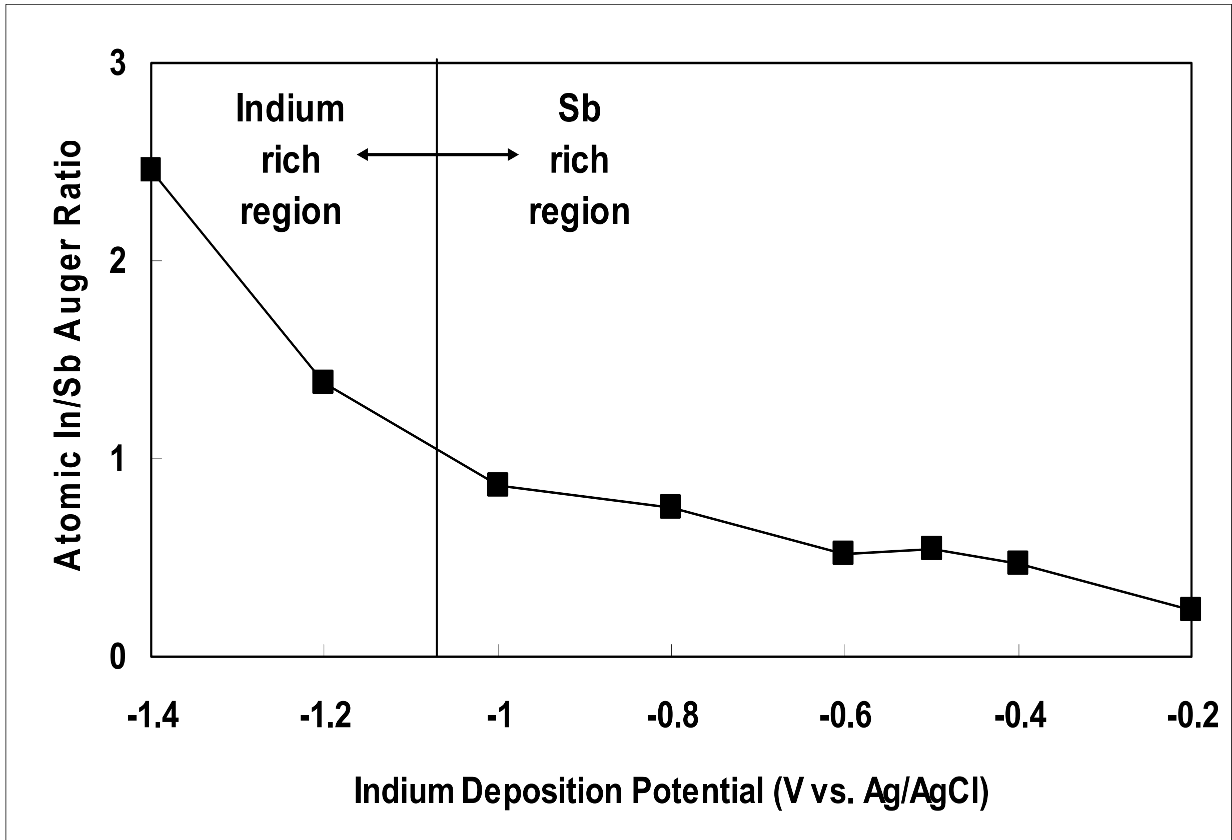

Figure 7.5 The atomic In/Sb Auger ratio versus indium deposition potential.

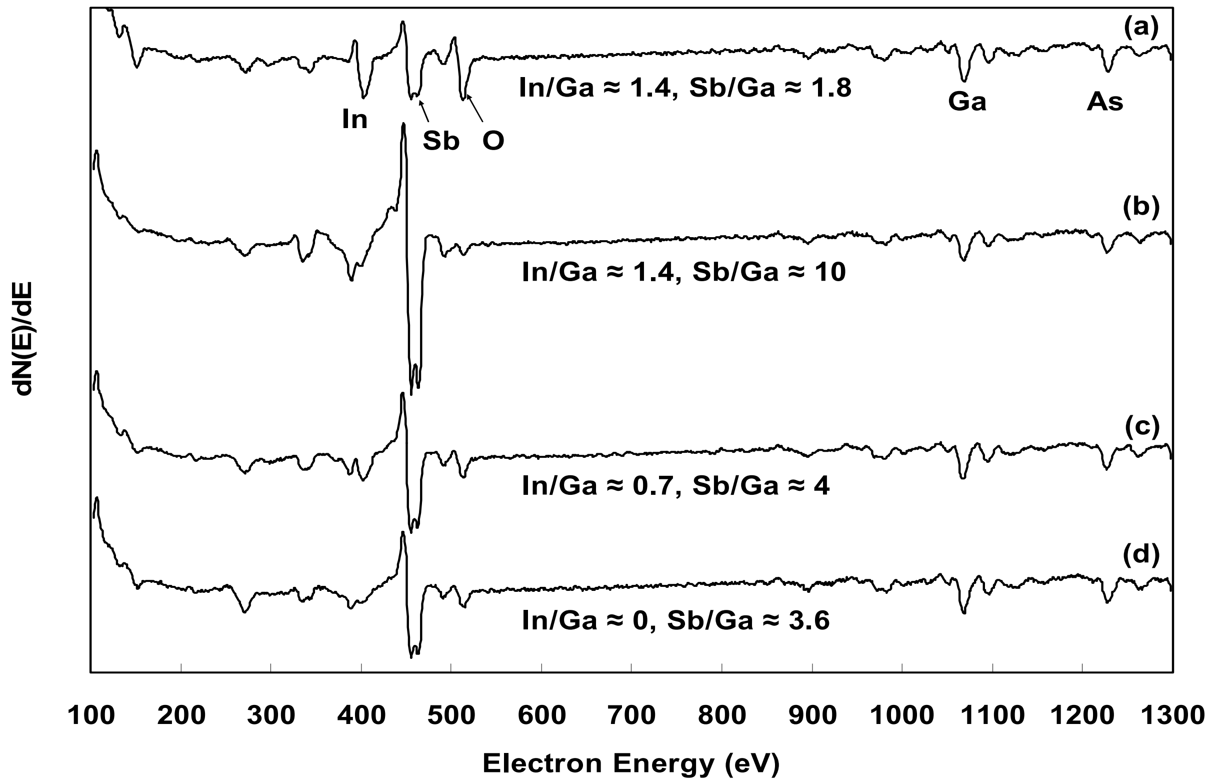

Figure 7.6 Auger spectra comparison of (a) InSb on n-GaAs(100), (b) Sb deposition at −0.5 V on (a), (c) Sb deposition at − 0.32 V on (a), and (d) Sb deposition at −0.15 V on (a).

CHAPTER 8

CONCLUSION AND FUTURE STUDIES

Electrochemical ALD of metal and semiconductor thin films is the main topic of this dissertation. Formation of Pt and Cu thin films on Au(111) substrate has been somehow successful by using SLRR. SLRR is an excellent method of growing a metal thin film on Au(111) by 2 dimensional layer-by-layer growth. Cu and Pb atomic layers were used as sacrificial layers for Pt and Cu thin films, respectively. Using halide ions in solutions, such as I^- or Cl^- anions, has been helpful for the electrochemical annealing and the modification of surfaces. With use of those halide ions, in-situ STM image patterns are identical to ex-situ LEED patterns.

GaAs(100) substrate has been used as a substrate since it is considered as the next generation substrate, to Si substrate. Since no photo-current flows in the reductive current region under illumination, a n-type GaAs(100) substrate has been used in these studies. Cleaning n-GaAs(100) substrate has been more challenging than cleaning Au(111) substrates, because of greater reactivity with oxygen and other contaminants. Cleaning n-type Ge(111) substrate has also been attempted, and some AES and LEED patterns were obtained (Chapter 5). Attempts were made to grow two binary compounds, In_2Te_3 (Chapter 6) and InSb (Chapter 7), on n-GaAs(100) substrate by electrochemical ALD. From several Auger ratios, a Te atomic layer appeared to be formed at −1 V on the substrate. An Indium atomic layer was grown at −0.4 V. In_2Te_3 compound has been grown, layer-by-layer, up to three cycles. Indium appeared to be grown via nucleation and growth on the clean substrate, and a Te atomic layer on the substrate appeared to be the precursor for an In atomic layer. A Sb atomic layer was formed at −0.1 V on the clean substrate, and a subsequent Sb oxide reduction step was required. Then, an Indium atomic layer was formed on a Sb atomic layer between −0.6 V and −0.4 V. However, the formation of another Sb atomic layer on the InSb layer needs yet to be studied and developed.

Future studies with metal SLRR would be to grow thicker films, 10 ~ 20 nm or thicker, of Cu, Ru, or Pt, by using SLRR on Au(111) substrate. Cu thicker film grown by using SLRR would be applied to Cu Damascene, which is used in Cu on-chip interconnect. Ru and Pt films are expected to be applied to grow electro-catalysts for fuel cells. The qualities of the resulting metal films grown by SLRR should be compared with the ones grown by conventional bulk electrodeposition with similar amounts. Regarding electrochemical ALD on n-GaAs(100) substrate, more lattice-matched binary compound to the substrate, such as ZnSe, can be grown on the substrate by using electrochemical ALD. Some morphological studies, such as in-situ STM or AFM, should be done on the surface after growing binary compounds by electrochemical ALD, which would give stronger and more direct evidence. Furthermore, it would be very interesting to see whether Cu thin film can be grown layer-by-layer on n-GaAs(100) by using SLRR.